FACULTY OF ENGINEERING AND ARCHITECTURE

Automated EEG Source Imaging to Localize the Epileptogenic Zone in Patients with Drug-Resistant Epilepsy

Amir Ghasemi Baroumand

Doctoral dissertation submitted to obtain the academic degree of
Doctor of Biomedical Engineering

Supervisors

Prof. Pieter van Mierlo, PhD* - Prof. Sandor Beniczky, PhD**

* Department of Electronics and Information Systems
Faculty of Engineering and Architecture, Ghent University

** Department of Clinical Medicine - Department of Clinical Neurophysiology
Aarhus University, Denmark

June 2024

GHENT UNIVERSITY

ISBN 978-94-6355-840-2
NUR 954
Wettelijk depot: D/2024/10.500/46

Members of the Examination Board

Chair

Prof. Luc Dupré, PhD, Ghent University

Other members entitled to vote

Geertjan Huiskamp, PhD, UMC Utrecht, the Netherlands
Prof. Alfred Meurs, PhD, Ghent University
Prof. Pierre Mégevand, PhD, Université de Genève, Switzerland
Prof. Christian Vanhove, PhD, Ghent University

Supervisors

Prof. Pieter van Mierlo, PhD, Ghent University
Prof. Sandor Beniczky, PhD, Aarhus University, Denmark

Acknowledgment

Before completing my master in Control Engineering and Automation, I had the opportunity to participate in an experiment involving the recording of the brain's electrical activities, known as EEG, as part of a research project. This experiment illuminated the profound insights we can gain by studying the brain, revealing how we learn from its functions and how I could contribute to this field. Motivated by this experience, I was inspired to apply my engineering skills to clinical research. This journey ultimately led me to pursue a PhD focused on studying EEG signals in patients with drug-resistant epilepsy.

Conducting this PhD journey and writing this dissertation has been a remarkable experience. My initial steps began with the MEDISIP group, which introduced me to the field. I later transitioned to Epilog, where I deepened my knowledge and conducted all my studies and research. Finally, I returned to MEDISIP to complete my thesis. The most memorable moments of this journey included the joy of fatherhood with Djanan and expecting of our second child. These experiences, along with numerous opportunities and challenges, defined my journey. Balancing the acquisition of new knowledge outside my initial background, working at Epilog, and embracing the responsibilities of 24/7 fatherhood were integral parts of this process. The work presented in this PhD thesis is the result of many collaborations. Without the support and contributions of many wonderful individuals, this thesis would not have been possible. I am truly grateful for the opportunity to acknowledge and thank them here.

First of all, I want to express my gratitude to **Prof. dr. Pieter van Mierlo** for giving me the opportunity to conduct my research in MEDISIP and later in Epilog. I appreciate the guidance and support I received, especially in the early stages of my work, which helped me gain a better understanding of my research topic. I am grateful for the freedom I was given to pursue my academic and professional work. The experiences of running PreOp and ictal cases and the discussions that followed have been memorable. Moreover, I enjoyed the travel we had to Exeter, Dublin, and Geneva. I hope that Epilog, also known as Clouds of Care, continues to be a leader in healthcare technology. I am hopeful that MEDISIP's fruitful contributions to the upcoming revolution in neuroscience will remain enduring.

I would like to express my sincere gratitude to my promoter, **Prof. dr. Sándor Beniczky**, for the invaluable clinical input and insights provided throughout my PhD journey. Although we first met when I sought advice on another clinical project in Aarhus University Hospital before starting my PhD, I could not have anticipated that you would one day become my promoter. Your feedback on the interictal and ictal ESI projects was instrumental in streamlining our processes. Additionally, your assessment of the sliding ictal ESI reports significantly contributed to elevating the standard of my work, enabling me to present it confidently in my PhD dissertation. Thank you for your guidance and support.

I would also like to extend my heartfelt thanks to **dr. Gregor Strobbe**. Thank you, Gregor, for giving me the opportunity to begin my first study at MEDISIP, for introducing me to Pieter, and for taking me to Epilog. It was a privilege to witness and contribute to the birth and growth of a start-up company. I am truly grateful to have been part of it. I have fond memories of the bachelor party you and Pieter organized for me, as well as our many discussions during Thirsty Thursdays, including those related to Leadfields topics. Additionally, our rehearsal session of the Googoosh's song went really well. I would also like to thank **Prof. dr. Vincent Keereman** for providing valuable clinical insights about seizures and spikes, as well as for being present in the crucial moment. Your support has been instrumental, and I wish great success for Xeos.

The very initial steps of this journey began when I joined ICELAB, the research group led by **Prof. dr. Farshad Moradi** at Aarhus University, Denmark. Farshad, a special thank you goes to you for taking me on as a research assistant, providing the necessary equipment for EEG recordings, and supporting me with writing PhD grants. Your guidance and support have been invaluable. I would also like to thank **dr. Nathalie Van Den Berge**. Although we only met a few times in Aarhus, you did a wonderful job introducing me to Gregor and MEDISIP. Your help has been greatly appreciated. I further would like to thank **dr. Willeke Staljanssens** for mentoring me after I joined MEDISIP and teaching me the fundamentals of EEG Source Imaging. Your support was invaluable in conducting the first Ictal ESI study, even though we did not have the chance to publish it.

I must thank **Prof. dr. Riëm El Tahry**, **dr. Simone Vespa**, and **dr. Bernd Vorderwülbecke** for the fruitful and contributive collaborations we had together. Your clinical inputs and feedback were essential to the success of this PhD project and the development of the Ictal pipeline. Moreover, I would like to express my appreciation to **dr. Geertjan Huiskamp**, **Prof. dr. Alfred Meurs**, **Prof. dr. Pierre Mégevand**, and **Prof. dr. Christian Vanhove** for serving as my jury members, reading my PhD dissertation, and providing me with their technical and clinical feedback to enrich its content. In addition, I appreciate my group mates, **Emma** and **Jolan**, at MEDISIP. Although I was with you for only one year in the university office, our discussions and your comments, especially those for my internal defense, were extremely helpful.

Beyond your technical knowledge, I admired your sense of happiness and zest for life. Furthermore, thank you so much, Jolan, for translating my summary into Dutch and for sharing your ideas for my PhD dissertation.

I wish to thank all my colleagues at Epilog, Somnilog, and Clouds of Care over the past years. I had the great fortune to work with a professional and amazing team. I would like to start by thanking **Tanja**. Although we didn't meet often due to working on different continents, we built a collaborative and effective friendship. **Jurgen**, your attitude and experience significantly boosted the company and paved the way for other colleagues to join. **Natasja** and **Delphine**, thank you for all nice works and for organizing all the great events. Additionally, I want to thank Mr. **Maxim** for being a great friend and neighbor, sharing information about Sint-Truiden. Thank you, **Benjamin**, **Brecht**, **Caroline**, **Ekatherina**, **Eline**, **Eline DS**, **Emiel**, **Enid**, **Gilles**, **Jeroen**, **Joachim**, **Maria**, **Nathan**, **Nick**, **Nigel**, **Laura**, **Sander**, **Tom**, and **Victor**, for all the discussions, collaborations, and great moment we had together. I wish you success in both your personal lives and professional careers.

Sarineh, we became colleagues after you joined Somnilog, and later we also developed a friendship. I was really happy to hand over my tasks to someone as responsible as you. Thanks for being a nice friend and colleagues. I would like to extend special thanks to **Kavous** and **Mitra** for giving me the opportunity to participate in the EEG experiment that shaped my career path. **Banafsheh**, we are grateful to have a special friend like you— a friend forever.

I wish to express my gratitude to all my colleagues at MEDISIP and Biommeda for creating a wonderful work environment over the years. I want to thank **Prof. dr. Stefaan Vandenberghe**, **Prof. dr. Patrick Segers**, **Prof. dr. Charlotte Debbaut**, and **Prof. dr. An Ghysels** for fostering a dynamic and scientific atmosphere. I also want to thank **Saskia** and **Inge** for their hard work and support for the entire team. I appreciate all the wonderful lunch sessions, Christmas parties, and coffee breaks we've had together with my frinds there, including **Zoe**, **Yousef**, **Wouter**, **Tim**, **Simeon**, **Sarah**, **Saar**, **Rabia**, **Melissa**, **Maya**, **Lise**, **Jessie**, **Jens**, **Jellis**, **Florence**, **Elias**, **Beatrice**, **Boris**, **Ariana**, **Amith**, and **Annette**. I especially enjoyed the Iranian coffee breaks at 3 p.m. with my friends. Thank you to **Samaneh**, **Sina**, **Mohammad**, **Meysam**, and **Hooamn** for making our everyday routine so enjoyable and for being such the great friends.

I want to acknowledge my family, who have fully supported me over the years. While it is difficult to name all of you, I want to extend my gratitude to each of you. Special thanks to **Aya** and **Babadi**, who have elevated my life. Your intuition about life and family is amazing, and I strive to learn from you. Thank you, **Amir**, **Omid**, **Mar**, and **Hana**, for your incredible hospitality and all you do for us when we are with you. I am amazed by the wonderful parties and the great spirits of **Homa**, **Bardiya**, and **Hooman**. Additionally, I want to thank **Elnaz** for being not only an old friend and an irreplaceable sister but also for her constant support and the positive vibes she brings to the whole family. My deepest gratitude goes to my parents, **Ama** and **Aba**.

Your love, encouragement, and unwavering support have been my foundation throughout my life. Thank you for believing in me, teaching me important values, and shaping who I am. Also, thank you, **Djanan**, my lovely sweet daughter. I will always cherish the unforgettable moment when I held you in my arms and you gazed at me on your first night. I am so proud of you. Together with you and your mamanii, we eagerly await **Nn's** safe arrival. I want to express my heartfelt gratitude to my wife, **Hakimeh**. Together, we have built a family and embarked on a lifelong journey filled with hopes, dreams, and love, from Hafezieh and Haj-Baba to Høegh Guldbergs Gade, and then to Wolterslaan. Thank you for motivating me to start the PhD journey, being the best partner, and sacrificing at crucial moments. You have made me a better person, and I could not have achieved all of this without you. I hope we continue to enjoy all that we have created together, cherishing each moment of our life, ke khodaeest dar in nazdike!

Amir

30 May 2024

Ghent

The 18th European Congress of Clinical Neurophysiology, Marseille, France. Reprinted from LinkedIn, by Sándor Beniczky, 2023. Retrieved from `https://www.linkedin.com/embed/feed/update/urn:li:share:7062361674187452416`.

Contents

English summary

In the name of the Lord of both life and mind, To nothing sublimer can thought be applied

Ferdowsi

The primary objective of this dissertation research is to precisely localize the epileptogenic zone (EZ) in patients with drug-resistant epilepsy. This will be achieved through automated pipelines utilizing interictal and ictal activities present in electroencephalography (EEG) data.

Epilepsy is a neurological disorder that affects approximately 1% of the global population. It is characterized by unprovoked recurrent seizures caused by abnormal electrical activities in the brain. Seizures can be classified into three types: focal, generalized, or unknown. In a focal seizure, abnormal electrical activities occur in one brain region, in contrast to a generalized seizure during which multiple areas of the brain are involved. Focal seizures could be with or without impaired awareness, and symptoms of this type can be generally conflated with other brain conditions. Generalized seizures can manifest in various types, such as absent seizures, tonic seizures, atonic seizures, and more. Among them, tonic-clonic seizures, formerly known as grand mal seizures, are quite dramatic. They can cause sudden loss of consciousness, body stiffening, shaking, and other symptoms.

There are several medications available for stabilizing the electrical activity in the brain, which can help to prevent or reduce the frequency and severity of seizures. Despite advancements in pharmacology and the availability of new medications, 7-20% of children and 30-40% of adult epilepsy patients remain drug-resistant. In such cases with drug-resistant epilepsy, surgery remains the most effective treatment option. To accomplish this, the epileptogenic zone (EZ) must be resected to render the patient seizure-free. EZ is a conceptual-clinical term rather than an anatomical-physiological area, and it refers to a critical region in the brain responsible for epileptic seizures and whose removal leads to seizure-freedom. Precise localization of the EZ is essential before the epilepsy operation since it has a crucial role in the clinical management of

patients to achieve seizure freedom and minimize the impact of surgery on essential brain functions.

The process of EZ localization, which is a part of presurgical evaluation, involves various tests. Firstly, the patient's medical history will be reviewed. Then, a group of multimodal neuroimaging techniques will be performed, including noninvasive methods such as video-EEG monitoring, magnetic resonance imaging (MRI), magnetoencephalography (MEG), positron emission tomography (PET), single-photon emission computerized tomography (SPECT), and Functional MRI (fMRI). If necessary, invasive intracranial electroencephalography (iEEG), which includes electrocorticography (ECoG) and stereo-electroencephalography (sEEG), can be used. Each technique provides information about the EZ. Long-term video-EEG recording detects those abnormal activities linked to the EZ, including sharp spikes (Interictal epileptiform discharges) or epileptic seizures (ictal activity). Analyzing spikes helps to identify the irritative zone (IZ), while seizure analysis can locate the seizure onset zone (SOZ). Apart from EEG data, brain lesions are detectable in the MRI, hypometabolism in the PET, and hyperperfusion during seizures in the ictal SPECT. All this information will be considered, and a multi-disciplinary team of epileptologists, neurologists, neurosurgeons, and other specialists will evaluate them to identify the EZ and plan treatment.

Among the above-mentioned neuroimaging modalities, scalp EEG is a useful, safe and non-invasive technique that is used to evaluate candidates for epilepsy surgery. It provides valuable insights into seizure onset, propagation, localization, and lateralization. EEG is capable of detecting rapid changes in brain electrical activity with high temporal resolution. However, this method has some limitations. The spatial resolution is relatively low. It records data from the scalp rather than directly from the sources, and the recorded signals may be distorted after passing through the skull and scalp tissues. Additionally, it primarily captures data from cortical regions, while detecting electrical activity from deep brain structures remains challenging. On the other hand, structural MRI, as a safe and non-invasive modality, has a high spatial resolution. This technique can provide information about the brain's structure and detect abnormalities like brain lesions. However, it cannot provide any insight into the brain's functioning.

EEG source imaging (ESI) is a neuroimaging technique that combines EEG and MRI to locate the sources of scalp potentials or reconstruct the source signals from scalp EEG. To perform ESI, a head model is created using either the patient's own MRI or a template MRI. It describes the anatomy of the head and provides information about its electrical conductivity. Then, the electrodes in the EEG recording are placed on the scalp and other extracranial regions of the head model. A forward model is used to investigate how electrical information flows between sources and electrodes. Finally, an inverse solution is used to estimate the origin of electrical brain activity from scalp EEG or the source signals. ESI has been used in various studies to localize the IZ and SOZ by analyzing spikes and seizures. While ESI is considered a useful technique for

the presurgical evaluation, it presents some challenges in clinical application. The procedure is time-consuming and requires specialized expertise for its operation. Additionally, there is a need for more extensive validation studies to establish its performance.

The main goal of this dissertation is to investigate two ESI methodologies developed in-house for the purpose of localizing the EZ in a standardized and objective manner. Initially, the investigation focused on the validation of PreOp, designed to automatically identify the epileptogenic focus through the localization of automatically detected interictal spikes. Subsequently, the dissertation focuses on the development and validation of ictal ESI intended to automatically determine the SOZ based on the analysis of marked seizure activity. Multiple studies were conducted with both pipelines.

PreOp, our in-house interictal ESI pipeline analysis, comprises two stages - spike detection and ESI. In brief, the EEG analysis begins with automated spike detection, followed by clustering of detected events based on their morphology. To conduct ESI analysis, we first create a head model that is specific to the patient's MRI. This is done by segmenting the MRI into six tissues: grey matter, white matter, cerebrospinal fluid (CSF), skull, scalp, and air. The dipoles, which are the solutions of ESI, are distributed over the grey matter. Then, we use the finite difference method (FDM) as the forward model to calculate the leadfields matrix. This matrix explains the electrical relations between dipoles and EEG electrodes using the reciprocity theorem. Finally, we apply sLORETA as the inverse solution and conduct ESI analysis on the detected spikes at three-time points: the onset time, the half-rising time, and the peak of the averaged spike waveforms. PreOp underwent a validation study in 41 consecutive patients of the Danish Epilepsy Centre. The study was performed blindly using only EEG and pre-operative MRI, without any information on surgery or outcome. The analysis was evaluated in two ways: fully automated and semi-automated. Both evaluations were carried out after automated ESI. In the fully automated assessment, the dominant cluster was quantitatively determined first, and the analysis was always selected at the half-rising phase of the spike. In the semi-automated evaluation, the physician chose the dominant cluster and the time point based on the clinical context. For the assessment, the resected area and the outcome one year after surgery are reference standards, considering the concordance at the sub-lobar level. The accuracy increased from 61% in the fully automated to 78% in the semi-automated assessment. Automated ESI demonstrated accuracy similar to the previously reported neuroimaging methods. Moreover, PreOp showed its potential to increase the utilization of source imaging in the presurgical evaluation of patients with epilepsy.

PreOp was involved in multiple studies. One study investigated the impact of electrode setup on automated interictal ESI. PreOp was applied to data of 30 patients from HUG, Geneva, Switzerland. The presurgical 257-channel EEG was down-sampled to 25, 40, and 204 channels for separate analyses. The results showed that the low-density EEG was found to be sufficient for

interictal ESI if high numbers of spikes were available. In another study, PreOp was used to evaluate the accuracy of automated interictal low-density ESI to define the insular IZ by comparing the simultaneous interictal ESI localization with the sEEG interictal activity. Here, sEEG was used as the reference standard. The outcomes of this study demonstrated the potential of PreOp as a useful tool in the presurgical work-up. Additionally, three prospective projects were conducted at various epilepsy centers, including one involving MRI-negative patients, one involving patients of HUG in Geneva, Switzerland, and one involving 17 European centers. Patients of these prospective studies had resection later. The first prospective project evaluated the clinical value of a fully automated ESI analysis using PreOp in patients with MRI-negative epilepsy. The study assessed sublobar concordance with sEEG results, surgical resection, and outcome. To achieve this, a multidisciplinary team developed EZ hypotheses at the sub-lobar level and made decisions on further management at two-time points: first blinded to ESI, then after clinical interpretation of ESI. The data from 29 patients were analyzed, and the study found that PreOp led to a change in the management plan in 12 out of 29 patients (41%). This single-center prospective study demonstrated that PreOp had the added value in helping to plan the implantation of depth electrodes for sEEG. In the second prospective project, a single-center prospective study was conducted to evaluate the performance of PreOp. The study took place at HUG in Geneva, Switzerland, and included data from 122 patients between 2017 and 2022. Out of these patients, 40 were found to match the inclusion criteria. The study suggests using PreOp in the evaluation of all patients who are referred for epilepsy surgery. In the last prospective project, PreOp was used in the PROMAESIS study. This multi-center study aims to evaluate the accuracy and clinical relevance of automated ESI in presurgical epilepsy assessment. The performance assessment of this project is pending and will be evaluated once the results are available. Finally, a study was conducted to assess the time required to integrate interictal ESI data into the clinical workflow of a specialized epilepsy center. Three pipelines, including PreOp, were employed for the analysis. The study findings demonstrated that PreOp requires significantly less working time as compared to the other two ESI algorithms.

The second part of research focused on developing the ictal pipeline analyzing seizures to localize SOZ. This pipeline was necessary to overcome some of the challenges posed by scalp EEG data during a seizure. These challenges include artifacts, low signal-to-noise ratio, and the propagation of ictal activity throughout the brain. Functional connectivity was shown as a promising technique in the literature for localizing SOZ. It involves identifying the source with the highest outdegree among sources with high ESI power in the time domain. We used this pipeline as a starting point for further development. We performed the ESI power in the frequency domain to reduce the impact of noise or artifacts on the analysis. In the first ictal study, we analyzed data from 24 cases of extra-temporal lobe epilepsy (ETLE), which are more challenging cases for localization in comparison to temporal lobe epilepsy (TLE). Although

power+connectivity performed better than ESI power at both the seizure and patient levels, the challenges associated with connectivity made it difficult to use, especially for clinical practices. The choice of seizure onset is critical for accurate connectivity. Moreover, ESI power generally showed reasonable results at the seizure level. To improve ictal ESI method that focuses on power, we have developed a semi-automated ictal ESI power pipeline. The marking of seizure onset and identifying the frequency band of interest was performed by experts as part of the clinical work-up, while the ESI analysis was fully automated. This pipeline contains both EEG analysis and ESI analysis. In the EEG processing stage, we used time-frequency analysis of the ictal epoch at the sensor level to obtain the window of interest (WoI) via a region-growing procedure. For the ESI analysis, we generated a head model, distributed dipoles in the grey matter, used FDM as the forward model, and calculated the leadfields matrix. The grey matter was parcelled into 50 sublobes, with 25 in each hemisphere. Using a modified version of LORETA as the inverse solution, the ictal epoch was reconstructed in each sublobe. Time-frequency analysis was performed on the activity estimated in each sublobe, and the one with the highest power during the WoI was estimated as the SOZ. A retrospective validation study was conducted in 50 consecutive patients of the Danish epilepsy centre. The reference standard was concordance with the resected area and one-year postoperative outcome. The automated ictal ESI achieved a sensitivity and specificity of 64.5% and 89.5%, respectively. The accuracy of 74% achieved by the ictal ESI is considered high for localizing the SOZ.

The automated ictal power pipeline had some limitations, as it only worked if the ictal onset occurred within 0 seconds and +3s after the marked onset. Additionally, it only functioned if the band of interest matched the marked band. These limitations were overcome by updating the pipeline, which led to the development of sliding-window ictal ESI. In simple terms, the analysis starts from -2 seconds to +5 seconds after the onset and applies ESI in every 2-second sliding window with a 1-second overlap. In each 2-second time bin, spectrogram analysis is performed, followed by region growing to select the two time-frequency (TF) islands with the highest energy. The power distribution of the TF islands over the channels is then calculated to construct the topography. Finally, an ESI analysis of these topographies is performed. This methodology was evaluated using the identical data as previous study. It's worth noting that the pipeline's performance has been maintained at the same level as the previous ictal pipeline, but it has successfully addressed some of the limitations of its predecessor.

The performance of PreOp to localize the EZ was assessed across our multiple studies on around 225 patients and compared with the results of Sliding Ictal ESI. Additionally, the performance of our in-house ESI pipeline was compared to other presurgical methods in the literature, including interictal-ESI/MSI, ictal-ESI/MSI, MRI, PET, and ictal-SPECT. PreOp is more sensitive than Sliding Ictal ESI but less specific, and they both have similar accuracy. Both PreOp

and Sliding Ictal ESI have accuracy similar to interictal-ESI/MSI and MRI, and they outperform the other methods.

In conclusion of this dissertation, we have validated two in-house ESI pipelines to localize the epileptogenic zone from interictal and ictal EEG recordings. These pipelines were tested in clinical studies in patients with focal drug-resistant epilepsy. Our methods demonstrated the importance of automated interictal and ictal ESI, which can complement each other. Also, these methods are easily applicable in clinical settings and potentially enhance the EZ localization accuracy during the presurgical evaluation in patients with refractory epilepsy.

Nederlandstalige samenvatting

In de naam van de Heer van zowel de wijsheid als de geest, Op niets verhevener kan de gedachte worden toegepast

Ferdowsi

Het hoofddoel van dit proefschriftonderzoek is om de epileptogene zone (EZ) nauwkeurig te lokaliseren bij patiënten met medicijnresistente epilepsie. Dit zal worden bereikt door geautomatiseerde pijplijnen die gebruik maken van interictale en ictale activiteit in elektro-encefalografie (EEG).

Epilepsie is een neurologische aandoening die ongeveer 1% van de wereldbevolking treft. Het wordt gekenmerkt door terugkerende, niet-uitgelokte aanvallen die worden veroorzaakt door abnormale elektrische activiteit in de hersenen. Aanvallen kunnen worden ingedeeld in drie typen: focaal, gegeneraliseerd of onbekend. Bij een focale aanval vindt de abnormale elektrische activiteit plaats in één hersenregio, in tegenstelling tot een gegeneraliseerde aanval waarbij meerdere delen van de hersenen betrokken zijn. Focale aanvallen kunnen al dan niet gepaard gaan met verminderd bewustzijn, en de symptomen kunnen vaak verward worden met andere aandoeningen van de hersenen. Gegeneraliseerde aanvallen kunnen zich manifesteren in verschillende vormen zoals absences, tonische aanvallen, atonische aanvallen, enz. Hieronder zijn tonisch-clonische aanvallen, vroeger bekend als grand mal aanvallen, behoorlijk dramatisch. Ze kunnen plotseling bewustzijnsverlies, stijfheid van het lichaam, trillingen en andere symptomen veroorzaken.

Er zijn verschillende medicijnen beschikbaar om de elektrische activiteit in de hersenen te stabiliseren. Deze kunnen helpen bij het voorkomen van aanvallen, of het verminderen van de frequentie en ernst ervan. Ondanks ontwikkelingen in de farmacologie en de beschikbaarheid van nieuwe medicijnen, blijft 7-20% van de kinderen en 30-40% van de volwassen epilepsiepatiënten resistent voor medicatie. In dergelijke gevallen van medicijnresistente epilepsie blijft chirurgie de meest effectieve behandeloptie. Hierbij wordt de epileptogene zone weggenomen om de patiënt aanvalsvrij te maken. EZ is geen anatomisch-

fysiologisch gebied, maar een klinisch conceptuele term die verwijst naar een kritische regio in de hersenen die verantwoordelijk is voor epileptische aanvallen en waarvan de verwijdering leidt tot aanvalsvrijheid. Nauwkeurige lokalisatie van de EZ is essentieel voor de epilepsieoperatie, aangezien het cruciaal is om aanvalsvrijheid te bereiken en de impact van de operatie op essentiële hersenfuncties te minimaliseren.

Het proces van EZ-lokalisatie, wat deel uitmaakt van de prechirurgische evaluatie, omvat verschillende stappen. Allereerst wordt de medische voorgeschiedenis van de patiënt beoordeeld. Vervolgens worden verschillende beeldvormingstechnieken gebruikt, met onder andere niet-invasieve methoden zoals video-EEG monitoring, magnetische resonantiebeeldvorming (MRI), magneto-encefalografie (MEG), positron emissie tomografie (PET), "single photon emissie computer tomografie" (SPECT) en functionele MRI (fMRI). Indien nodig kan invasieve intracraniale elektro-encefalografie (iEEG), waaronder elektrocorticografie (ECoG) en stereo-elektro-encefalografie (sEEG), worden gebruikt. Elke techniek biedt specifieke informatie over de EZ en kan complementair ingezet worden met de andere technieken. Langdurige video-EEG metingen kunnen gebruikt worden om abnormale activiteiten te detecteren die verbonden zijn met de EZ, zoals scherpe piekgolven (interictale epileptiforme ontladingen) of epileptische aanvallen (ictale activiteit). Het analyseren van piekgolven helpt bij het identificeren van de irritatieve zone (IZ), terwijl men door analyse van de aanvallen zelf de epileptische aanvalszone kan lokaliseren. Afgezien van EEG-gegevens zijn hersenlaesies detecteerbaar in de MRI, hypometabolisme in de PET, en hyperperfusie tijdens aanvallen in de ictale SPECT. Al deze informatie wordt samen overwogen, en een multidisciplinair team van epileptologen, neurologen, neurochirurgen en andere specialisten zal deze evalueren om de EZ te identificeren en de behandeling te plannen.

Onder de genoemde technieken voor beeldvorming van de hersenen is scalp-EEG een nuttige, veilige en niet-invasieve techniek die wordt gebruikt om kandidaten voor epilepsiechirurgie te evalueren. EEG is in staat om snelle veranderingen in de elektrische activiteit van de hersenen met hoge temporele resolutie te detecteren, en biedt waardevolle inzichten in het begin, de verspreiding, de lokalisatie en de lateraliteit van aanvallen. Deze methode heeft echter enkele beperkingen, zoals een relatief lage spatiale resolutie. De metingen gebeuren op de hoofdhuid in plaats van rechtstreeks aan de bronnen (in de hersenen), en de geregistreerde signalen kunnen vervormd zijn tijdens hun verspreiding door de schedel- en hoofdhuidweefsels. Bovendien legt het voornamelijk gegevens vast van corticale regio's, terwijl activiteit uit diepere hersenstructuren maar moeilijk opgemeten kan worden. Structurele MRI heeft aan de andere kant, ook als een veilige en niet-invasieve modaliteit, een hoge spatiale resolutie. Deze techniek kan informatie verschaffen over de structuur van de hersenen en afwijkingen zoals hersenlaesies detecteren. Het biedt echter geen inzicht in de werking van de hersenen.

EEG-bronlokalisatie (ESI) is een neurologische beeldvormingstechniek die EEG

en MRI combineert om de bronnen te lokaliseren van de signalen die we opmeten op de hoofdhuid, en de activiteitsignalen in deze bronnen te reconstrueren. Om ESI uit te voeren wordt een hoofdmodel gemaakt met behulp van patiënt-specifieke MRI beelden of een sjabloon-MRI. Het hoofdmodel beschrijft de anatomie van het hoofd en geeft informatie over de elektrische geleidbaarheid ervan. Vervolgens worden de EEG elektroden op de hoofdhuid en andere extracraniële regio's mee opgenomen in het hoofdmodel. Een voorwaarts model wordt gebruikt om te onderzoeken hoe elektrische informatie zich van de dipolen (bronnen in de hersenen) naar de elektroden verspreidt. Vervolgens wordt een invers model gebruikt om op basis van de gemeten EEG-signalen de activiteit in de bronnen te schatten. ESI wordt vaak gebruikt in onderzoek om de irritatieve zone en epileptische aanvalszone te lokaliseren door analyse van piekgolven en epileptische aanvallen. Hoewel ESI wordt beschouwd als een waardevolle techniek voor de prechirurgische evaluatie, zijn er enkele drempels die overwonnen moeten worden voor toepassing in de kliniek. De procedure is tijdrovend en vereist gespecialiseerde expertise. Bovendien is er behoefte aan uitgebreidere validatiestudies om de accuraatheid ervan te bepalen.

Het hoofddoel van dit proefschrift is om twee eigen ESI-methodologieën te onderzoeken die zijn ontwikkeld voor het lokaliseren van de epileptogene zone op een gestandaardiseerde en objectieve manier. In eerste instantie richt het onderzoek zich op de validatie van PreOp, een methode ontworpen om automatisch de epileptogene focus te identificeren op basis van gedetecteerde interictale piekgolven. Vervolgens richt het proefschrift zich op de ontwikkeling en validatie van Ictal ESI, bedoeld om automatisch de epileptische aanvalszone te bepalen op basis van gemarkeerde activiteit tijdens aanvallen. Beide pijplijnen werden toegepast in meerdere studies.

PreOp, onze zelf-ontwikkelde interictale ESI-pipeline, bestaat uit twee delen: piekgolf-detectie en ESI. Kort samengevat begint de EEG-analyse met geautomatiseerde detectie van piekgolven, gevolgd door clusteren van de gedetecteerde pieken op basis van hun morfologie. Voor de ESI-analyse creëren we een patiënt-specifiek hoofdmodel op basis van een MRI. Dit wordt gedaan door de MRI beelden te segmenteren in zes verschillende weefsels: grijze stof, witte stof, hersenvocht (CSF), schedel, hoofdhuid en lucht. De dipolen, de bronnen in de ESI-analyse, worden verdeeld over de grijze stof. Vervolgens gebruiken we de eindige-differentiemethode (EDM) om het voorwaartse model en de zogenaamde leadfield-matrix te berekenen. Deze matrix verklaart de relaties tussen activiteit in de dipolen en EEG-elektroden met behulp van de reciprociteitstheorema. Ten slotte passen we sLORETA toe als inverse oplossing en voeren we ESI-analyse uit op de gedetecteerde pieken op drie tijdstippen: het begin, de half-oplooptijd en op de piek van de gemiddelde piekgolfvormen. PreOp werd onderworpen aan een validatiestudie met 41 opeenvolgende patiënten van het Deense Epilepsiecentrum. De studie werd geblindeerd uitgevoerd met alleen EEG en pre-operatieve MRI, zonder enige informatie over de operatie of de uitkomst ervan. De analyse werd op twee

manieren geëvalueerd: volledig geautomatiseerd en half-geautomatiseerd. Bij de volledig geautomatiseerde beoordeling werd eerst kwantitatief de dominante cluster bepaald, en de rest van de analyse werd steeds uitgevoerd op de half-oplooptijd van de piek. Bij de half-geautomatiseerde evaluatie werden de dominante cluster en het geanalyseerde tijdstip van de piek gekozen door een arts op basis van de klinische context. De hieropvolgende ESI verliep steeds automatisch. Om de resultaten te beoordelen werd de aangeduide EZ vergeleken met de operatief verwijderde regio en de klinische uitkomst één jaar na de operatie. Hierbij werd rekening gehouden met overeenkomst op sub-lobair niveau. Geautomatiseerde ESI vertoonde een nauwkeurigheid die vergelijkbaar is met eerder gerapporteerde beeldvormingstechnieken. De nauwkeurigheid steeg van 61% bij de volledig geautomatiseerde naar 78% bij de half-geautomatiseerde beoordeling. Bovendien toonde PreOp potentieel om het gebruik van bronafbeelding te vergemakkelijken in de prechirurgische evaluatie van patiënten met epilepsie.

PreOp werd in nog verschillende studies gebruikt. In een eerste studie werd de impact onderzocht van de elektrodeopstelling op geautomatiseerde interictale ESI. PreOp werd hiervoor toegepast op metingen van 30 patiënten van HUG, Genève, Zwitserland. Een preoperatieve 257-kanaals EEG werd gereduceerd tot 25, 40 en 204 kanalen voor afzonderlijke analyses. De resultaten toonden aan dat lage-densiteit EEG voldoende is voor interictale ESI indien er voldoende pieken beschikbaar zijn. In een andere studie werd PreOp gebruikt om te evalueren hoe nauwkeurig geautomatiseerde interictale lage-densiteit ESI de insulaire IZ kan definiëren. Hiervoor werd interictale ESI-lokalisatie vergeleken met de interictale activiteit opgemeten met (invasieve) sEEG als referentie. De resultaten van deze studie toonden het potentieel van PreOp als een waardevol instrument in het preoperatief onderzoek. Bovendien werden drie prospectieve studies uitgevoerd met verschillende epilepsiecentra: een met MRI-negatieve patiënten, een tweede met patiënten van HUG in Genève, Zwitserland, en een laatste met 17 Europese centra. Patiënten in deze prospectieve studies werden later -na de analyse- geopereerd. In de eerste prospectieve studie werd de klinische waarde geëvalueerd van een volledig geautomatiseerde ESI-analyse met behulp van PreOp bij patiënten met MRI-negatieve epilepsie. De studie beoordeelde de sublobaire overeenstemming met sEEG-resultaten, chirurgische resectie en klinische uitkomst. Hiertoe ontwikkelde een multidisciplinair team hypotheses over de EZ op sub-lobair niveau en nam het beslissingen over verdere behandeling op twee momenten: eerst geblindeerd voor ESI, daarna na klinische interpretatie van ESI. De gegevens van 29 patiënten werden geanalyseerd, en de studie vond dat PreOp leidde tot een wijziging in het behandelplan bij 12 van de 29 patiënten (41%). Deze prospectieve studie toonde aan dat PreOp toegevoegde waarde had bij het plannen van de implantatie van diepte-elektroden voor sEEG. In een tweede prospectieve studie werd de accuraatheid van PreOp geëvalueerd. Bij deze studie werden gegevens gebruikt van 122 patiënten tussen 2017 en 2022 uit het HUG in Genève, Zwitserland. Van deze patiënten voldeden er 40 aan de inclusiecriteria. Deze studie wees op de meerwaarde van PreOp bij de

evaluatie van alle patiënten die worden doorverwezen voor epilepsiechirurgie. In het laatste prospectieve project werd PreOp gebruikt in de PROMAESIS-studie. Deze multicentrische studie heeft tot doel de nauwkeurigheid en klinische relevantie van geautomatiseerde ESI te evalueren in de preoperatieve beoordeling van epilepsie. De beoordeling van dit project is nog lopende en wordt afgerond zodra alle resultaten beschikbaar zijn. Tot slot werd een studie uitgevoerd om te beoordelen hoeveel tijd nodig is om interictale ESI-gegevens te integreren in de klinische werkstroom van een gespecialiseerd epilepsiecentrum. Drie methodes, waaronder PreOp, werden gebruikt en vergeleken tijdens deze analyse. De onderzoeksresultaten toonden aan dat PreOp aanzienlijk minder werktijd vereist in vergelijking met de twee andere ESI-algoritmen.

Het tweede deel van het onderzoek was gericht op de ontwikkeling van de "Ictal" pipeline voor de analyse van aanvallen om de epileptische aanvalszone te bepalen. Deze pijplijn was nodig om enkele uitdagingen rond scalp-EEG metingen van een epileptische aanval te overwinnen. Deze uitdagingen zijn onder andere artefacten, een lage signaal-ruisverhouding en de verspreiding van ictale activiteit door de hersenen. Functionele connectiviteit werd in de literatuur getoond als een veelbelovende techniek voor het lokaliseren van de aanvalszone. Het omvat het identificeren van de bron met het meest uitgaande connecties onder de bronnen met hoge ESI-energie in het tijdsdomein. We gebruikten deze pijplijn als startpunt voor verdere ontwikkeling. We voerden de ESI-energie analyse uit in het frequentiedomein om de impact van ruis of artefacten op de analyse te verminderen. In de eerste Ictal-studie analyseerden we gegevens van 24 patiënten met extratemporale kwabepilepsie (ETLE). Deze gevallen zijn uitdagender voor lokalisatie in vergelijking met temporale kwabepilepsie (TLE). Hoewel ESI met informatie over energie en connectiviteit beter presteerde dan ESI op basis van enkel energie, op zowel het aanvals- als het patiëntniveau, maakten de uitdagingen die gepaard gingen met connectiviteit het moeilijk om te gebruiken in klinische praktijk. Voor nauwkeurige resultaten van de connectiviteit is het cruciaal om het begin van de epileptische aanval exact aan te duiden. Bovendien toonde ESI op basis van energie over het algemeen redelijke resultaten op aanvalsniveau. Om de ictale ESI-methode die zich richt op energie verder te verbeteren, hebben we een half-geautomatiseerde Ictal ESI-energie pijplijn ontwikkeld. Hierbij werd het aanvalsbegin en de belangrijke frequentieband gemarkeerd door experts als onderdeel van het klinische onderzoek, terwijl de ESI-analyse volledig geautomatiseerd was. Deze pijplijn bevat zowel EEG-analyse als ESI-analyse. In de EEG-verwerkingsfase gebruikten we tijd-frequentie analyse van het ictale tijdsinterval op het sensorniveau om het tijdsinterval van belang te bepalen via een groeiende-regio-procedure. Voor de ESI-analyse genereerden we een hoofdmodel, verdeelden dipolen in grijze stof, gebruikten EDM als het voorwaartse model en berekenden we de leadfields-matrix. De grijze stof werd verdeeld in 50 subkwabben (25 in elke hemisfeer). Met behulp van een aangepaste versie van LORETA als de inverse oplossing werd het ictale tijdsinterval in elke subkwab gereconstrueerd. Tijd-frequentie-analyse

werd uitgevoerd op de activiteit in elke subkwab, en de subkwab met de hoogste energie tijdens het tijdsinterval werd aangeduid als de aanvalszone. Een retrospectieve validatiestudie werd uitgevoerd met 50 opeenvolgende patiënten van het Deense epilepsiecentrum. Als referentie voor de resultaten werd gekeken naar overeenstemming met het gereseceerde gebied en de klinische uitkomst een jaar na de operatie. De geautomatiseerde Ictal-ESI behaalde een sensitiviteit en specificiteit van respectievelijk 64,5% en 89,5%. De nauwkeurigheid van 74% behaald door de Ictal ESI wordt als hoog beschouwd voor het lokaliseren van de aanvalszone.

De geautomatiseerde Ictale energie-pijplijn had enkele beperkingen, omdat deze alleen werkte als het effectieve begin van de aanval plaatsvond binnen een tijdsvenster van 0 tot 3 seconden na het gemarkeerde begin. Bovendien werkte het ook alleen als de relevantee frequentieband overeenkwam met de gemarkeerde band. Deze beperkingen werden overwonnen door de pijplijn aan te passen, wat leidde tot de ontwikkeling van de schuifvenster-ictale ESI. In eenvoudige bewoordingen begint de analyse van -2 seconden tot +5 seconden rond het aangeduide begin van de aanval en wordt ESI toegepast in een tijdsvenster van 2 seconden dat doorschuift in stappen met een overlap van 1 seconde. In elk 2-seconden tijdvak wordt een spectrogramanalyse uitgevoerd, gevolgd door regioo-groeien om de twee tijdfrequentie (TF) clusters met de hoogste energie te selecteren. De energiedistributie van de TF-eilanden over de kanalen wordt vervolgens berekend om de topografie op te bouwen. Ten slotte wordt een ESI-analyse van deze topografieën uitgevoerd. Deze methodologie werd geëvalueerd met dezelfde gegevens als de vorige studie. Het is belangrijk om te vermelden dat de prestaties van de pijplijn op hetzelfde niveau zijn gebleven als de vorige Ictale pijplijn, maar dat het met succes enkele beperkingen van zijn voorganger heeft aangepakt.

De accuraatheid van PreOp om de EZ te lokaliseren werd beoordeeld in meerdere studies met ongeveer 225 patiënten, en vergeleken met de resultaten van de schuifvenster-Ictale ESI. Bovendien werd de prestatie van onze zelf-ontwikkelde ESI-pipeline vergeleken met andere preoperatieve methoden in de literatuur, waaronder interictale ESI/MSI, ictale ESI/MSI, MRI, PET en ictale-SPECT. PreOp is sensitiever dan Schuifvenster Ictale ESI maar minder specifiek, en ze hebben allebei een vergelijkbare nauwkeurigheid. Zowel PreOp als Schuifvenster Ictale ESI hebben een nauwkeurigheid die vergelijkbaar is met interictale ESI/MSI en MRI, en ze presteren beter dan de andere methoden.

In deze dissertatie hebben we twee zelf-ontwikkelde methodes voor ESI gevalideerd om de epileptogene zone te lokaliseren uit interictale en ictale EEG-metingen. Deze methodes zijn getest in klinische studies bij patiënten met focale medicijnresistente epilepsie. Onze methoden hebben het belang aangetoond van geautomatiseerde interictale en ictale ESI, die mekaar kunnen aanvullen. Ook zijn deze methoden gemakkelijk toepasbaar in klinische omgevingen en kunnen ze de nauwkeurigheid van de lokalisatie van de EZ verbeteren tijdens de preoperatieve evaluatie van patiënten met medicijnresistente epilepsie.

List of Figures

List of Tables

Chapter 1

Introduction

Every breath that goes in is an extension of life; and when it comes out it is a relief of life. Therefore, in every breath there are two benefits, and for each benefit thanks are necessary.

Saadi Shirazi

1.1 Context

Epilepsy is a neurological disorder that affects around 1% of the global population. It is characterized by recurring seizures that are caused by unprovoked abnormal electrical activity in the brain. Seizures are classified into three types: focal, generalized, or unknown. In a focal seizure, abnormal electrical activity occurs in a specific part of the brain, while in a generalized seizure, multiple areas of the brain are involved. Focal seizures can occur with or without impaired awareness, and symptoms can be easily mistaken for other brain conditions. Generalized seizures can manifest in various forms.

There are a variety of medications available to help prevent or reduce seizures, however, around 30-40% - remain resistant to drug treatment despite advances in pharmacology and the availability of new medications. In these cases, epilepsy surgery is often the best course of action. For patients with drug-resistant epilepsy, removing the epileptogenic zone (or EZ) result in seizure freedom. The EZ is a specific cortical region in the brain that initiates seizures. It is a crucial area that must be entirely removed or disconnected to attain complete freedom from seizures. Accurate estimating of the location and boundaries of the EZ is the primary goal of epilepsy pre-surgical evaluation. This process involves a range of tests, including a review of the patient's medical history and various multi-modal neuroimaging techniques, such as electroencephalogram (EEG), Magnetic Resonance Imaging (MRI), magnetoencephalography (MEG), positron emission tomography (PET) scans, Ictal single photon emission computed tomography (SPECT), and functional MRI. Invasive techniques, such as electrocorticography (ECoG) or stereoelectroen-

cephalography (sEEG), may also be used if necessary. By analyzing the data gathered from these tests, a team of specialists can identify the EZ and plan the best course of treatment for the patient.

Scalp EEG and MRI are valuable tools in assessing candidates for epilepsy surgery. EEG offers insights into the seizure onset, propagation, and lateralization, but has limitations in detecting activity from deep brain structures. MRI provides detailed information regarding the brain's structure and detects abnormalities like brain lesions.

EEG source imaging (ESI) is a powerful neuroimaging technique that combines EEG and MRI data to localize the sources of scalp potentials or reconstruct source signals from scalp EEG. To perform ESI, a head model is created using the patient's MRI or a template MRI. This model describes the head's anatomy and electrical conductivity. Electrodes are then placed on the surface of the head model, and a forward model is used to investigate the flow of electrical information between sources and electrodes. Finally, an inverse solution is used to estimate the origins of electrical brain activity from scalp EEG or the source signals. ESI has been used successfully in various studies to localize the Irritative Zone (IZ) and Seizure Onset Zone (SOZ) by processing spikes and seizures. However, ESI has its limitations in clinical application, including being a time-consuming procedure that requires specialized expertise for its operation. Additionally, more extensive validation studies are needed to establish its effectiveness.

In this dissertation, we evaluated two in-house automated ESI pipelines to localize EZ objectively, consistently, and standardizedly. We began by validating the automated interictal ESI pipeline. It was designed to automatically identify the epileptogenic focus through the processing of spikes that are automatically detected. Following that, we focused on developing and validating the automated ictal ESI pipeline, which aims to determine the seizure onset zone based on manually marked seizure activity analysis.

1.2 Outline

This dissertation is divided into 7 chapters that can be read independently. The chapters are arranged in a bottom-up hierarchy. The structure of this dissertation is detailed as follows:

Chapter 2 of this PhD dissertation establishes a framework that sheds light on the concepts related to this research. It first delves into the fundamental aspects of epilepsy and seizures, including definitions, numbers, and classification. The chapter also explores traditional diagnostic methods such as using EEG, as well as the treatment options. The concept of drug-resistant epilepsy is introduced, leading to a detailed discussion of presurgical evaluation for surgical resection. Finally, an overview is given of the conventional neuroimaging modalities utilized during the presurgical evaluation.

In **Chapter 3** of our study EEG and ESI are introduced. To thoroughly examine these subjects, we introduce the origins of EEG signals in the brain, as well

as the methods used to record EEG data using scalp electrodes. Additionally, we explore the various rhythms and artifacts present in EEG signals. Moving on to ESI, we start by introducing the head model and explaining how it is constructed. We investigate the forward model, providing additional physical and mathematical background information to introduce the leadfields matrix. Finally, we discuss the concept of inverse solutions, providing an overview of conventional inverse techniques found in literature.

Chapter 4 focuses on the automated interictal ESI pipeline (PreOp) and related studies. The chapter commences by presenting a detailed analysis of the clinical blinded validation study of PreOp. In the second study, we analyze the impact of the number of scalp electrodes on automated interictal ESI. In the third study, we evaluate the application of PreOp to a cohort with a complex epilepsy type. Additionally, we present the PreOp application to epilepsy patients with MRI-negative through a prospective study in the fourth study. Subsequently, we examine the assessment of PreOp through the second prospective study. In the following study, the integration of interictal ESI data into the clinical workflow of a specialized epilepsy center is evaluated based on the time required for the work. Finally, we conduct a comprehensive evaluation of PreOp across multiple studies at the end of this chapter.

Chapter 5 explores the automated ictal ESI pipeline and its related studies, which aim to identify the SOZ. The first study presents a modified version of an existing algorithm for ictal ESI pipeline. The second study focuses on the clinical validation of the automated pipeline by optimizing the first algorithm. Additionally, we have addressed some of the limitations of the pipeline and improved it further. Our efforts resulted in the development of Sliding Ictal ESI, which is discussed in the last section of this chapter.

In **Chapter 6**, we conduct a comparison between automated interictal ESI and automated ictal ESI to determine their performance. To further enhance our understanding, we analyze literature articles that discuss EZ localization using both interictal-ESI/MSI and ictal-ESI/MSI techniques. We extract the performance metrics from these techniques and also gather the results from other modalities like MRI, PET, and ictal-SPECT when available. Lastly, we compare the results from our in-house ESI pipelines with the outcomes of these different modalities.

Chapter 7 summarizes and discusses our results, future research perspectives, and final conclusions.

Chapter 2

Drug-resistant epilepsy and the presurgical evaluation

> *It is more important to know what sort of person has a disease than to know what sort of disease a person has.*
>
> Hippocrates

2.1 Epilepsy: definition, numbers, and classification

2.1.1 Epilepsy definition

In 2005, the International League Against Epilepsy (ILAE) formulated the definitions for "seizure" and "epilepsy" through a Task Force [1]:

1. *An epileptic seizure is a transient occurrence of signs and/or symptoms due to abnormal excessive or synchronous neuronal activity in the brain.*
2. *Epilepsy is a disorder of the brain characterized by an enduring predisposition to generate epileptic seizures, and by the neurobiologic, cognitive, psychological, and social consequences of this condition. The definition of epilepsy requires the occurrence of at least one epileptic seizure.*

In December 2013, The ILAE Executive Committee updated the epilepsy definition to be more practical for clinical use [2]:

> *Epilepsy is a disease of the brain defined by any of the following conditions:*

1. *At least two unprovoked (or reflex) seizures occurring >24 h apart,*
2. *One unprovoked (or reflex) seizure and a probability of further seizures similar to the general recurrence risk (at least 60%) after two unprovoked seizures, occurring over the next 10 years.*
3. *Diagnosis of an epilepsy syndrome*

Epilepsy is considered to be resolved for individuals who had an age-dependent epilepsy syndrome but are now past the applicable age or those who have remained seizure-free for the last 10 years, with no seizure medicines for the last 5 years.

2.1.2 Epilepsy numbers

According to the World Health Organization (WHO) [3], epilepsy is the fourth most prevalent neurological disorder worldwide, affecting over 50 million patients. At any given time, approximately 4 to 10 out of every 1000 individuals in the general population have active epilepsy. Additionally, approximately 5 million new cases of epilepsy are diagnosed worldwide each year.

Almost 80% of people with epilepsy live in low- and middle-income countries, where the ratio is nearly 139 cases per 100000. In high-income countries, however, it drops to 49 cases per 100,000.

Meta-analytic studies have explored the global prevalence and incidence of epilepsy. Fiest et al. reviewed 222 studies covering 197 papers on prevalence and 48 on incidence [4]. They measured the prevalence of active epilepsy and lifetime epilepsy, which are 6.38 and 7.60 per 1,000 persons, respectively. In addition, the annual cumulative incidence of epilepsy is 67.77 per 100,000 persons, but the incidence rate is lower and around 61.44 per 100,000 person-years.

2.1.3 Epilepsy classification

In 2017, the ILAE introduced a revision of epilepsy classification containing three levels (Fig. 2.1) [5]. In the first level, it presents the epileptic seizure types. The seizure type classification is based on the new nomenclature explained in an article by Fisher and colleagues [6]. According to them, seizures are categorized into focal onset, generalized onset, and finally, unknown onset. The second level is about epilepsy type, which includes focal, generalized, combined generalized and focal epilepsy, and finally unknown epilepsy type. The third level determines the epilepsy syndrome, which is a group of characteristics that commonly appear together. These include specific types of seizures, EEG characteristics, and imaging features. Identifying the epilepsy syndrome provides more information on which underlying causes should be considered and which medication or treatment options may be more effective. Epilepsy syndrome helps to guide the management of the condition, but it is not directly correlated with a specific diagnosis of the underlying cause.

In addition, it is important to determine the etiology of epilepsy as early as possible. To date, six etiologic categories have been recognized, namely structural, genetic, infectious, metabolic, immune, and known. It is worth noting that a patient with epilepsy may fall under multiple etiologic categories.

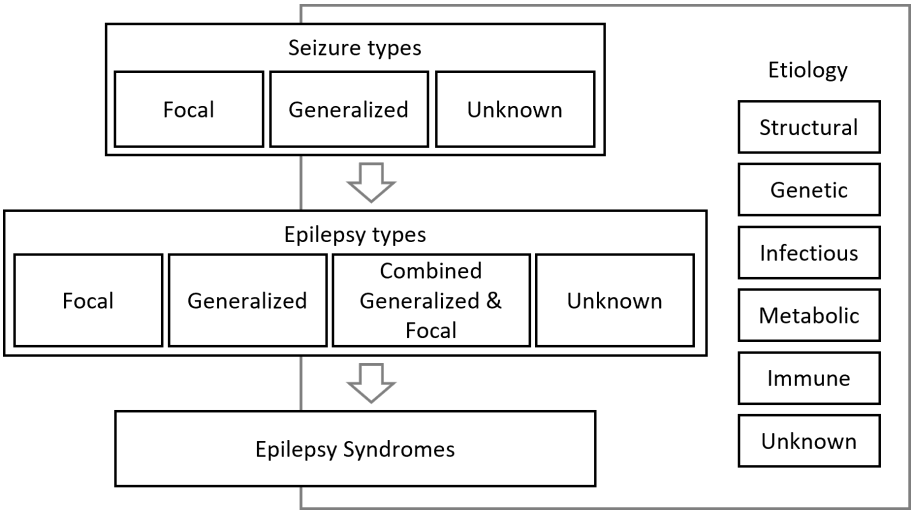

Figure 2.1: Epilepsy classification.

2.1.4 Seizure classification

An overview of seizure type classification can be found in figure 2.2. Seizure classification begins by verifying if the onset signatures of seizures are focal, generalized or unknown.

Focal seizures are a type of seizures that occur within specific networks localized to one hemisphere of the brain, even in subcortical regions. These seizures can either be localized separately or propagated in a large area in the brain. The semiology of seizures, which refers to the symptoms or signs, helps identify the regions involved in seizure onset and propagation. The focal seizure classification contains two levels. It is primarily based on the patient's level of awareness during the seizure. This means that the patient's ability to maintain full awareness of themselves and their surrounding environment, even if they are immobile, is considered. If there is any impairment in the patient's awareness during the seizure, it is classified as a focal impaired awareness seizure. Focal seizures are also categorized by their motor and non-motor features, which are the signs and symptoms that occur at the onset of a seizure. Motor onset seizures are characterized by changes in muscle contraction, which can affect individual muscles or groups of muscles and result in motor activity. In addition, there is a type of seizure called focal to bilateral tonic-clonic seizure, where focal seizures propagate widely in the brain to involve the networks of both hemispheres. This results in a tonic-clonic seizure, which comes with loss of consciousness.

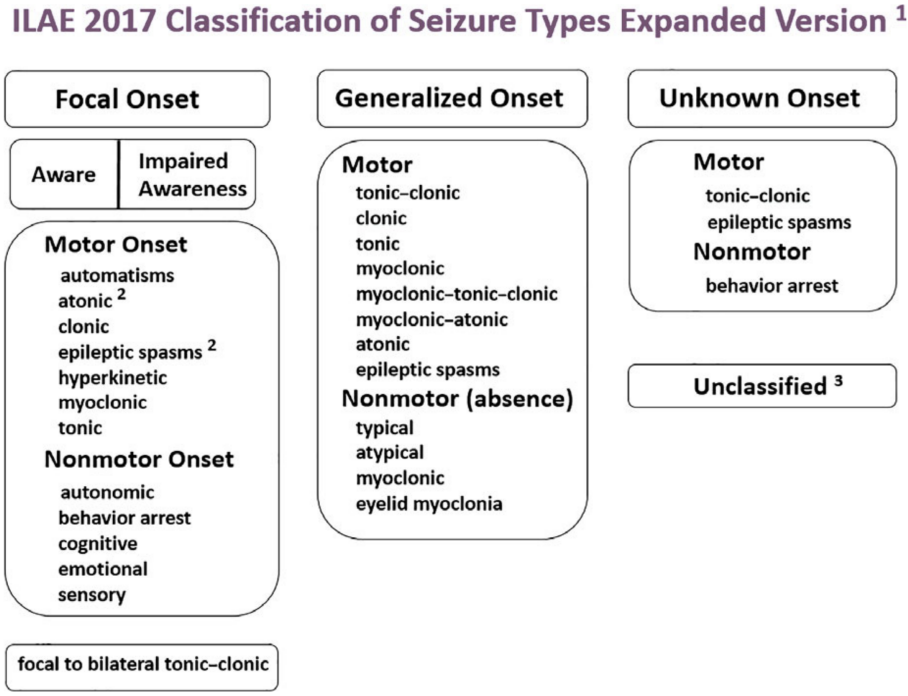

Figure 2.2: The expanded classification of seizure types presented by the ILAE. Figure is adapted from [6]

A generalized seizure is a neurological condition that typically begins in a localized area of the brain, but rapidly spreads to involve large networks spanning both hemispheres. These networks may include cortical or subcortical regions, but not necessarily the entire cortex. Generalized seizures are classified into two main types - motor onset and non-motor (absent) onset. The 1981 classification remains unchanged, but myoclonic-atonic seizures, myoclonic absence, and absence seizures with eyelid myoclonia have been added as subtypes.

Furthormore, there are some seizures that cannot be categorized as either focal or generalized in onset and are classified as having an unknown onset. These seizures can be further sub-classified as either motor or non-motor in type. Motor-type seizures include epileptic spasms and tonic-clonic seizures, while non-motor-type seizures include behavior arrest.

2.2 Epilepsy: diagnosis and treatment

2.2.1 Epilepsy diagnosis

The first step in diagnosing epilepsy is evaluating the patient's medical history. Then, a neurologist will conduct a neurological exam to examine the brain's function. Computerized Tomography (CT) or MRI scans can investigate

brain structure and they can confirm the diagnosis of epilepsy with possible structural causes (known as structural epilepsy). However, EEG plays a critical role in monitoring brain function, particularly in cases where MRI results are negative. Furthermore, the classification of epilepsy type is commonly determined using EEG recordings.

2.2.2 EEG in epilepsy

EEG is a useful diagnostic tool for epilepsy. It can confirm epileptic seizures and aid in presurgical workup, among other benefits. EEG guides the clinical management of epilepsy. Although there are various EEG abnormal patterns associated with epilepsy, our focus is on studying epileptic seizures and interictal epileptiform discharges (IEDs).

Epileptic seizures are caused by abnormal neural activity, which is detectable in EEG recordings. During a seizure, known as ictal activity, the EEG signals show significant deviations from the baseline. Seizure patterns are typically defined as follows [7]:

> ***Seizure pattern, EEG****: Phenomenon consisting of repetitive epileptiform EEG discharges at >2 cycle per second or Hz and/or characteristic pattern with quasi-rhythmic spatio-temporal evolution (i.e. gradual change in frequency, amplitude, morphology and location), lasting at least several seconds (usually >10 s). Two other short duration (<10 s) EEG seizure patterns are: electrodecrement and low voltage fast activity seen during clinically apparent epileptic seizures. Frequent interictal epileptiform discharges are usually not associated with clinical seizures and thus should be differentiated from EEG seizure patterns.*

Patients with epilepsy can experience IEDs, which are abnormal sharp waves between seizures. These discharges also known as interictal activity, are defined as [7]:

> ***Epileptiform pattern****: Describes transients distinguishable from background activity with a characteristic morphology typically, but neither exclusively nor invariably, found in interictal EEGs of people with epilepsy.*
>
> ***Sharp wave****: An epileptiform transient clearly distinguished from the background activity, although amplitude varies. A pointed peak at a conventional time scale and duration of 70–200 ms, usually with a steeper ascending phase when compared to the descending phase. Main component is generally negative relative to other areas, and may be followed by a slow wave of the same polarity.*
>
> ***Spike****: A transient, clearly distinguished from background activity, with pointed peak at a conventional time scale and duration from*

20 to less than 70 ms. Amplitude varies but typically below 50 microvolts. Main component is generally negative relative to other area.

***Spike-and-slow-wave complex**: An epileptiform pattern consisting of a spike and an associated following slow wave, clearly distinguished from background activity. May be single or multiple.*

***Multiple spike-and-slow-wave complex**: Use of term discouraged. An epileptiform graphoelement consisting of two or more spikes associated with one or more slow waves. Synonym: polyspike and-slow-wave complex.*

Figure 2.3 demonstrates an example of some of the discussed waveforms.

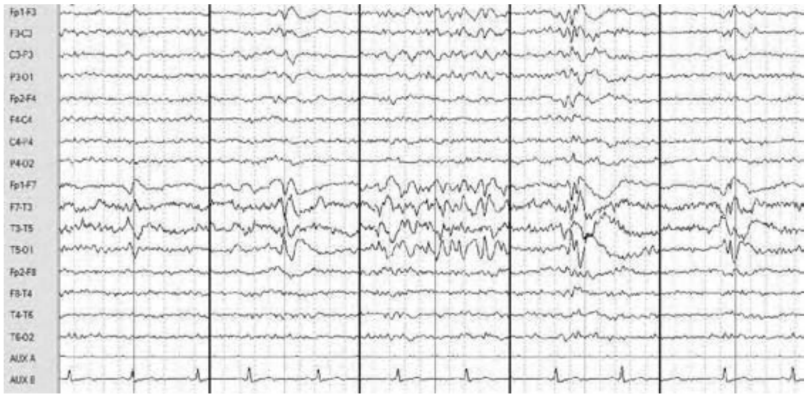

Figure 2.3: Examples of various morphologies include sharp waves demonstrated during seconds 1 and 2, spikes and sharp waves seen in second 3, and spike-and-wave discharges in the last second. Picture is adapted from [8]

Figure 2.4 illustrates a focal spike and seizure in focal epilepsy, where abnormal waves are recorded in electrodes near the seizure origin. In contrast, generalized epilepsy involves activity in both hemispheres.

2.2.3 Epilepsy treatment

The primary goal of treating epilepsy is to eliminate seizures as quickly as possible without causing any harmful side effects. When epilepsy is not well-controlled, it can lead to complications and health risks like [9]:

- physical injuries due to the seizure,
- deterioration in memory or analytical skills,
- depression or/and anxiety,
- developmental delays in children,

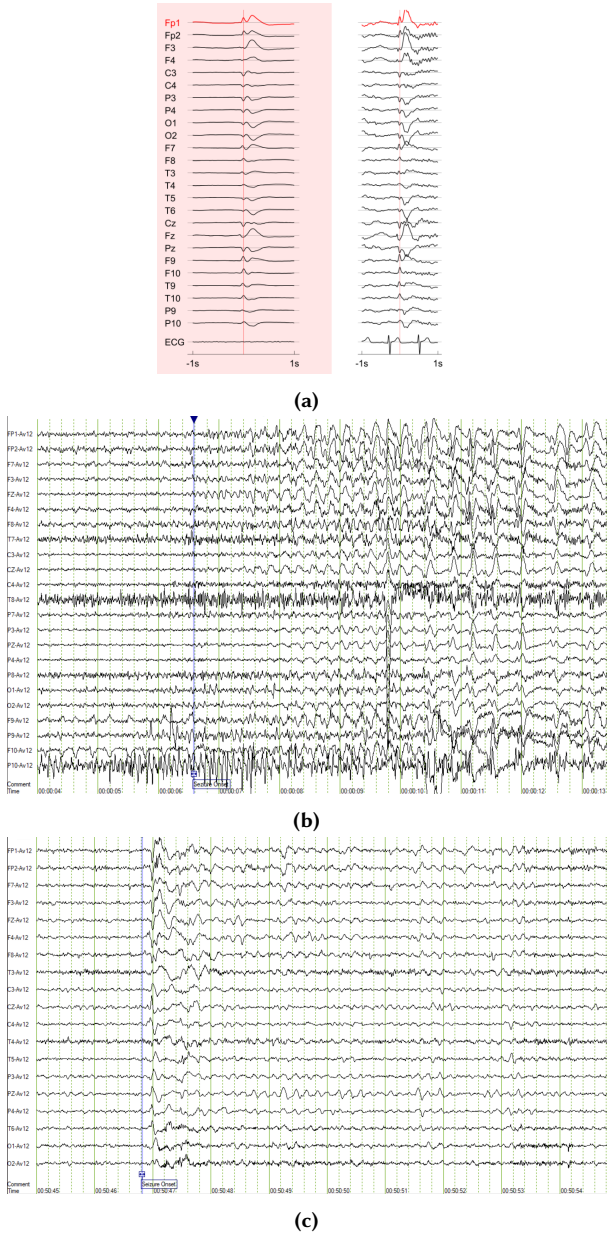

(a)

(b)

(c)

Figure 2.4: Illustrative examples of a focal spike and a focal seizure in an identical patient, and a generalized seizure. a) Focal spike: An average of 300 spikes (on the left) and the single spike with the highest similarity to the average spike (on the right). b) Focal seizure: This is marked by ictal activity with a frequency of 4Hz starting from Fz. c) Generalized seizure: It starts bilaterally from the frontal lobe with onset marked by a blue line.

- sudden death, a rare complication of epilepsy, etc.

The classification of epilepsy and seizure helps the treatment by choosing the appropriate anti-epileptic drugs (AED). They are the most commonly used treatment option for epilepsy, and their ultimate goal is to eliminate seizures. Around 66.5% epilepsy patients can manage their seizures with AEDs [10], but some remain resistant. Even with newer AED combinations, seizure freedom is unlikely.

2.2.4 Refractory epilepsy

The ILAE created a Task Force to establish a definition for drug-resistant epilepsy with the goal of enhancing patient care [11]. According to them drug-resistant epilepsy is defined as:

> *the failure of adequate trials of two tolerated and appropriately chosen and used antiepileptic drugs (AED) schedules (whether as monotherapies or in combination) to achieve sustained seizure freedom.*

In children, drug-resistant epilepsy affects 7-20% [12] of patients, while in adults it varies from 30-40% [13].

For patients with drug-resistant epilepsy, surgery offers the most effective treatment option [14, 15, 16]. Different types of surgery are performed depending on the type of epilepsy, including:

- focal resection; temporal or/and extratemporal lobe resection,
- lesionectomy,
- anatomic hemispherectomy,
- other epileptic surgery.

The possibility of epilepsy surgery is assessed during the presurgical evaluation.

2.3 Presurgical evaluation

2.3.1 History of epilepsy surgery

In ancient and medieval times, techniques like trepanation were employed to treat conditions such as epilepsy. Early neurosurgical interventions did not emerge until the early 19th century. A significant advancement occurred in 1886 when Victor Horsley performed the first documented successful brain tumor resection to treat epilepsy. In the early 20th century, advancements in neurosurgical techniques enabled more systematic approaches to surgical

epilepsy treatment. For example, Wilder Penfield and his team developed the Montreal Procedure that uses electrical stimulation to map brain function during surgery. This technique helped to preserve eloquent brain tissue and minimize functional loss. In the mid-20th century, neuroimaging advancements significantly improved brain structure visualization. During this time, temporal lobectomy, which involves resecting part of the temporal lobe, including the hippocampus and amygdala, became the standard procedure for treating temporal lobe epilepsy. In the late 20th century, advancements in CT and structural MRI significantly enhanced presurgical planning. Additionally, invasive EEG techniques improved the precision of locating brain targets before surgery. Stereotactic procedures, such as the Gamma Knife, further paved the way for less invasive surgical interventions.

2.3.2 Epileptogenic zone localization

The presurgical workup aims to identify and delineate the epileptogenic zone (EZ), which is defined as [17]:

> "*the area of cortex that is necessary and sufficient for initiating seizures and whose removal (or disconnection) is necessary for complete abolition of seizures*"

EZ is a conceptualized definition that cannot be directly measured. To solve this issue, all contributing regions are mapped to estimate the EZs [18]:

1. symptomatogenic zone: an area of cortex producing the ictal symptoms when triggered by an epileptiform discharge,
2. Irritative Zone (IZ): a cortical area in tissue generating interictal spikes,
3. Seizure Onset Zone (SOZ): an cortical area making clinical seizures,
4. epileptogenic lesion: a radiographic lesion causing the epileptic seizures,
5. functional deficit zone: a cortical area which is functionally abnormal during interictal period.

Determining the precise location of the epileptic focus is still a challenging undertaking. Therefore, relying on a single modality is not sufficient to accurately identify the resection area and to ensure that the patient becomes seizure-free.

2.3.3 Multi-modal neuroimaging

When pinpointing the EZ for presurgical evaluation, it is essential to use non-invasive techniques such as long-term video-EEG monitoring, MRI scanning, MEG, and nuclear imaging methods like PET and SPECT. A team of experts including neurologists, neurosurgeons, neuropsychologists, neuroradiologists, and other specialists are in charge of conducting these examinations.

The team identifies the epilepsy sub-type, evaluates surgical candidacy, hypothesizes the area of EZ, and confirms if surgery benefits the patient. If the estimated resection area is not properly taken into account, there is a risk of developing post-operative deficits. Thus, all surgical risks are assessed before proceeding, ensuring a high success rate. In the following, we review some presurgical workups:

I. Scalp Video-EEG Monitoring

In general, video-EEG can accurately distinguish epileptic seizures from other clinical events and provide additional EEG-based diagnostic information such as IEDs and ictal activities. IEDs, originating from the IZ, are presented more at night when rapid eye movement (REM) sleep happens. Moreover, ictal activities originating from the SOZ help to interpret the observed semiology.

Apart from the scalp EEG setup, invasive channels like sphenoidal or Foramen ovale electrodes support picking up activities from mesiotemporal or basotemporal regions [19, 20, 21].

II. MEG

As a functional and noninvasive neuroimaging modality, it records the magnetic fields of the brain produced by the electrical activities of neurons. It is similar to EEG in measuring brain activities, and the two methods can provide complementary information. Unlike EEG signals, MEG fields can pass through tissues and bone with minimal distortion, and conductance in the skull or scalp tissue has little impact on them. A helmet-shaped device records data using an array of highly sensitive magnetometers (>300) inside a magnetically shielded room. Recently, a new wearable MEG scanner has also been developed [22]. Analysis of interictal and ictal recordings in MEG can help localize the EZ, similar to EEG.

III. Structural MRI

Studies show that successful surgery is more likely if MRI detects structural abnormalities [23, 24]. After surgery, any remaining lesion increases the chance of seizure persistence. MRI epilepsy scanning should monitor the whole patient's brain and head. The recording protocol includes 3D slices of T1- and T2-weighted images, as well as fluid attenuated inversion recovery (FLAIR) images [25]. Both T2 and FLAIR imaging can provide an accurate anatomical representation of the hippocampus. Additionally, using high-field strength MRI can enhance the signal-to-noise ratio, as stated in [26].

IV. Nuclear Imaging

PET and SPECT use various tracers to evaluate physiological functions and biochemical changes at the molecular level. PET tracers are utilized to assess multiple physiological activities of the brain, such as glucose metabolism, neurotransmitter function, and blood flow. This data analysis enables the development of metabolic brain imaging. In case the tracer detects hypometabolism in a specific brain region, it could signify a dysfunctional cortex, which can potentially be associated with the epileptic focus.

SPECT can provide 3D images from radioisotopes using gamma rays, making it a helpful technique in ETLE cases and non-lesional cases. During interictal and ictal phases, the relevant tracer (^{99m}Tc-hexamethylpropyleneamine oxime (^{99m}Tc-HMPAO)) is injected and results are compared. Ictal hyperperfusion occurs in the SOZ and linked networks, making SPECT results complementary for EEG and MRI findings.

V. EEG and MEG source localization

EEG and MEG signals record the electrical and magnetic field of the brain with electrodes placed on the scalp or magnetometers close to the head, respectively. Advances in computer technology and mathematical modeling during the 1980s led to dipole modeling techniques that estimate the sources generating the scalp potentials [27, 28]. EEG source localization allowed localizing the origin of interictal epileptiform discharges in the brain. From the 1990s, the integration of MEG with MRI allowed more accurate anatomical localization of epileptic foci [29]. In the 2000s, advanced source localization techniques, such as beamforming and distributed source modeling, were developed for both EEG and MEG, improving the ability to localize epileptic activity with greater accuracy. Although numerous studies have demonstrated the added value of EEG and MEG source localization ([30]), these methods are not widely used in epilepsy centers for presurgical evaluations [31]. This is due to the need for specialized technical expertise and the time-consuming nature of the analysis. Additionally, there is a lack of a standard EEG/MEG source localization procedure to estimate the EZ.

VI. Invasive Video-EEG Monitoring

Invasive EEG recording (iEEG), performed via ECoG or sEEG, can directly record seizure onset and propagation from the cortex. In iEEG, the onset of seizures is determined by recognizing specific discharge patterns. Among them, focal fast activity is the specific biomarker associated with the outcome of epileptic surgery [32]. This emphasizes the importance of successful iEEG recording. To accomplish this, electrodes are surgically implanted within the brain.

In ECoG, subdural strip or grid electrodes are directly placed on the brain surface to record cortical activities. This could determine the extent of the IZ and SOZ networks and their relation to other regions, such as the Eloquent cortex.

sEEG enables the recording of electrical activities from deep brain structures. This is achieved through the use of implanted electrodes that are precisely placed in specific target areas. They can reach all cortical areas but have limited spatial sampling. Regarding lateralization in patients with temporal epilepsy (TLE), bilateral sEEG recordings provide better localization results than subdural bilateral recordings.

2.3.4 Preoperative process

This section outlines the diagnostic process for patients with refractory epilepsy. Firstly, the patient is hospitalized for long-term video-EEG monitoring (VEM) for several consecutive days. During this period, AED dosages are reduced to induce epileptic seizures, which help record ictal and interictal activities and identify clinical symptoms. VEM is a crucial investigation to accurately diagnose epilepsy subtypes. In addition to EEG, MR scans with an epilepsy protocol are taken. Any additional presurgical diagnostics follow the findings in EEG and standard MR [33].

As discussed, only the patients with focal or unknown epilepsy will undergo presurgical investigations. In contrast, those with generalized epilepsy receive alternative treatments like vagus nerve stimulation (VNS).

Chapter 3

EEG and EEG Source Imaging

There is only one good, knowledge, and one evil, ignorance.

Socrates

3.1 Introduction

EEG is a non-invasive method for recording electric signals from the brain. In this chapter, we will discuss how EEG is generated, how EEG is recorded from the scalp, and how to localize EEG for clinical use.

3.2 EEG: from source to sensor

3.2.1 EEG origin

To study the sources of EEG signals, it is essential to understand the nature of brain communication, how neurons communicate with each other, how electrical potentials are generated, and how these potentials contribute to the measurable signals on the scalp.

Neurons are the fundamental building blocks of the human brain. The brain contains around 86 billion neurons, interconnected into a complex network. Each neuron has three main parts: a cell body (soma), an axon, and up to a thousand dendrites. Figure 3.1 shows the detailed structure of a neuron. The soma, the control center of the neuron, maintains the cell, keeps the neuron functional, and houses the nucleus. An axon is a long, slender projection that extends from the soma. Its primary function is to carry electrical impulses away from the soma to other neurons. The dendrites are tree-like extensions from the soma, and their primary role is to receive incoming signals from other neurons, conducting this information towards the soma. The area of the neuron where the soma meets the axon is known as the axon hillock. The axons are typically covered by the myelin sheath, a fatty, insulating layer, that protects the axon and enhances the speed and efficiency of electrical signal transmission. A synapse is the junction where a neuron communicates

with another cell, which could be another neuron, a muscle cell, or a gland cell. The synapse plays a critical role in transmitting information within the nervous system, allowing the transfer of electrical and chemical signals between cells. The transmission of a signal within a neuron occurs along the dendrites, soma, and axon via electrical conduction. The communication at the synapse between the presynaptic axon terminal and the postsynaptic dendrite relies on neurotransmitters, a process known as chemical transmission. Here, neurotransmitters housed in the axon terminal are released into the synaptic cleft upon the firing of the pre-synaptic neuron.

Communication between neurons involves two types of electrical potentials: action potentials (APs) and postsynaptic potentials (PSPs). Action potentials utilize electrical conduction, while postsynaptic potentials involve chemical transmission. An AP is a rapid, transient electrical signal that travels along the neuron's membrane from the axon hillock to the axon terminal. A PSP is a change in the membrane potential of the postsynaptic neuron due to neurotransmitters released from the presynaptic neuron (Fig. 3.2). It occurs at the postsynaptic membrane of neurons in the dendrites or cell body. Moreover, a synapse can be excitatory or inhibitory and generates either an excitatory postsynaptic potential (EPSP) or an inhibitory postsynaptic potential (IPSP), depending on whether the postsynaptic membrane potential becomes more positive or more negative, respectively.

This mechanism of generating electrical impulses involves a series of steps, including maintaining the resting membrane potential, triggering an action potential, and propagating the action potential along the neuron. Voltage-gated channels and pumps in the neuronal cell membrane play a pivotal role in this process. These include voltage-gated sodium (Na^+) and potassium (K^+) channels, as well as Na^+/K^+ pumps. Each of these channels opens and closes at different polarities and thresholds. The Na^+ channel, for example, opens and closes at -55 mV and +40 mV, respectively, while the K^+ channel opens and closes at +40 mV and -80 mV, respectively. The Na^+/K^+ pumps maintain a higher extracellular concentration of Na^+ compared to the intracellular environment, and a higher intracellular concentration of K^+ compared to the extracellular environment across the neuron's membrane. Generating an action potential occurs during four phases, including resting state, depolarization, repolarization, and hyperpolarization (Fig. 3.3). During the resting state phase, neurons exhibit a resting membrane potential of approximately -70 mV, which results from several factors, including the high permeability of the neuronal cell membrane to K^+ and the low permeability to Na^+. Consequently, at the resting membrane potential, the inside of the cell is more negative than the outside. When a neuron receives enough excitatory stimuli, the membrane potential becomes less negative (depolarizes), potentially triggering an action potential. In this situation, the number of EPSPs is greater than IPSPs, leading to a sufficient increase in potential at the axon hillock. If the depolarization reaches a threshold of around -55 mV, voltage-gated Na^+ channels open, leading to a rapid influx of Na^+ into the neuron. As a result, the membrane

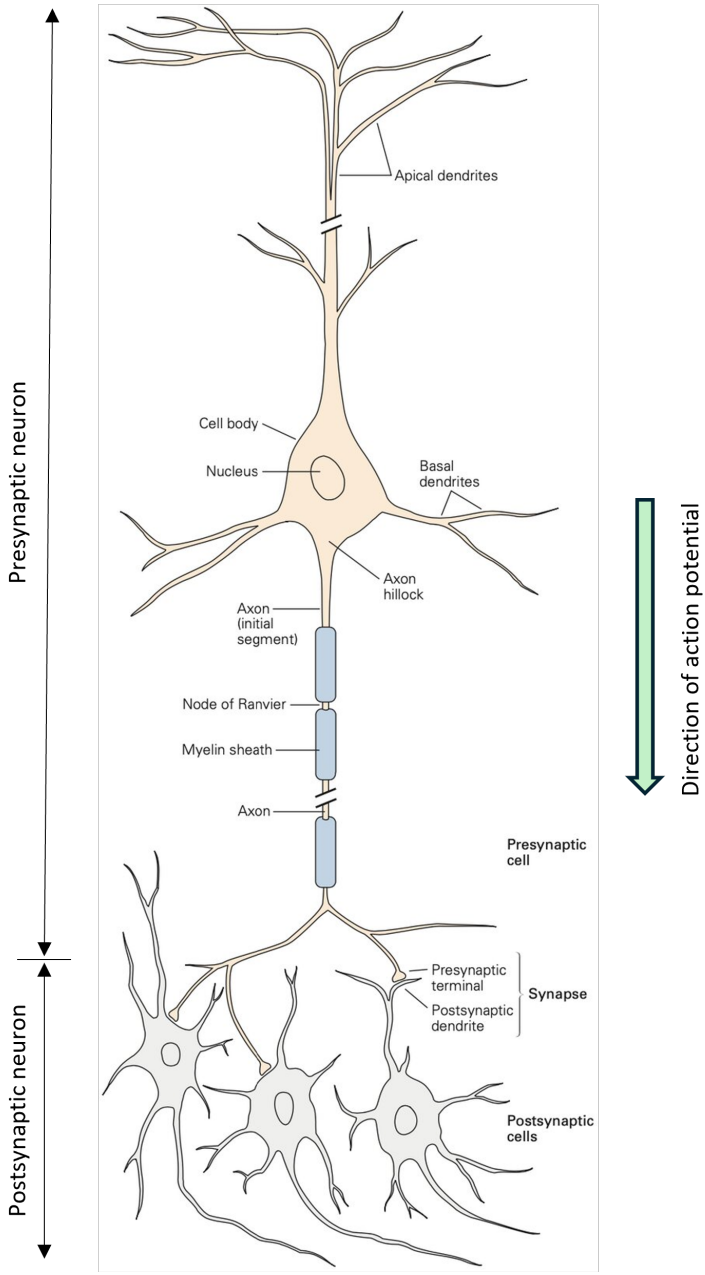

Figure 3.1: Anatomy of neuron. Picture adapted from [34].

potential becomes positive, typically reaching about +30 to +40 mV. The propagation of the action potential begins with this depolarization until the peak is reached. Following the peak of the action potential, voltage-gated

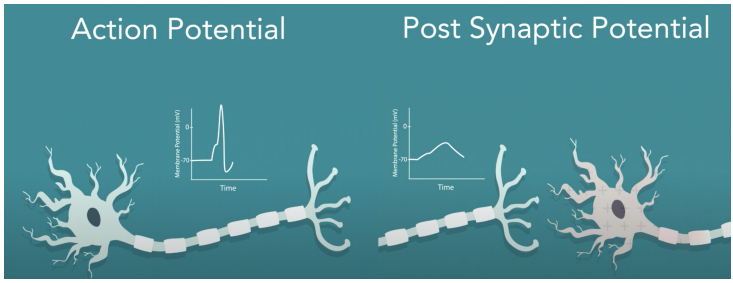

Figure 3.2: Action Potential vs Postsynaptic Potential. Picture adapted from [35].

Na^+ channels shut, and voltage-gated K^+ channels open, allowing K^+ to exit the neuron. This results in the membrane potential becoming more negative, a process known as repolarization. The resting potential of the neuron briefly drops below -70 mV due to the slow closure of K^+ channels, allowing excessive K^+ to exit the neuron, resulting in hyperpolarization.

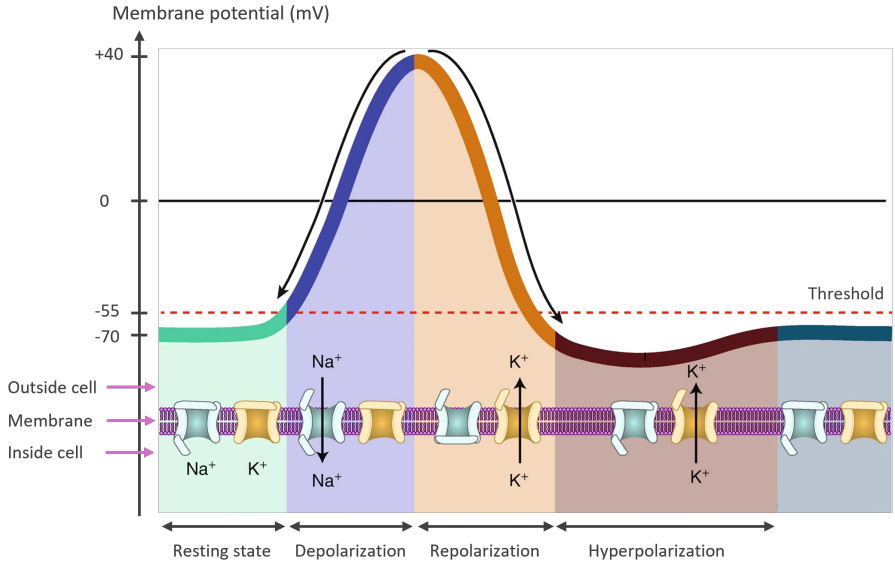

Figure 3.3: The four phases of generating an AP. Picture adapted from [36].

While APs are the fundamental units of electrical signaling in neurons, their duration is very short. In addition, during an action potential, different segments of the axon are at different stages of depolarization and repolarization. This creates regions of inward and outward current flow that can form a complex pattern. The inward and outward currents are not only opposite but also spatially separated, creating a pattern that can be approximated by a quadrupole when viewed from a certain distance.

PSPs are slower and can be detected by scalp EEG. A postsynaptic potential

can be modeled as an electric current dipole, characterized by inward and outward flows of ions (current), creating a separation of charges across the neuronal membrane. This results in a dipole with a positive region (source) and a negative region (sink) separated by a certain distance. The EEG is produced by pyramidal neurons located in the cortex. When a postsynaptic neuron receives an excitatory signal from the synapse, positive ions flow into the dendrites. It makes the intracellular space more positive and the extracellular more negative. Therefore, the extracellular space at the opposite end of the postsynaptic neuron becomes more positive. This pair of equal charges in extracellular space between the cell body and the dendrite makes the electric current dipole. Alternatively, for IPSP the dipole direction is opposite. Figure 3.4 overviews how excitatory and inhibitory PSPs can be modeled by current dipoles.

Figure 3.4: Generating an electric current dipole via EPSP and IPSPS. Picture adapted from [37].

The scalp sensor cannot detect the single electric current dipole activity from postsynaptic potentials since they are weak in strength. However, the synchronized activities of current dipole groups can create a measurable signal. The timing of neuronal activities and the orientation of dipoles are critical factors in producing detectable signals. When neurons fire asynchronously, the current dipoles will not sum up and the overall signal is weak. Neurons also cancel their activities when they have opposite orientations because positive and negative charges neutralize each other. The most powerful signal is produced when neurons are oriented in the same direction and fire at the same time, which is the case for pyramidal neurons.

Action potentials (APs) are less detectable by scalp EEG compared to postsynaptic potentials (PSPs) for several reasons:

- Spatial Summation: the PSPs involve synchronized activity of a large area involving many neurons, while the AP are localized to the axon and do not synchronize over large populations.
- Dipole configuration: the PSPs generate electric current dipoles with strong electrical fields that can propagate to the scalp, while the APs generate quadrupoles with closely spaced opposite charges having weaker electrical fields.

- Duration: the duration of PSPs is longer than that of the APs, tens to hundreds of milliseconds compared to 1-2ms. This gives the PSPs more probability to be summed up and detected by the scalp EEG electrodes.

- Source Orientation: PSPs primarily occur in the dendritic trees of pyramidal neurons, which are oriented parallel to each other and can be summed to produce stronger signals. In contrast, APs occur along axons, often oriented in various directions, leading to greater signal cancellation.

3.2.2 Scalp EEG recording

It is essential to have a standardized setup for clinical EEG recordings. The international 10-20 system with 19 electrodes is a widely used method for recording scalp EEG signals. The system derives its name from the distances between neighboring electrodes, which are placed at 10% or 20% of the total length between two landmarks - nasion and inion. Nasion is a bony landmark situated between the eyes and above the nasal bridge, while inion is the most prominent point of the external occipital protuberance on the back of the skull. The measurement of the distance between nasion and inion involves two paths: right-left and front-back. Considering this information in the right-left path results in pinpointing ten electrodes, which are Fp1/2, F7/8, T3/4 (now known as T7/8), T5/6 (now known as P7/8), and O1/2. Similarly, the electrodes Fz, Cz, and Pz are placed considering the front-back path. Afterward, the F3(4) electrode is positioned at the midpoint between the Fz and F7(8) locations, while the C3(4) electrode is placed midway between the Cz and T3(4) locations. Similarly, the P3(4) electrode is placed at the midpoint between Pz and T5(6) locations. Nasion, inion, right-left and front-back paths, as well as the electrodes placement utilized in the 10-20 system, are illustrated in Figure 3.5-a. Channels are labeled using a standard nomenclature system based on the anatomical location of the electrodes on the scalp. This system uses the letters "F", "T", "P", and "O", representing the frontal, temporal, parietal, and occipital lobes, respectively, while "C" is used to represent the central brain region. Additionally, electrodes on the left side of the head are labeled using odd numbers, while those on the right side are labeled using even numbers.

One limitation of this setup is that it does not cover sublobes such as the anterior or basal temporal lobes, which are the most common sources of epileptogenic activity [38, 39]. Therefore, it was proposed to add six extra electrodes, including the inferior temporal chain (F9/10, T9/10, and P9/10), for all standard clinical recordings [40] (Fig. 3.5-b left). A high-density EEG setup is recommended to ensure accurate EEG source localization [40]. This can be achieved using montages with more electrodes, such as a 10-10 system subgroup or the entire set of 10-10 system (Fig. 3.5-b right), or by utilizing EGI-256 electrodes, as illustrated in Fig. 3.5-c.

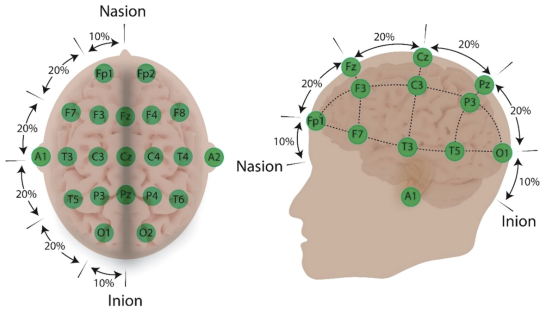

(a)

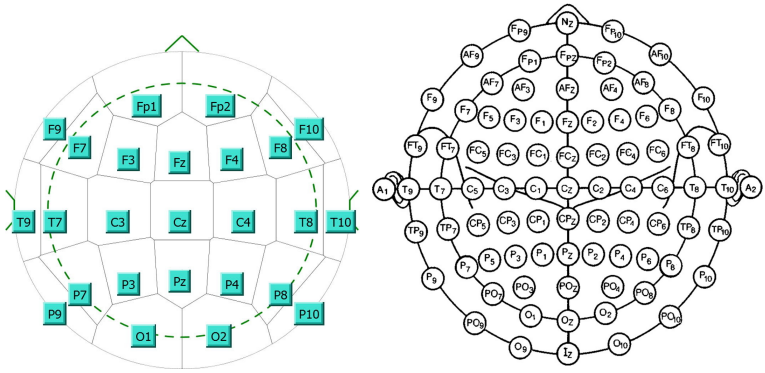

(b)

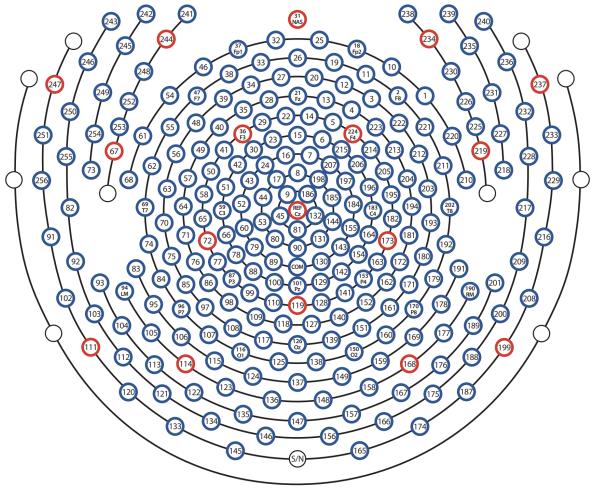

(c)

Figure 3.5: Standard scalp EEG setups, a) Nineteen electrodes of the international 10–20 system. Figure utilizes more details including nasion, inion, right-left, and front-back paths. Picture adapted from [41], b) The modified 10-20 system (left) vs 10-10 electrodes (right) [40], c) high-density setup with 256 electrodes.

3.2.3 EEG rhythms

EEG signals are identified as normal and abnormal brain activities based on the amplitudes and frequencies of signals. It varies from person to person according to their age and physical/mental conditions. Generally speaking, the EEG signals are categorized into five rhythms [42] (Fig. 3.6):

- Delta (δ): the high amplitude wave with a frequency below 4 Hz. It is observed in babies and slow-wave sleep in adults. However, it can indicate a brain disease in awake adults.
- Theta (θ): the frequency range of these waves is between 4Hz and 7Hz. They are more predominant in young children and are also linked to idling and drowsiness during certain sleep stages in teenagers and adults.
- Alpha (α): the waves have frequencies between 8Hz and 12Hz. It is associated with the relaxing mode and is visible in awake individuals with eyes closed, especially in the electrodes located in the parietal-occipital region.
- Beta (β): the low amplitude wave with a frequency range of 13Hz to 30Hz. Generally, it is associated with alertness and is visible in specific sleep stages. The range varies from active calm to mild obsessive that intense, and stressed in between. Higher frequencies are also linked to thinking and alertness.
- Gamma (γ): the low amplitude waves with a freqency above 30Hz. It displays during cross-modal sensory processing and is associated with the cortex's active information.

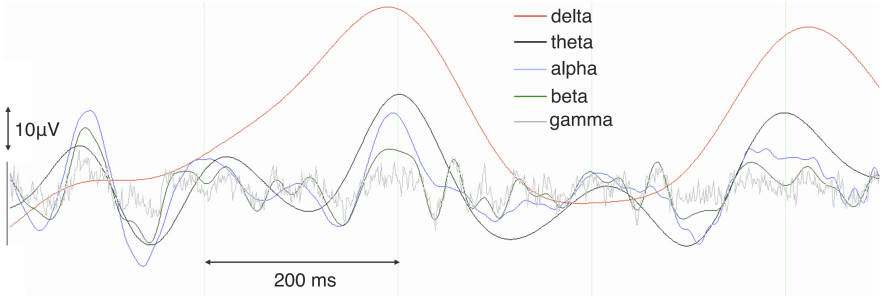

Figure 3.6: Comparison of 5 EEG bands. Figure adapted from [43]

3.2.4 EEG artifacts

EEG signals are often recorded alongside other activities near the electrodes, which can contaminate the recordings with non-brain activity artifacts. Figure 3.7 gives an overview of five frequent artifacts. There are two types of such artifacts:

- Physiological: it arises from the body's artifacts such as ocular, muscular, and electrocardiac artifacts. The ocular artifacts typically occur due to the eye's movements and are visible in the frontal polar channels like Fp1 and Fp2. The amplitude could rise up to 10x the actual brain signals and last 100 ms to 400 ms. However, facial activities like chewing, jaw movements, teeth grinding, etc, trigger muscular artifacts. Both amplitude and frequencies of the signals could be high in size (> 100 Hz). Finally, electrocardiac artifacts arise when the EEG electrodes detect heartbeats.

- Environmental: it is practically the disturbances in the EEG recording that are caused by external factors or devices that include the power line noises (50 Hz in Europe; 60 Hz in the US), poor electrode attachment, subject movements, etc.

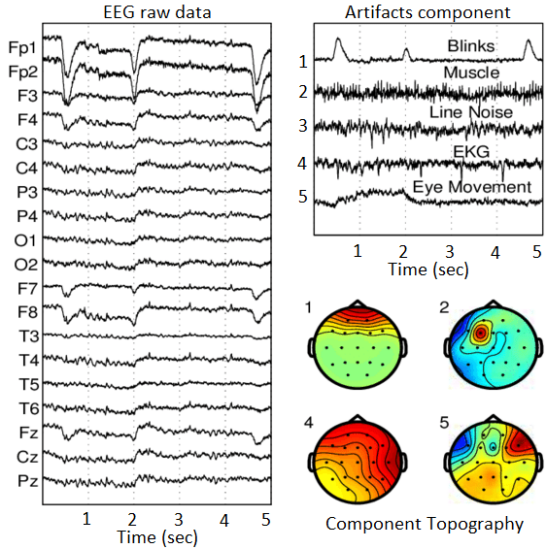

Figure 3.7: On the left, five typical artifacts can be seen in EEG signals. On the right, the morphology of related components is displayed, along with the topographies of four physiological components. Figure is adapted from [44]

3.3 EEG: from sensor to source

3.3.1 EEG Source Imaging

ESI is a technique that identifies the brain sources responsible for generating the measured electric potentials at the scalp. It consists of a forward method and an inverse solution. The forward method calculates how a source's electric signal generates scalp potentials, while the inverse solution estimates brain sources from measured scalp potentials. Figure 3.8 shows the forward model and inverse solution.

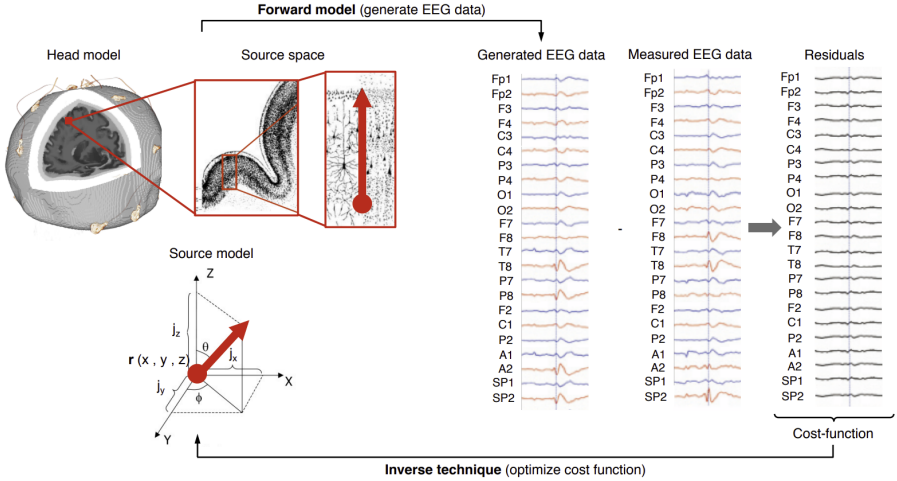

Figure 3.8: An overview of ESI is presented, which involves using a forward model to generate "Generated EEG data" from electrical source activities using the head model. However, this is different from the "Measured EEG data". The residuals are calculated and used in the "Inverse technique" to calculate the ESI outcome. Figure is adapted from [43]

3.3.2 Head model

The head model describes the anatomical structure and electrical conductivity of the head. The complexity of the model increases with the number of modeled brain tissues, resulting in a more realistic model. The most basic head model consists of a concentric sphere with three tissue types: inner brain, skull, and scalp. However, this model is inadequate for clinical purposes, which require more complex and realistic models.

In order to create a head model suitable for clinical applications, high-resolution MRI slices (typically T1- or T2-weighted images) are used to segment the head tissues into six individual types, including grey matter (GM), white matter (WM), cerebrospinal fluid (CSF), skull, scalp, and air (Fig. 3.9). Each segmented tissue has a specific electrical conductivity value (table 3.1). In this step, all the potential ESI sources, the dipoles, are located in the GM.

3.3.3 Forward model

The forward model computes how the activities of the current dipoles propagate through various brain tissues, generating measurable signals at the scalp based on the constructed head model.

I. Physical theory

This section explains the physical and mathematical background of the forward model. It describes the scalp potentials generated by the current dipole source at position $r = [x, y, z]$ and dipole moment intensity $j = [j_x, j_y, j_z]$ as:

Conductivity S/m								
Tissues	[45]	[46]	[47]	[48]	[49]	[50]	[51]	Ours
GM	0.33	0.22	0.3333	0.33	0.26	0.11	0.59	0.33
WM	0.33	0.22	0.1428	0.14	0.19	0.07	0.34	0.14
CSF	-	-	1.79	1.79	-	-	2.14	1.79
Skull	0.0041	0.015	0.0041	0.01	-	-	0.06	0.0132
Scalp	0.33	0.22	0.3279	0.43	-	-	-	0.33
Air	0	0	0	0	-	-	-	0

Table 3.1: Summary of tissue electrical conductivity in the literature. The last columns is the numbers we used in our studies.

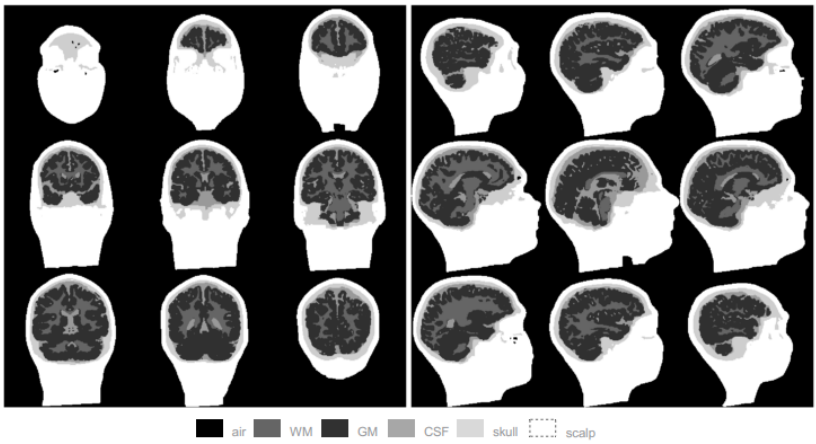

Figure 3.9: Geometry of a headmodel that consists of six tissues in axial and sagittal views

$$V = L(r)j(r) \tag{3.1}$$

where $V \in \mathbb{R}^{N_c \times 1}$ is EEG signal recorded from N_c electrodes and $j(r) \in \mathbb{R}^{3\times 1}$ is the current dipole amplitude at the location r. Moreover, $L(r) \in \mathbb{R}^{N_c \times 3}$ is the lead field matrix that describes how the current dipole links to the generated potentials on the scalp. By considering N_d sources at the locations $r_i (i = 1...N_d)$ with the dipoles moments $j_i (i = 1...N_d)$, Eq. (3.1) can be rewritten as:

$$V = LJ \tag{3.2}$$

where J is the current dipole vector at N_d locations. Here, $J = [j_1, ..., j_{N_d}]^T$ and $j_i = [j_{x,i}, j_{y,i}, j_{z,i}]^T$ contains both amplitude and orientation of the i-th dipole. Additionally, $L = [L(r_1), ..., L(r_{N_d})] \in \mathbb{R}^{N_c \times 3N_d}$ is the lead field matrix. It connects the amplitudes of the source dipoles in J with fixed

orientation in the x, y and z-direction to the EEG data recorded at the scalp.

To calculate the lead field matrix, it is essential to consider Maxwell's equations that describe the electromagnetic model including the different electrical properties of the tissues in the head. This leads to the derivation of Poisson's equation, which allows to solve the forward model.

The Maxwell's equations are:

$$\nabla.E = \frac{\rho}{\epsilon} \tag{3.3}$$

$$\nabla.B = 0 \tag{3.4}$$

$$\nabla \times E = -\frac{\partial B}{\partial t} \tag{3.5}$$

$$\nabla \times B = \mu j + \mu\epsilon\frac{\partial E}{\partial t} \tag{3.6}$$

where E, B, and j are the electric, magnetic, and current density fields, respectively. In addition, ρ, ϵ, and μ are the charge density, electrical permittivity, and magnetic permeability, respectively. Assuming isotropic conductivity in the forward model, we can use Ohm's law:

$$j = \sigma E \tag{3.7}$$

where $\sigma(x, y, z)$ is the conductivity matrix and j stands for surface charge density, it describes that the current passing the head model is proportional to the electrical field.

Finally, we add the continuity equation, which emphasizes that electric charge cannot be created or destroyed:

$$\nabla.J = -\frac{\partial \rho}{\partial t} \tag{3.8}$$

We can use Eq. (3.3) to (3.8) to explain all electromagnetic phenomena that occur in the head. Current density, denoted by J, is defined as the amount of current per unit area, in A/m^2. The divergence of J, ie, $\nabla.J$, also known as the current source density, has units of A/m^3.

For measuring EEG signals, only the electrical field E needs to be considered. The head model has negligible capacitance, causing electric charges to distribute on the tissue interface and not accumulate in the brain volume. This simplifies the interpretation of Maxwell's equations and allows ignoring the terms $\frac{\partial E}{\partial t}$ and $\frac{\partial B}{\partial t}$ in the calculation of E. The instantaneous current density depends only on the instantaneous current sources, Eq.(3.5) simplifies

to $\nabla \times E = 0$. The electric field E can be formulated as the negative gradient (∇) of the scalar potential function $U(x, y, z)$, which is determined by the position, as follows:

$$E = -\nabla U. \tag{3.9}$$

The negative sign in Eq. (3.9) indicates that the electric field orients from high-to-low potential at a given area.

The total current density j_{tot} that flows through the brain is composed of two components: the first, called forced current source j_f, originates from the dipole source, while the second, called j_r, results from the macroscopic electric field in the brain, as expressed by Ohm's law. Then:

$$j_{tot} = j_f + j_r = j_f + \sigma E = j_f - \sigma \nabla U \tag{3.10}$$

As previously discussed, the capacitance of the head tissues can be ignored. This leads to $\nabla j_{tot} = 0$. Poisson's equation can be obtained by calculating the divergence of Eq. (3.10):

$$\nabla.(\sigma \nabla U) = \nabla.j_f \tag{3.11}$$

Eq. (3.11) is the primary equation connecting the electric potential U to the current source dipole j_f in the EEG forward model.

There are several methods to solve Equation (3.11), including the "Boundary Element Method" (BEM) [52, 53, 54], the "Finite Difference Method" (FDM) [55, 56, 57, 58, 59] and the "Finite Element Method" (FEM) [48, 60, 61, 62, 63, 64]. The BEM approach divides the head model into subvolumes with homogeneous conductivity and calculates the potentials only on the surface of these separating subvolumes. However, both FEM and FDM don't have this limitation. They divide the head model into small volume elements. In FEM, this volume has an arbitrary shape, while it is cubic in FDM. Although FEM offers more flexibility, it is computationally more intensive. In this thesis, we used FDM to to compute the EEG forward model.

II. Finite Difference Method (FDM)

The FDM approach uses a cubic grid to represent the head model as a network of volume elements. Figure 3.10 shows the scheme, with h_x, h_y, and h_z representing the grid size in the x, y, and z directions. Element 0 is the central node of the grid, surrounded by six elements at potential U_i, where $i = 1...6$.

This technique involves a dipole model consisting of two monopoles, I and $-I$, that extend three voxel nodes in the x, y, and z directions. The dipole is positioned in the center node. Figure 3.11 provides an example of the dipole in the z-direction. Node $r_1(x_1, y_1, z_1)$ serves as a current source that represents the injection of positive charges into the pyramidal cell. The current source

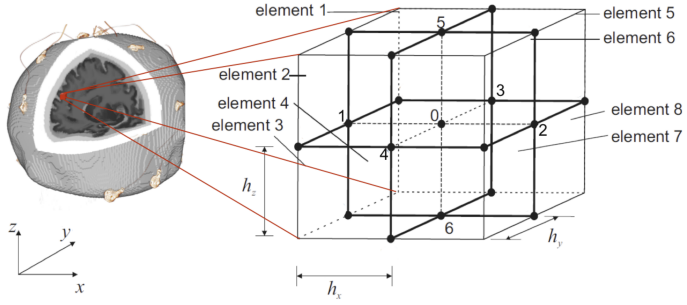

Figure 3.10: The computational scheme is used in FDM when conductivities are incorporated. There are six potentials in nodes 1 to 6 surrounding the center node, i.e., 0. Figure adapted from [43]

density is $+I\delta(r-r_1)$, and the δ function confirms that the current is deleted at one point in space [65]. On the other hand, node $r_2(x_2, y_2, z_2)$ is a current sink that represents the removal of positive charges from the pyramidal cell. It is equivalent to $-I\delta(r-r_2)$. By using the two monopoles, Eq. (3.11) can be rewritten as [49, 60]:

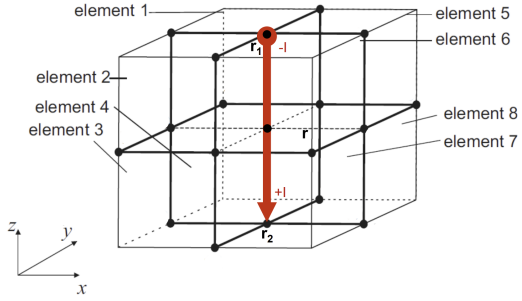

Figure 3.11: A typical dipole model of FDM solution in z-direction. Figure adapted from [43]

$$\nabla.(\sigma\nabla U) = +I\delta(r-r_1) - I\delta(r-r_2) \tag{3.12}$$

After expanding Equation (3.12), the following result was obtained:

$$\begin{gathered}\sigma\frac{\partial^2 U}{\partial x^2}+\sigma\frac{\partial^2 U}{\partial y^2}+\sigma\frac{\partial^2 U}{\partial z^2}+\frac{\partial\sigma}{\partial x}\frac{\partial U}{\partial x}+\frac{\partial\sigma}{\partial y}\frac{\partial U}{\partial y}+\frac{\partial\sigma}{\partial z}\frac{\partial U}{\partial z} \\ = \\ I\delta(x-x_1)\delta(y-y_1)\delta(z-z_1)-I\delta(x-x_2)\delta(y-y_2)\delta(z-z_2)\end{gathered} \tag{3.13}$$

Let's use U_0 for the potential at the central point and $U_i, i = 1...6$ for the surrounding potentials. Then, according to Eq. (3.13), we get [56, 59, 66]:

$$\sum_{i=1}^{6} A_i U_i - \left(\sum_{i=1}^{6} A_i\right) U_0 = I_P \tag{3.14}$$

The Saleheen coefficients, A_i, depend on the conductivities of the eight surrounding volumes of the central node, as shown in Fig. 3.11. The value of current, I_P, depends on the position of the center node. If the center node is at the monopole of the current source or sink, then I_P is either 1 or -1, respectively. Otherwise, I_P is 0. Figure 3.12 explains how the Saleheen coefficients are calculated using four fixed-position volumes:

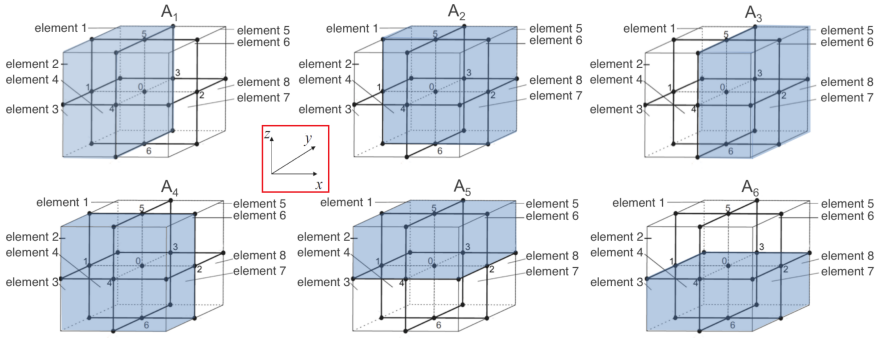

Figure 3.12: The active volume elements to compute the Saleheen coefficients A_1 to A_6. Figure adapted from [43]

$$A_1 = \frac{1}{4h_x^2}[\sigma_1 + \sigma_2 + \sigma_3 + \sigma_4] \tag{3.15}$$

$$A_2 = \frac{1}{4h_y^2}[\sigma_1 + \sigma_4 + \sigma_5 + \sigma_8] \tag{3.16}$$

$$A_3 = \frac{1}{4h_x^2}[\sigma_5 + \sigma_6 + \sigma_7 + \sigma_8] \tag{3.17}$$

$$A_4 = \frac{1}{4h_y^2}[\sigma_2 + \sigma_3 + \sigma_6 + \sigma_7] \tag{3.18}$$

$$A_5 = \frac{1}{4h_z^2}[\sigma_1 + \sigma_2 + \sigma_5 + \sigma_6] \tag{3.19}$$

$$A_6 = \frac{1}{4h_z^2}[\sigma_3 + \sigma_4 + \sigma_7 + \sigma_8] \tag{3.20}$$

where σ_v, $v = 1, ..., 8$ is the conductivity at the volume v. It's important to note that potential values are calculated at the center node, with volume elements covering that node representing the head model's conductivity and geometry. When considering n nodes and taking equations (3.15) to (3.20)

into account, Eq. (3.14) can be rewritten for each node as follows:

$$A.U = I \tag{3.21}$$

By considering n nodes, $A \in \mathbb{R}^{n \times n}$ represents the stiffness matrix that captures the relationship between the displacements at different nodes and the conductivity values in the elements connecting these nodes. Furthermore, A_{nc} is the c-th coefficient of the n-th node, assumed as the center node. The potential vector at each computational node is represented by $U = (U_1, ..., U_n)^T \in \mathbb{R}^{n \times 1}$, and the vector of current sources and sinks is represented by $I \in \mathbb{R}^{n \times 1}$. If the current source/sink monopole is located at the a-th/b-th node, then $I_a = +1/I_b = -1$, otherwise it equals zero.

Eq. (3.21) must be solved in terms of U to determine the potential of each node using direct or iterative methods. Then:

$$U = A^{-1}.I \tag{3.22}$$

Solving Eq. (3.22) for each electrode allows us to determine the potentials produced by current dipoles. The lead fields matrix in Eq. (3.1) is calculated using Eq. (3.22). Evaluating U at N_{ch} scalp electrodes in x, y, and z directions with unit amplitude input produces $V_u \in \mathbb{R}^{N_{ch} \times 3}$. V_u represents the lead fields matrix L for each source dipole.

For accurate results, we need to calculate the forward solution for all sources in the head model. Depending on the size of the head model, even up to 10,000,000 source needs to be considered for the calculation, which makes the forward solution quite intensive. Instead of computing the lead fields matrix directly, we can employ the reciprocity principle to reverse the roles of the dipoles-electrodes. This approach limits the lead fields calculation to the number of electrodes rather than the number of sources.

3.3.4 Lead fields calculation

In order to explain the calculation of the lead fields matrix, we first discuss the concept of the reciprocity theorem using the circuit shown in Fig. 3.13. Clamps A and B are EEG electrodes on the scalp, and two other clamps, described by r, measure a dipole source in the brain. Introducing current I_r at clamps generates potential $V_{AB}I_r$ in the network (Fig. 3.13A). Meanwhile, current I_{AB} at clamps A and B causes potential difference $I_{AB}U_r$ at r (Fig. 3.13B). The reciprocity principle hypothesizes [67]:

$$V_{AB}I_{AB} = I_rU_r \tag{3.23}$$

We assume a dipole in the x-direction located at r, as shown in Fig. 3.13. The dipole is formed by a pair of current monopoles: $+I_r$ and $-I_r$ as a source and a sink, respectively. The monopoles are positioned at opposite nodes and separated by a distance of $2h_x$, where h_x is the spacing of nodes in the x-direction. The dipole moment has a magnitude of $2h_xI_r$. Therefore, we can

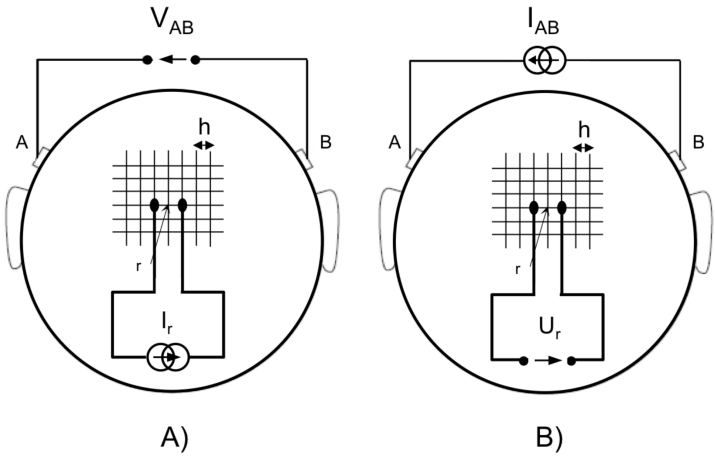

Figure 3.13: The circuit network illustration demonstrates the reciprocity theorem for the brain model. A) When a current source I_r is generated in the brain, V_{AB} is created at the scalp electrodes. Conversely. B) a current source I_{AB} at the scalp generates a potential U_r in the brain. Figure adapted from [68].

assume the presence of a dipole field at this location, and the scalp electrodes are far enough from the sources with a $2h_x$ distance. As a result, we rewrite (3.23) as:

$$V_{AB} = \frac{U_r I_r}{I_{AB}} \tag{3.24}$$

We include the dipole orientation in x, y, and z-direction and describe the dipole based on its location at $r = [ih_x, jh_y, kh_z]$ in the 3D head model. Here, i, j, k and h_x, h_y, h_z indicate the number of nodes and the dipole spacing in x, y and z-direction, respectively. Then, by considering $d_x = 2h_x I_x$ and

$$\frac{\partial U}{\partial x}(r) \approx \frac{[U(r + h_x e_x) - U(r - h_x e_x)]}{2h_x} \tag{3.25}$$

where e_x is unit vector in x direction. Then (3.24) is rewritten as:

$$V_{AB} = \frac{d_x(r)\frac{\partial U}{\partial x}(r)}{I_{AB}} \tag{3.26}$$

Equation (3.26) gives the scalp potential V_{AB} for a dipole oriented in the x direction at location r, with $\frac{\partial U}{\partial x}(r)$ specified. We can also calculate V_{AB} for dipole orientations in the y and z directions. In general, for a dipole with moments $d = (d_x, d_y, d_z)^T \in \mathbb{R}^{3\times 1}$ located at r, the scalp potential V_{AB} is:

$$V_{AB}(r,d) = \frac{d^T.\nabla U(r)}{I_{AB}} \tag{3.27}$$

where $\nabla U(r) = (\partial U(r)/\partial x, \partial U(r)/\partial y, \partial U(r)/\partial z)^T \in \mathbb{R}^{3\times 1}$. Equation (3.27) shows how EEG lead fields are calculated using the reciprocity approach with pairs of scalp electrodes. The potential $U(ih_x, jh_y, kh_z)$ from Eq. (3.22) is calculated for each pair by taking the gradient of $U(r)$ with respect to x, y, and z.

Equipotential lines and current density ($J = \sigma\nabla U$) in the brain are visualized in Fig. 3.14, where:

- $\nabla U = (\frac{\partial U}{\partial x}, \frac{\partial U}{\partial y}, \frac{\partial U}{\partial z})^T$, and
- $\frac{\partial U}{\partial x} \approx \frac{[U((i+1)h_x,jh_y,kh_z) - U((i-1)h_x,jh_y,kh_z)]}{2h_x}$
- $\frac{\partial U}{\partial y} \approx \frac{[U(ih_x,(j+1)h_y,kh_z) - U(ih_x,(j-1)h_y,kh_z)]}{2h_y}$
- $\frac{\partial U}{\partial z} \approx \frac{[U(ih_x,jh_y,(k+1)h_z) - U(ih_x,jh_y,(k-1)h_z)]}{2h_z}$

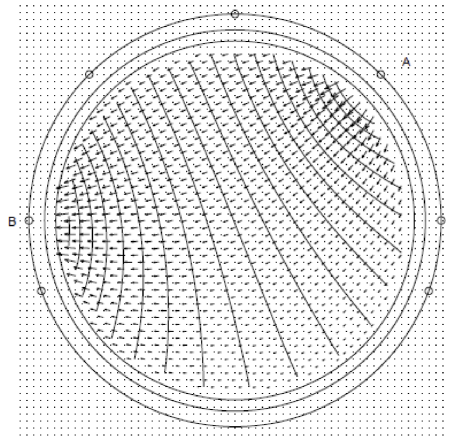

Figure 3.14: Current source A and sink B cause potential difference at scalp electrodes and current density through the brain. Figure adapted from [69]

Furthermore, $I_{AB} = 1$ is a current that travels from electrode A to B through the brain as shown in Fig. 3.13-B. V_{AB} is the potential difference between scalp sensors A and B, and it is caused by a dipole with dipole moment d located at r.

Equation (3.27) measures the voltage difference V_{AB} between two EEG electrodes, and this equation can be applied to other pairs of electrodes as well. If

there are N_{ch} channels for EEG recording, then $N_{ch} - 1$ pairs of electrodes with independent potential difference can be defined. Therefore, $N_{ch} - 1$ numerical forward measurements can be obtained, and consequently, $N_{ch} - 1$ potential differences can be calculated [59]. This data is then used to calculate lead fields matrix in x, y, and z directions by transforming it into N_{ch} average reference potentials at N_{ch} EEG electrodes.

3.3.5 Inverse solution

As previously discussed, Fig. 3.8 illustrates how the scalp EEG signals are generated by source-level activities in the forward solution. In contrast, the EEG inverse solution aims to identify the source(s) responsible for the measured scalp potentials. This is an ill-posed problem due to its non-uniqueness and instability. To solve this, the cost-function is defined as the difference between the generated and measured scalp EEG and minimized accordingly.

I. The theory

In general, inverse solutions operate differently depending on the:

- type of forward model, and
- assumption used to minimize the cost-function parameters.

However, the way dipoles are used in the forward models plays a crucial role in the EEG inverse problem. A dipole is characterized by six parameters: three spatial coordinates and three moment components, which are then reduced by applying constraints on the sources. Different inverse approaches are introduced depending on the number of dipoles, as well as the number of them with fixed position, magnitude, and orientation [70]. Four examples of all possibilities are described below:

- an individual dipole; position, orientation, and magnitude are time-varying unknown,
- a fixed number of dipoles; positions and orientations are fixed unknown but amplitudes are varying,
- a fixed number of dipoles; positions are fixed, but orientations and amplitudes are varying,
- variable number of dipoles, but with a group of constraints.

Depending on the nature of forward modeling, inverse solutions are classified into 2 categories:

1. The parametric approach, the equivalent current dipole (ECD), also known as overdetermined (dipolar) models: it assumes EEG is generated by small numbers of focal sources, equal or fewer than the number of electrodes [71, 72]. The forward model is explained in Eq. (3.1).

2. The non-parametric approach, the distributed dipole approach, also known as underdetermined (distributed) source models: it considers all possible sources in the gray matter [73, 74, 75], and the forward model is characterized as Eq. (3.2).

Although ECD techniques may be suitable for focal EEG sources, they are sensitive to initialization parameters such as the number, location, and orientation of dipoles. In addition, there are other limitations to using ECD techniques, such as limited spatial resolution and dependence on electrode placement, that must be considered when analyzing epilepsy cases.

Because the distributed dipole approach does not require any prior assumptions, this solution was used throughout this dissertation. An infinite number of different dipole distributions within the head model can generate the same scalp EEG signals, resulting in a highly underdetermined inverse problem. Consequently, inverse solutions in literature apply different assumptions to identify the optimal or most likely solutions, with differences arising from constrains' choice and implementations.

The distributed dipole approach is an equivalent dipole solution where dipoles have fixed positions, and their strengths and orientations vary. Theoretically, a matrix that linearly relates the measured EEG to the estimated source solution can be introduced. Therefore, the equations representing distributed inverse solutions are linear, and they can reproduce the measured EEG from the 3D current source estimate. However, in practice, this situation does not hold due to the noise in the EEG data. Regularization parameters are necessary to cope with the noise and provide more stability to the solution [76].

In respect of the EEG inverse solution and considering Eq. (3.2),

$$\hat{J} = \min[F(J)]$$

where,

$$F(J) = \underbrace{||V - LJ||^2}_{\text{Data fit}} + \underbrace{\alpha f(J)}_{\text{Regularization}} \tag{3.28}$$

The terms *data fit* and *regularization* are key concepts that the inverse solutions uses. They represent various aspects of the optimization process for estimating neural sources from recorded scalp signals. Different inverse solution techniques differ in how they define the *data fit* and *regularization* terms. In general, these techniques use various methods to measure the agreement between the scalp EEG recordings and the predicted data that is based on the estimated neural sources. Additionally, these techniques apply different types of constraints and regularization to stabilize the solution and prevent over-fitting. For additional information on the EEG inverse solutions, please refer to article [77].

In the following, we will present some appropriate inverse solutions for the distributed dipole approach and investigate how they solve Eq. (3.28). These

techniques include Minimum Norm (MN), Weighted Minimum Norm (WMN), Low Resolution Electromagnetic Tomography (LORETA), and Standardized Low Resolution Brain Electromagnetic Tomography (sLORETA).

II. Minimum Norm (MN)

Minimum norm is the general estimation of the dipole solutions without any a priori information [78]. This technique assumes that the current distributions have the minimum overall intensity. However, the assumption is not physiologically always valid. Its solution is unique, and saying only one combination of sources can generate the lowest overall intensity that fits data simultaneously. Consequently, this method mainly localizes the superficial sources since they can generate a certain current distribution with fewer activities. The solution of this technique for a given α is as following:

$$\hat{J}_{MN} = L^T(LL^T + \alpha I_N)^{-1}V \tag{3.29}$$

III. Weighted Minimum Norm (WMN)

WMN was designed to address the issue of MN localizing superficial sources. Various weighting strategies have been proposed in the literature, such as PROMS [79], FOCUSS (Focal Underdetermined System Solution) algorithm [80], and RWMN (radially weighted minimum norm solution) [81]. Although all of the weighting solutions mentioned above overcome the problem of surface-oriented MN, they are purely mathematical solutions without any physiological explanation. Based on a given α, the solution is:

$$\hat{J}_{WMN} = (W^TW)^{-1}L^T(L(W^TW)^{-1}L^T + \alpha I_N)^{-1}V \tag{3.30}$$

where

$$W = \Omega^2 \otimes I_3$$

and $\otimes$ denotes the Kronecker product and I_3 is the 3x3 identity matrix. By considering M dipoles, N_{ch} EEG channels, and introducing Ω as a diagonal MxM matrix,

$$\Omega_{\beta\beta} = \sqrt{\sum_{n=1}^{N_{ch}} l_{n\beta}^T l_{n\beta}}, \forall\beta = 1, ..., M$$

Considering n^{th} row of the lead fields matrix is $(l_{n1}^T, l_{n2}^T, ..., l_{nM}^T)$ where $n = 1, ..., N_{ch}$, then,

$$l_{n\beta} = (l_{xn\beta}, l_{yn\beta}, l_{zn\beta})^T$$

The lead field matrix strength is reflected in the weighting matrix, resulting in an equally valid solution where deep and superficial sources occur with the same probability.

IV. LORETA

More advanced techniques introduced constraints to ensure spatial coherence and smoothness. LORETA, as an inverse solution, merges the normalization of the lead field with the Laplacian operator to achieve this objective [82]. This approach provides the current distribution of the entire brain without limiting the volume of solutions. As previously discussed, EEG scalp measurements lack information about the generators, resulting in an infinite set of possible solutions for inverse solutions. LORETA assumes simultaneous and synchronous activity for neighboring neurons, helping find a unique solution for the 3D current distribution. The single-cell recordings and synchronized activities in adjacent neurons confirmed the assumption. The solution of this approach is:

$$\hat{J}_{LOR} = (B\Delta^T\Delta B)^{-1}L^T(L(B\Delta^T\Delta B)^{-1}L^T + \alpha I_N)^{-1}V \tag{3.31}$$

that:

$$B = \frac{6}{d^2}(A - I_{3M})$$

$$A = A_0 \otimes I_3$$

$$A_0 = [diag(A_1 1_M)]^{-1}A_1$$

$$[A_1]_{\gamma\beta} = \left\{ \begin{matrix} 1/6, & if||v_\gamma - v_\beta|| = d \\ 0, & otherwiose \end{matrix} \right\}, \forall\gamma, \beta = 1, ..., M$$

the term v is the voxel in the space solution and d represents the minimum distance between grid points.

V. sLORETA

Standardized low resolution brain electromagnetic tomography (sLORETA) is a modified version of LORETA that does not use the Laplacian operator [83]. However, it works similarly to the approach Dale et al. developed [84]. Here, localization is based on the images of standardized current density. It uses the current density estimated by the minimum norm and standardizes it. To make this happen, sLORETA uses variance and variations of the current density that achieves zero-error localization. The solution of this method is:

$$\hat{J}_{sLOR} = L^T H(HLL^T H + \alpha H)^{-1}V \tag{3.32}$$

where

$$H = I - 11^T/1^T 1$$

and $H \in \mathbb{R}^{N_{ch}\times N_{ch}}$ is the centering matrix, $1 \in \mathbb{R}^{N_{ch}\times 1}$ is a vector of ones, and $I \in \mathbb{R}^{N_{ch}\times N_{ch}}$ is an identity matrix.

Chapter 4

Automated Interictal ESI

The universe is not outside of you. Look inside yourself; everything that you want, you already are.

Rumi

4.1 Introduction

In this chapter, we focused on the EZ localization through the interictal ESI analysis. We introduced our in-house automated interictal ESI pipeline, PreOp, which has been clinically validated and utilized in several retrospective and prospective studies on different patient cohorts. The structure of this chapter is as follows:

1. we delivered the complete manuscripts of the clinical validation study of PreOp,
2. we assessed the impact of various electrodes on the ESI results,
3. we examined PreOp to localize insular epilepsy patients, which is a challenging task due to the complex anatomy of the insula,
4. we presented the first prospective study using PreOp on MRI-negative epilepsy patients,
5. we presented the second prospective study, where PreOp performed the ESI analysis over a 4-year period,
6. we presented the third prospective study, PROMAESIS, where 17 European epilepsy centers joined to evaluate the clinical performance of automated ESI in presurgical epilepsy evaluation,
7. we evaluated the time aspect of automated ESI analysis to integrate it into the clinical setups.

8. Finally, the overall performance of PreOp was assessed in all studies using this pipeline.

4.2 Automated Interictal ESI; clinical validation study

Title: "Automated EEG source imaging: A retrospective, blinded clinical validation study"

4.2.1 Introduction

Approximately 1/3 of patients with epilepsy are drug-resistant [85]. In this patient group, epilepsy surgery of the presumed epileptogenic focus is currently the treatment option with highest efficacy [86, 15, 16]. However, accurate localization of the epileptic focus is often challenging. Since there is no single-modality that reliably can localize the area that needs to be resected in order to render the patient seizure-free (EZ, epileptogenic zone), the presurgical evaluation is based on a multimodal approach [87]. This comprises semiology, EEG (obtained during long-term video-EEG monitoring), magnetic resonance imaging (MRI), and in selected cases positron emission tomography (PET), single photon emission computed tomography (SPECT) and magnetoencephalography (MEG).

Using this approach, only half of the investigated patients can be operated and of them only 2/3 become seizure free [88, 89]. Thus, there is need for additional methods, using post-processing and signal analysis that help localizing the EZ. EEG source imaging (ESI) estimates the underlying brain activity from the measured EEG, using an electric conduction model built from the patient‘s MRI. The value of ESI in the presurgical evaluation to localize the EZ has already been shown in several studies [90, 101, 104, 30, 105, 106, 107, 108, 109, 91, 92, 93, 94, 95, 96, 97, 98, 99, 100, 102, 103]. Methods based on high-density (HD) EEG recordings and using individual head models (derived from the patient´s own MRI) proved more accurate than low-density (LD) recordings and models using template head models [30].

In spite of the published compelling evidence on the accuracy of ESI, its use has not gained wide acceptance in clinical practice. In a recently published study, the E-pilepsy consortium showed that only 36% (9/25) of the European centers included ESI into their presurgical workup [110]. This is mainly because ESI is considered time-consuming and it requires special expertise in signal analysis that is not available in all centers. HD-EEG is typically recorded only for a few hours, since it is less feasible for long-term monitoring [111]. To overcome these obstacles and to contribute to more widespread use of ESI in presurgical evaluation, we have recently developed a fully automated process for identification and subsequent source localization of IEDs from long-term low-density EEG recordings [99]. Since almost all patients included in the presurgical evaluation undergo long-term EEG monitoring, preferably recorded using the standard electrode array setup of the IFCN [40], and MRI scanning, these datasets are widely available in the epilepsy centers worldwide.

In this study, we present a clinical validation study on 41 operated patients using the automated method to detect and localize IEDs. As reference standard, we used the location of the surgical resection and postoperative outcome. Our goal was to determine the localization accuracy at sub-lobar level of the automated ESI method. Although the analysis was done retrospectively, it was blinded to all data other than the EEG recordings. Furthermore, the analyzed dataset was from a different institution than the ones where the automated method was developed. We present our results according to the STARD criteria [112].

4.2.2 Methods

I. Patients and recordings

De-identified EEG and MRI data, from consecutive patients were analyzed retrospectively. These data were recorded as part of the clinical workup of the patients. Inclusion criteria were: patients with (1) drug-resistant focal epilepsy, (2) admitted to the Epilepsy Monitoring Unit (EMU) as part of the presurgical evaluation, (3) who underwent resective surgery, and (4) with postoperative follow-up of at least one year. Exclusion criterion was the lack of MRI sequences necessary for constructing the individual head model (see below). Patients gave their informed consent prior to admission to the EMU.

EEG was recorded at the Danish Epilepsy Centre, using the standardized IFCN array of 25 electrodes, including six electrodes in the inferior temporal chain (F9/10, T9/10 and P9/10) in addition to the 19 electrodes of the 10–20 system [40]. Electrode impedance was kept below 5KX. EEG was recorded with a sampling frequency of 256 Hz, using the NicoletOne system. For each patient, the complete, available EEG recording was analyzed (i.e. we did not select or exclude any EEG data).

MRI examination was done at Department of Radiology, Hvidovre Hospital, 3 T Siemens scanner. T1-3D-MPR-sequence was used for constructing the individual head models.

II. The analysis pipeline

De-identified long-term EEG and MRI data were analyzed using Epilog PreOp (Epilog NV, Ghent, Belgium). The analysis consists of automated spike detection, clustering of single detected spikes based on their morphology, and finally ESI analysis of the detected spikes at two time points: the half-rising time and the peak of the averaged spike waveforms. The whole analysis was performed blinded to all other data (clinical and para-clinical data, information on surgery and outcome). Fig. 4.1 shows the analysis pipeline.

III. Automated spike detection

Automated spike detection was performed using the Persyst Spike Detector P13 (Persyst, San Diego, CA, USA). Detected events with a spike-probability lower than 0.5 were rejected. After band-pass filtering the spikes from 0.5 to

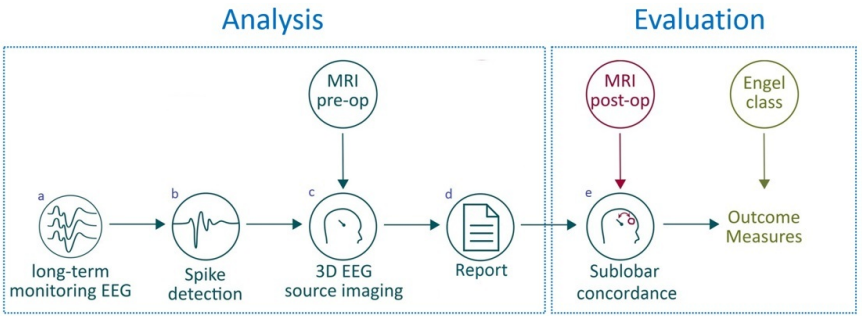

Figure 4.1: The automated ESI (Epilog PreOp) pipeline: (a) recording long-term EEG signals, (b) detecting spikes using Persyst P13 spike detector, clustering them and averaging afterwards, (c) building patient-specific head model from the pre-operative MRI to perform ESI, (d) generating a report that summarizes the findings and (e) comparing the spike-clusters depicted in the report with the resection zone.

30 Hz, those that contained a bad channel (i.e. a channel with a standard deviation that exceeds five times the median standard deviation of all channels) were excluded. The signals were baseline- corrected in a period of 200–100 ms before the peak of the spike. Afterwards, the spikes were averaged for each detected cluster and clusters were merged if the scalp topography at the peak had a correlation higher than 0.9. Clusters with less than 15 single spikes were excluded from further analysis. Up to four spike-clusters, with the highest number of spikes were further analyzed. The spikes within each cluster were averaged to increase signal-to-noise ratio [102].

Previously published, large-scale studies showed that although patients with focal epilepsy may have several interictal spike-clusters, analysis of the dominant cluster accurately localized the EZ [30]. However, criteria for determining the dominant spike-cluster have not been defined until now. We used two different criteria to determine which spike-cluster was dominant: quantitative and qualitative criteria. The quantitative criterion assumed that the cluster with much higher number of spikes, compared to the other clusters was the dominant one. Thus, we considered a spike-cluster as quantitatively dominant if it contained at least twice as many spikes as all other clusters. When none of the identified clusters fulfilled this criterion, the patient was considered multifocal. The qualitative criteria aimed at reproducing the clinical reasoning, according to which each information is set into the broad clinical context, and weighed against all other data. Selection of the qualitatively dominant spike-cluster was done after completion of the automated analysis, by a physician in charge with the presurgical workup of the patients, and hence un-blinded to the clinical context.

IV. Individual head model and inverse solution

For each patient, an individual head model with a 1 x 1 x 1 mm resolution was constructed from the T1-weighted MR image. The head model consisted of

six different tissues (scalp, skull, cerebrospinal fluid, grey matter, white matter and air) [113, 98]. To this end, each tissue probability map was estimated in the statistical parametric mapping software (SPM12). After smoothing, the maps were combined to form the head model. The skull thickness was set to a minimum of three voxels to ensure that no skull holes existed in the head models. The electrodes were placed on the head-model using the following procedure: (1) a 3D model was generated of the head model; (2) the nasion, inion and electrodes T7/T8, FT9/10, TP9/10 were marked on the 3D model; (3) the distances between the marked points over the surface of the head was used to place the other electrodes at inter-distances defined according to the 10– 20 system; (4) visual inspection of the electrodes was done and if necessary individual electrodes were slightly moved to ensure correct placement of each electrode. (In some cases, we noticed that the position of electrodes P3 and P4 was slightly too lateral: because of the head curvature at that position the algorithm put them a bit too lateral. In these cases, we moved the electrodes slightly more central, but never more than 1 cm. For all other electrodes the positioning was kept as calculated). Afterwards, dipoles were placed in the gray matter with 3 mm spacing and the finite difference method was used to compute the leadfields that describe the relation between the current dipoles in the gray matter and the measured scalp EEG [59, 114, 115].

The source of each spike-cluster was localized at the half-rising time and at the peak of the spikes using sLORETA as inverse technique [83].

V. ESI reporting format

The Epilog ESI reports summarized the results of the automated analyses. The first page gives an overview of the detected spike-clusters together with the spike lateralization, spike timing and spike interval diagram. Then, for each cluster, the averaged and the ten most representative spikes are shown in both referential and bipolar montages. In the next pages, the EEG source localization at half-rising time and at peak are shown, both for the averaged spike and for 100 single spike-events that have most similar morphology compared to the averaged spike.

After completing the automated analyses, ESI reports were forwarded to the physician, who evaluated the automatically detected clusters, classifying them as epileptiform or non-epileptiform (artifacts), and then the qualitatively dominant clusters were identified as described above. In addition, depending on the clinical context, the physician could choose the ESI either at the half-rise time or at the peak.

This procedure resulted in two sets of results: those derived from the fully automated process (automated ESI, quantitative determination of the dominant cluster and analysis always at the half-rise time) and the results of the semi-automated approach (automated ESI, then selection of the dominant cluster and of the analysis time-point by the physician, in the clinical context). Non-dominant clusters and especially artifacts were more widely scattered than the spikes of the dominant clusters. This was taken into consideration

when assessing the analysis reports. Three check boxes were included for each cluster (genuine spike, artefact, physiological) allowing the clinician to interpret and classify the clusters.

VI. Reference standard

For evaluating the accuracy of the ESI, we used as reference standard the resected area and the outcome one year after surgery. All locations were determined at sub-lobar level [116]. Patients with several clusters but without a dominant cluster were considered multifocal. Although distributed source models (such as sLORETA) result in spatially extended sources, similar to previous studies [30] we determined the location of the sources at the maxima automatically indicated by the cross-hair in the source images. When this was inside the resected region, the localization was considered positive. Patients were considered seizure-free if they were Engel class I, at one year post-operative follow-up. Results of the index test (ESI) were classified as follows: True Positive (TP): source within the resected area and seizure free outcome; False Positive (FP): source within the resected area and not seizure free outcome; True Negative (TN): source outside the resected area and not seizure free outcome; False Negative (FN): source outside the resected area and seizure free outcome. All patients with multifocal ESI and all patients without any spike-clusters were considered negative (i.e. discordant with the resected area).

VII. Outcome measures

We calculated sensitivity, specificity, overall accuracy, positive predictive value (PPV), negative predictive value (NPV), and Odd's Ratio (OR) according to the conventional formulae:

$$sensitivity = \frac{TP}{TP + FN}$$

$$specificity = \frac{TN}{TN + FP}$$

$$overalaccuracy = \frac{TP + TN}{TP + FP + TN + FN}$$

$$PPV = \frac{TP}{TP + FP}$$

$$NPV = \frac{TN}{TN + FN}$$

$$OR = \frac{sensitivity \times specificity}{(1 - sensitivity) \times (1 - specificity)}$$

95% confidence interval (95% CI) of a parameter was determined based on its standard error:

$$parameter \quad standard \quad error \quad = \sqrt{\frac{parameter \times (1 - parameter)}{sample \quad size}}$$

$$95\% \quad CI \quad = parameter \pm 1.96 \times parameter \quad standard \quad error$$

Where 1.96 expresses the normal distribution measure for 95% confidence interval. It could be used to measure intervals of sensitivity, specificity, accuracy, PPV and NPV [117, 118]. However, calculation of 95% CI for OR was done according to the definitions described below [119]:

$$standard \quad error \quad (log(OR)) = \sqrt{\frac{1}{TP} + \frac{1}{TN} + \frac{1}{FP} + \frac{1}{FN}}$$

$$95\% \quad CI \quad (OR) = \exp(log(OR) + 1.96 \times standard \quad error \quad (log(OR)))$$

4.2.3 Results

Out of 42 consecutive operated patients fulfilling the inclusion criteria, one patient was excluded due to the lack of a suitable MRI (Fig. 4.2). For this patient only CT imaging was available and not MRI. Data of 41 patients were analyzed (24 female; age: 12– 55 years, median: 43 years, duration of analyzed EEG recording: 29 ± 3.9 h). Fourteen patients (34.1%) had normal MRI. Twenty-eight patients (68.3%) had temporal and 13 patients (31.7%) had extratemporal resections (six frontal, two parietal, two occipital, one mesial parieto-occipital, one insular and one operculo-insular resection). Twenty-five patients (61%) were seizure-free at one year follow-up.

In two patients, no interictal epileptiform discharges occurred during the LTM. Twelve patients had a single spike-cluster. In 22 patients, a dominant spike-cluster was identified using the quantitative criterion. In five patients with multiple clusters, none of them fulfilled the quantitative criterion for dominant cluster, and were classified as multifocal (thus discordant with the resection site).

Figs. 4.3 and 4.4 show the results of the ESI of a patient with temporal and respectively extratemporal focus.

Table 4.1 summarizes the outcome measures. Using the fully automated method (quantitatively defined dominant cluster and analysis at half-rise time) gave an accuracy of 61%. In the semi-automated method, where physicians were allowed to choose the dominant cluster and the time-point of analysis (half-rise or peak) but still with automated detection and ESI, yielded an accuracy of 78%. The physician changed the choices of the fully automated method in seven patients (in one case the analysis time-point, in two cases the dominant cluster and in four cases both the time-point and the dominant cluster). Although artifacts were often detected, they rarely were

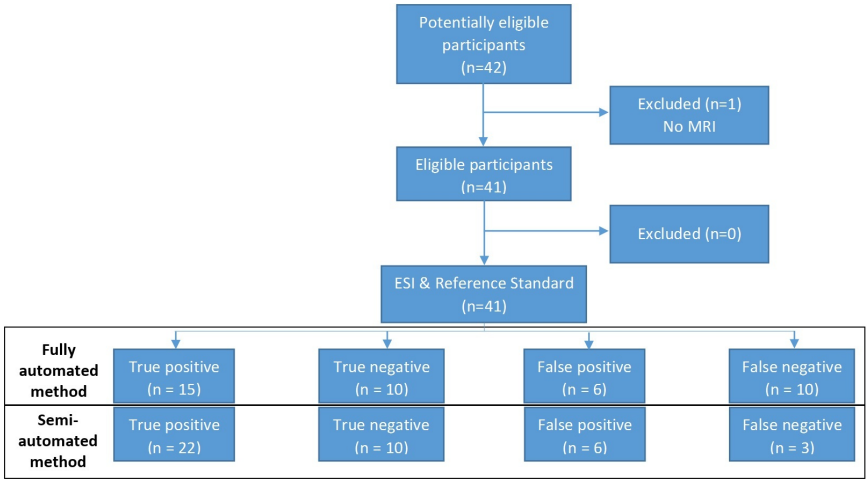

Figure 4.2: Study flowchart. The fully automated method included: automated ESI of the spike-cluster with quantitatively identified cluster, at the half-rising time. The semi-automated method included: automated ESI and manual selection of the dominant cluster and analysis time-point (either half-rise or peak).

the quantitatively dominant clusters. In three of the cases where the users overruled the quantitatively dominant spike, this was due to artifacts.

	Fully-automated method	Semi-automated method
Accuracy (95% CI)	61% (45–76%)	78% (62–89%)
Sensitivity (95% CI)	60% (41–79%)	88% (75–100%)
Specificity (95% CI)	63% (39–85%)	63% (39–85%)
PPV (95% CI)	71% (52–91%)	79% (63–94%)
NPV (95% CI)	50% (28–72%)	77% (54–100%)
Odds ratio	2.5 (0.7–9.1)	12.2 (2.5–59)

Table 4.1: Accuracy measures of the automated ESI. Abbreviations: PPV = positive predictive value, NPV = negative predictive value.

4.2.4 Discussion

In this study, we validated the performance of automated long-term EEG analysis [99] to localize the EZ. The algorithm detected interictal epileptiform discharges in the long-term EEG, clustered them and subsequently localized them using a realistic, patient-specific head model, built from the patient's MRI. The results were summarized in a concise report that was evaluated by a physician who was in charge with the presurgical evaluation of the patients. We evaluated two ways of implementing the automated ESI: a fully automated approach (quantitatively defined dominant cluster, analysis at half-rise) and a semi-automated approach, in which the physician was allowed to choose the dominant cluster and the analysis time-point (half-rise or peak).

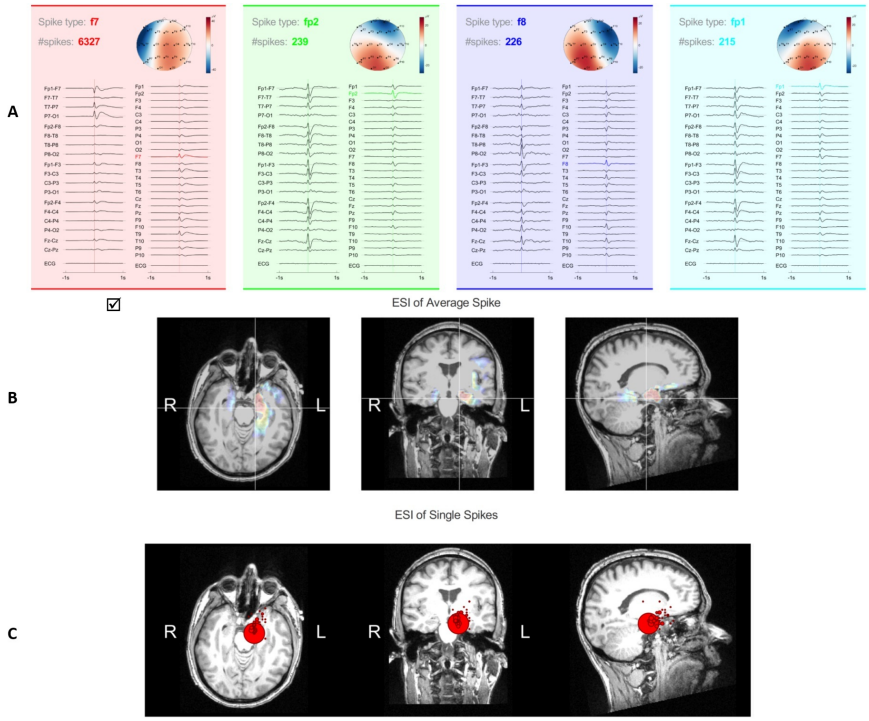

Figure 4.3: ESI in a patient with temporal focus (patient #8). A: Four automatically detected spike-clusters. For each cluster, the following data are shown: name of the electrode closest to the peak-negativity, the number of spikes in the cluster, the averaged waveform (in longitudinal bipolar and referential montages) and the voltage map. Note that the first cluster is quantitatively dominant (it contains almost 10 times as many spikes as the other three clusters together). The same cluster was considered dominant by the physician who interpreted this in the clinical context (choice of the qualitative dominant spike is shown in the checkbox below the spike-cluster). B and C: Results of the automated ESI of the dominant spike-cluster, at the half-rise time of the averaged waveform (maximum localized at the crosshair) (B) and of the individual spikes in the cluster (C), respectively. Note that both the maximum of the averaged waveform, and the majority of the individual spikes (red circle) indicate a source in the left mesial temporal region, which was in concordance with the resection site. The pathological examination showed hippocampal sclerosis. The patient was seizure-free (Engel I) at the one-year postoperative follow-up. (For interpretation of the references to colour in this figure legend, the reader is referred to the web version of this article.)

The fully automated approach yielded an accuracy of 61% (sensitivity: 60%, specificity, 63%). The semi-automated approach had better results (accuracy: 78%; sensitivity: 88%, specificity: 63%).

There are several important differences with respect to the previous study of automated ESI [99]. First of all, in this study, analysis was done completely blinded with respect to patients' outcome. Only the anonymized, unmarked

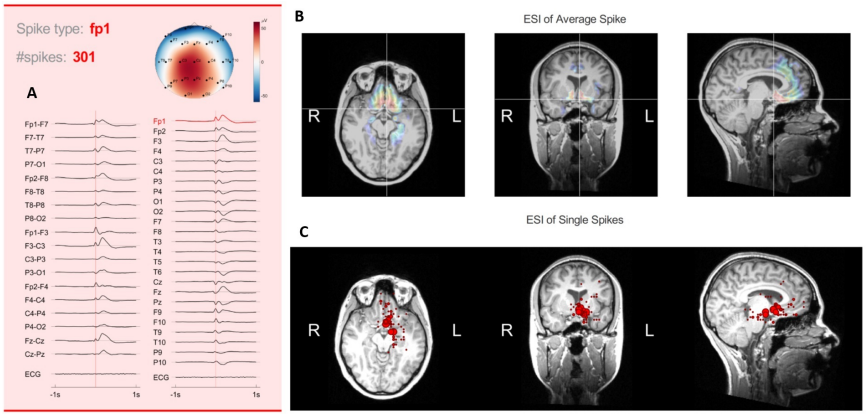

Figure 4.4: ESI in a patient with frontal focus (patient #34). A: The automatically detected spike-cluster, specifying the name of the electrode closest to the peak-negativity, the number of spikes in the cluster, the averaged waveform (in longitudinal and referential montages) and the voltage map. In this patient, two clusters were automatically detected, but the second cluster was artifact. B and C: Results of the automated ESI, at the half-rise time of the averaged waveform (maximum localized at the crosshair) (B) and of the individual spikes in the cluster (C). Note that both the maximum of the averaged waveform, and the majority of the individual spikes (red circle) indicate a source in the left frontal basal-mesial region, which was in concordance with the resection site. The pathological examination showed focal cortical dysplasia (type IIb). The patient was seizure-free (Engel I) at the one-year postoperative follow-up. (For interpretation of the references to colour in this figure legend, the reader is referred to the web version of this article.)

EEG recordings and T1-weighted MRI were included into the analysis dataset. The ESI-reports were made without any prior information and sent to the treating clinician, and then compared with the reference standard. Furthermore, the dataset used in this study was recorded in a different epilepsy center than those where the algorithm was developed, meaning that there is clear separation between the data used to develop the algorithm and the data used in this study to validate its performance. The algorithm was fixed upfront and was not tweaked based on the validation data. In this study, the concordance with the resection site (inside or outside the resected area) was used instead of the distance to the border of the resection to assess the clinical utility of the method.

An important finding of this study is that it identified two aspects that could not be optimally automated, and that needed intervention (decision) by the physician: the choice of the dominant cluster and the analysis time-point. This user-intervention was post-analysis, it was not time-consuming and did not need special expertise in signal analysis, since that part was automated. However, this step introduced subjective decisions and information outside ESI into the semi-automated analysis. This is a potential source of bias and we

would like to point out that it is an important limitation of the semi-automated method.

In all large studies in literature, the EZ was estimated by localizing the dominant spike-cluster [30, 92]. However, the term "dominant cluster" was never precisely defined. We built the fully automated method on the assumption that the cluster with the highest number of spikes is the dominant one. Our results showed that this was not always the case.

In this study, we use both a quantitative and qualitative definition of the dominant cluster, demonstrating that interpretation of the ESI results based on the clinical context, improves its performance. This is in accordance with the clinical decision process in which data are weighed against all other available data. Moreover, since the frequency of spikes in different clusters can change significantly throughout the long-term monitoring [120], the timing of the analyzed recording determines which cluster is quantitatively dominant: a cluster can contain many spikes one day, can only have few spikes the next day. In our study the mean duration of the EEG that was analyzed was 29 h. This ensures that a more general view of the occurrence of spikes was achieved compared to short recordings of 30 min to 1 h.

The other aspect that needs assessment by the physician is the time-point of the analysis. The half-rising time has previously been suggested as an ideal choice, because it is closer to the onset and the signal-to-noise ratio (SNR) is satisfactory in most clusters [121]. A problem with this strategy is that the spikes are averaged aligned to the peak time-point. Even within the same cluster, the morphology and duration of single spikes can vary. The further away from the peak the analysis is performed, the more variance (jitter) is introduced into the averaged signal (Fig. 4.5). This is consistent with a previous study that found source localization more reliable at the peak than at onset, in a sub-group of patients [122]. Although the signal of the peak can be generated by brain areas to which the epileptic activity propagates from the EZ, peak has some advantages: the signal-to-noise ratio at the peak is higher than the one of the onset and half-rising, and, the jitter is lower, since spikes are averaged aligned to the peak. This explains why in five patients in this study, a better result was obtained at the peak of the spike compared to the half-rising time.

Because there is no reliable objective (automated) way to determine which cluster is the dominant one, and whether ESI is better at half-rise or at peak, optimally these decisions are taken by the physician, in the clinical context. This approach improves the performance of the automated ESI. Because the ESI reports include all necessary information for the clinicians, only a short time investment is necessary to make these choices. This removes the significant time-burden of the analysis process, and makes this approach feasible in a busy clinical setting.

Due to their architecture and the closed fields, spikes confined to amygdala and hippocampus do not generate signals of amplitude high enough to cross

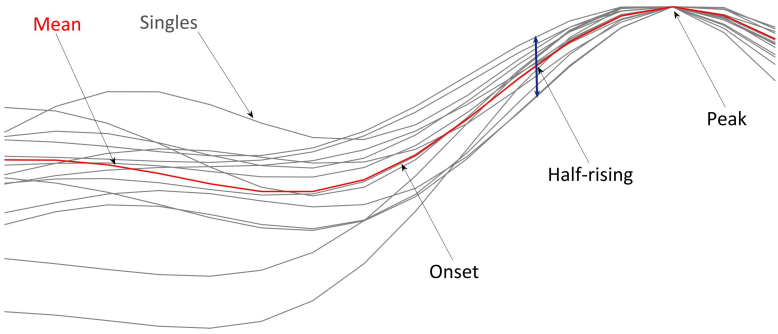

Figure 4.5: Superposition of the single-spikes in a cluster of spikes. Note that the jitter (difference between the single-spikes) is larger at the half-rising time-point compared to peak.

the scalp and these signals are not recorded by scalp electrodes, thus, these generators cannot be localized. This is an intrinsic limitation to any source imaging method. The maxima (cross-hair) of the mesial temporal sources we detected (like the one in 4.3) were in the nearby neocortical structures in the mesial part of the temporal lobe: the parahippocampal gyrus and the fusiform gyrus. Due to averaging of large numbers of spikes within each cluster, the signal-to-noise ratio is considerably improved, making possible localization of signals of lower amplitudes (like the middle third of the spike). This is in accordance with previously published large-scale studies that localized mesial temporal sources using distributed source models [30].

The performance of EEG source imaging for localization of the EZ has previously been evaluated in several studies (Table 4.2). Brodbeck et al., 2011 ([30]), indicated a sensitivity and specificity of 66% and 59% (n = 98) using low density EEG recordings, which increased to 84% and 88% (n = 52) using high density EEG. van Mierlo et al., 2017 ([99]) analyzed low density ESI and they reported the values of 70% and 100% for sensitivity and specificity when peak of the first cluster was analyzed. By considering the first two clusters however, the sensitivity increased to 79% and specificity decreased to 75%. A recently published prospective study using the same electrode-array (IFCN 25 electrode array) found that ESI had an accuracy of 57–62%, which was in the same range as the conventional neuroimaging: MRI (55%), PET (33%) and SPECT (40%) [123]. This emphasizes the need for multimodal approach, since none of the methods achieves a sufficient accuracy on its own. Mégevand et al., 2014 ([94]) and Lascano et al., 2016 ([92]) used HD-ESI which lead to sensitivity and specificity of 80% and 59% (n = 32) or 88% and 47% (n = 58), respectively. However, working with HD EEG recording requires its specific setup, which is not broadly available. A potential bias in the HD-EEG is related to the patient-selection, since patients without spikes in the long-term monitoring, are typically not referred to the short duration (30–60 min) HD-EEG recordings. This might have led to an overestimation of its performance, since normal EEG recordings were not included into the

evaluation of HD-EEG.

Study	LD-ESI			HD-ESI		
	Sens	Spec	N	Sens	Spec	N
Mégevand et al. 2014	-	-	-	80%	59%	32
Brodbeck et al. 2011	66%	59%	98	84%	88%	52
Lascano et al. 2016	-	-	-	88%	47%	58
van Mierlo et al. 2017	70%	100%	32	-	-	-
Sharma et al. 2018	63%	47%	47	-	-	-
Baroumand et al. 2018 (this study)	FA: 60%	FA: 63%	41	-	-	-
	SA: 88%	SA: 63%		-	-	-

Table 4.2: Performance of ESI for localization of EZ in some studies with the sample rates >20 patients. Abbreviations: LD = low-density, HD = high density, N = number of patients, Sens: sensitivity, Spec: specificity, FA: fully-automated, SA: semi-automated.

The performance of the ESI methods, including the automated methods described in this paper, are comparable (or even better) than the conventional neuroimaging methods. Nevertheless, each method delivers part of the complete picture. We cannot tell up front which investigation will be meaningful in which patient. Therefore, the inclusion of more techniques in the presurgical evaluation is beneficial for the localization of the EZ.

The added value of ESI could not be inferred from our retrospective dataset. Our study addressed the accuracy and not the clinical utility. A recently published systematic review and IFCN guideline on the utility of EEG in diagnosing and monitoring epilepsy [124] concluded that in spite of the compelling published evidence for the accuracy of ESI, there is lack of evidence for its clinical utility (i.e. diagnostic added value). Prospective studies, in which the multidisciplinary epilepsy surgery team makes first a preliminary decision blinded to the ESI data, and then modifies the decision based on ESI data are needed to elucidate the clinical utility of ESI.

The input data to our automated ESI (long-term EEG using $\geq$ 25 electrodes and T1-weighted MRI) are largely available in most centers doing presurgical evaluation, this method can be added to the multimodal work-up without additional time-burden. We hope that automating the analysis pipeline will contribute to increased utilization of ESI in the epilepsy centers.

4.3 The impact of electrode setup on automated interictal ESI

4.3.1 Introduction

The location and number of EEG channels are crucial for automated spike detection. In theory, using more EEG electrodes increases the likelihood of detecting genuine spikes and decreases the localization error. Additionally, it

is important to investigate the ESI results of the same event recorded with different EEG setups. In this chapter, we studied the impact of various EEG setups on the interictal ESI results, combining the above objectives. ESI with more electrodes leads to lower localization errors.

4.3.2 Methods

This study included 30 patients with refractory focal epilepsy who underwent 257-channel EEG recordings at Hôpitaux Universitaires de Genève (HUG), Switzerland. The EEG recording was down-sampled to 204, 40, and 25 channels for each respective recording (Fig. 4.6).

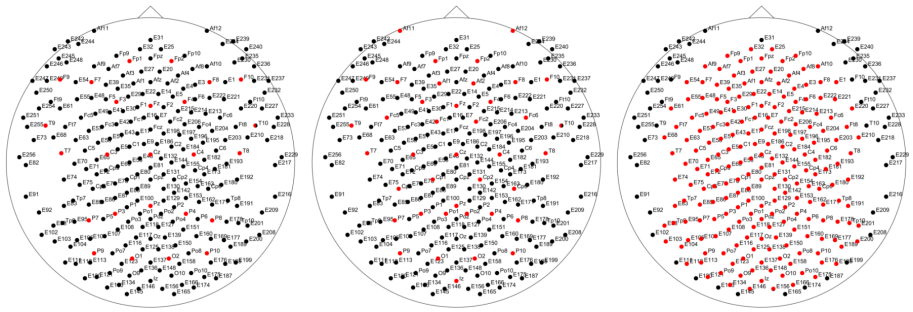

Figure 4.6: 2D visualization of EEG setups with 25 (left), 40 (center), and 204 (right) electrodes, highlighted in red, and compared to 257-electrode setup. Figure adapted from [125].

First, automated spike detection is applied to each EEG setup, followed by the application of our automated interictal ESI analysis. Figure 4.7 gives an overview of the pipeline. The analysis results of each setup was presented in a PDF file, resulting in four reports per patient. The epileptologist reviewed spike detection and ESI results and compared them to post-operative MRI after one year of clinical follow-up. ESI outcomes were evaluated both at the sub-lobar level and in comparison with the resection region. During this period, 18 patients were either seizure-free or experienced auras, while 12 patients continued to have seizures.

4.3.3 Results

Epileptic spike detection occurred in 21 patients using EEG setups with 25, 204, and 257 channels and in 24 patients using 40 channels. The automated spike detector detected epileptic discharges in the 10-10 electrodes. However, the quality of EEG signals had a significant impact on the detector's sensitivity. To address this, we had to exclude all bad channels before running the detector. In HD recordings with more electrodes, we had to exclude more channels from the 204- and 257-channel setups before detecting spikes. In terms of low-density setups, detecting an epileptic event was more reasonable in the 40-channel setup than in the 25-channel setup. However, existing channels were less common in these low-density setups, which could explain why more

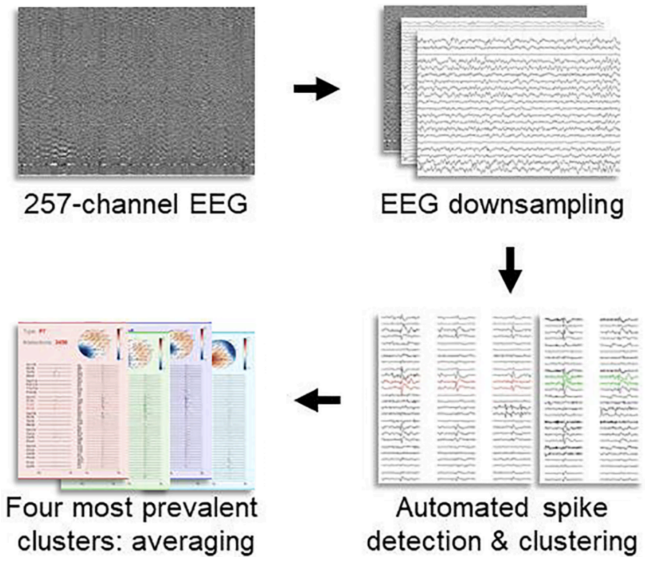

Figure 4.7: The processing pipeline: Automated spike detection was used on four EEG setups after down-sampling HD-EEG. All detections were post-processed and clustered into up to four groups. Then, ESI was applied to each cluster. Figure adapted from [125].

patients had genuine spikes in the setup with 40 channels. This resulted in overall accuracy rates ranging from 34% to 41% for spike detection (Fig. 4.8).

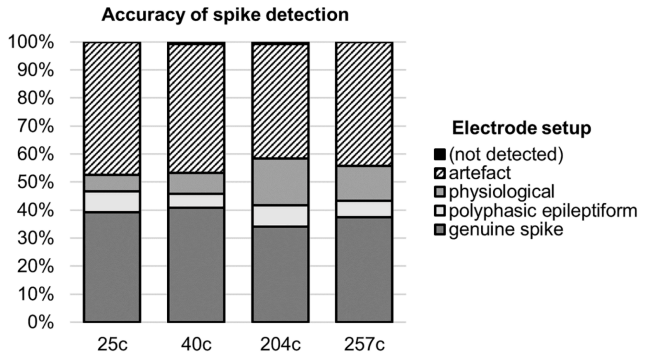

Figure 4.8: Demonstration of spike detection accuracy across all clusters of each setup. Figure adapted from [125].

For each setup and patient, the ESI evaluation was based on the genuine spike clusters with the highest number of detections. The ESI results were evaluated for concordance with the resected zone at various levels - sub-lobe, lobe, hemispheric and contralateral - for both favorable (ILAE class 1-2) and unfavorable (ILAE 3-5) postsurgical seizure outcomes, by selecting the half-rising time point as the basis for the outcomes (Fig. 4.9-top). Comparing

the ESI localization at the half-rising phase to the resection at the sublobar level led to the sensitivity and specificity varied between 58-75% and 50-67%, respectively. The result of this leads to an accuracy in the range of 55-71%. Moreover, performance assessment with respect to the resection volume retrieved from post-operative MRI led to a sensitivity of 40-68%, specificity of 67-80%, and accuracy of 54-72%. (Fig. 4.9-middle and 4.9-bottom). There were no significant differences noted between low- and high-density EEG setups.

4.3.4 Conclusion

Out of all the setups, the 204-channel setup has the lowest performance when it comes to detecting genuine epileptic spikes. As seen in Fig. 4.6-center, this setup lacks electrodes T9/10, Ft9/10, F9/10, and Af11/12, which are essential for capturing genuine epileptic spikes, particularly in patients with temporal lobe epilepsy. This could explain why the 204-channel setup performs less in detection and ESI procedures. Regarding performance within the sub-lobar level and resection zone, the 25-channel and 40-channel setups have the same overall accuracy. They are also comparable to the 257-channel setup's results. However, the 40-channel setup performed more effectively since it worked for three more patients. Low-density EEG can be used for interictal ESI if many spikes are available, showing it is comparable to high-density EEG.

For further information on this study, please refer to [125].

4.4 Interictal ESI for insular irritative zone localization

4.4.1 Introduction

Detecting epileptic activities originating from the insula in scalp EEG recordings is challenging. This is especially important for patients who have insular epilepsy. This section assesses PreOp's performance for localizing the IZ from long-term clinical EEG data and compares the results with stereo-EEG interictal activity.

4.4.2 Methods

The study included thirty patients who underwent iEEG and had at least one depth electrode that explored the operculo-insular area (Saint Luc University Hospital, Brussels, Belgium). Scalp EEG acquisition was performed using standard 10-20 montage and for some cases the inferior temporal chain electrodes T1/2, Ft9/10, and Tp9/10 were included. In addition, all patients underwent iEEG using depth electrodes, with some also using subdural grid or strip electrodes (Fig. 4.10). Subject-specific automated interictal ESI was applied on the long-term EEG and MRI. Electrodes T1/2 were excluded from the analysis because the location did not match the IFCN electrode setup.

The results were evaluated through a two-level analysis. In the first level, the outcomes of ESI from the first four clusters with the highest number of detections at both half-rising and peak were compared with sEEG electrode

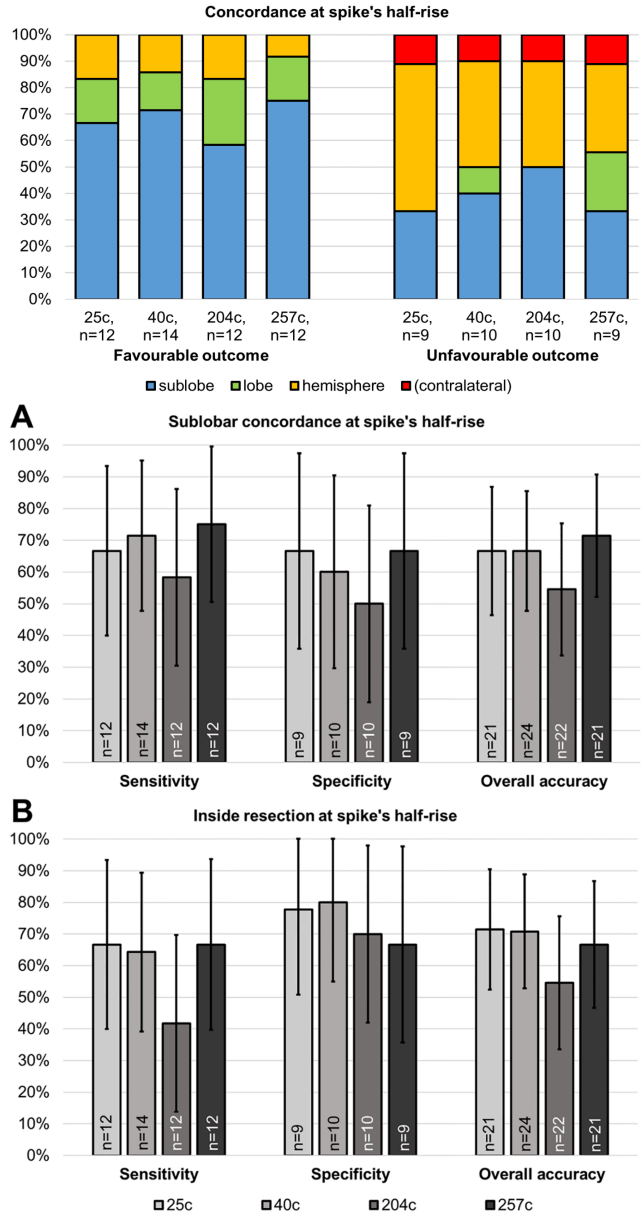

Figure 4.9: Top: Concordance with the resected area at various levels for favorable (ILAE class 1-2) and unfavorable (ILAE 3-5) post-surgical outcomes. Bottom: The performance of semi-automated ESI at the most prevalent spike average's half-rise in terms of, A) sub-lobar concordance of source maximum and resected zone, B) source maximum located inside the resected zone. Figure adapted from [125].

implementation for each patient. The patient was considered a positive ESI-insular-IZ if at least one concordance existed. Otherwise, the patient was

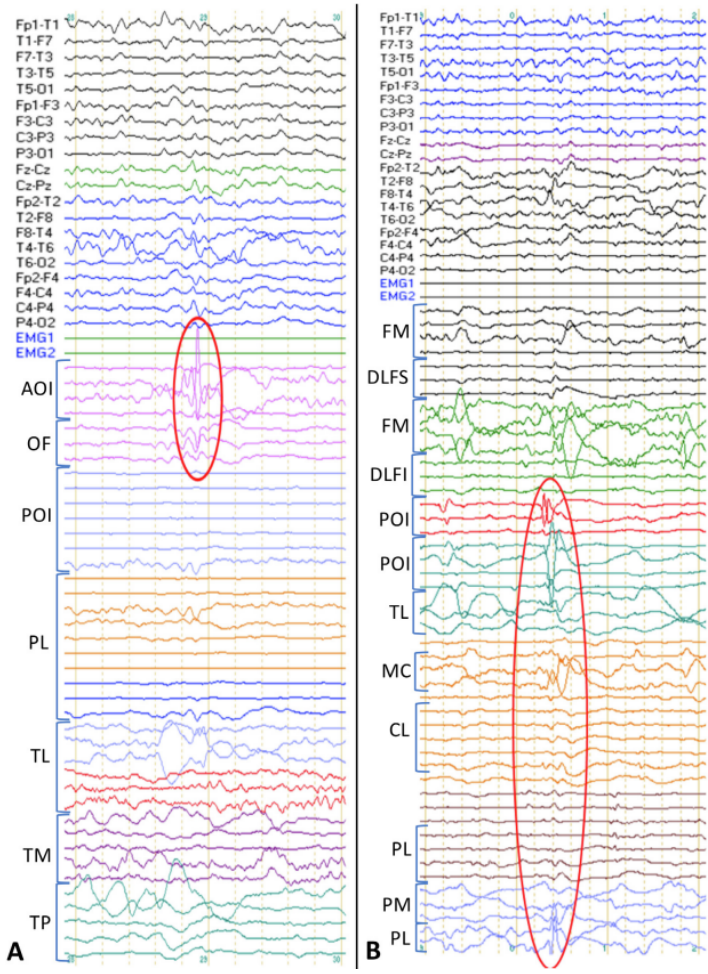

Figure 4.10: An example of insular spikes in simultaneous scalp EEG and iEEG. A) insular pure spike (red circle). B) insular diffusing spike; activity originates from the insula followed by propagations (red circle). Abbreviations: AOI - operculo-insular anterior, CL – central lateral, FM - frontal mesial, DLFI - dorsolateral frontal inferior, DLFS - dorsolateral frontal superior, MC - middle cingular, OF - orbitofrontal, PM - parietal mesial, PL - parietal lateral, POI - operculo-insular posterior, TL - temporolateral, TM - temporomesial, TP - temporopolar. Adapted from [126].

regarded as a negative ESI-insular-IZ. Considering sEEG as the reference standard, TP, TN, FP, and FN were defined at this level. For the second level of evaluation, only patients who had positive for ESI-insular-IZ were included. Simultaneous scalp EEG and sEEG were averaged in clusters showing insular activity from -1 to +1 of peak, called sEEG_average. Afterward, a visual analysis was conducted to determine if the average electrical activity of the sEEG, sEEG_average, matched the genuine sEEG spikes. Furthermore,

patients initially diagnosed as true positive at level 1 were re-evaluated as either true or false positive (Fig. 4.11).

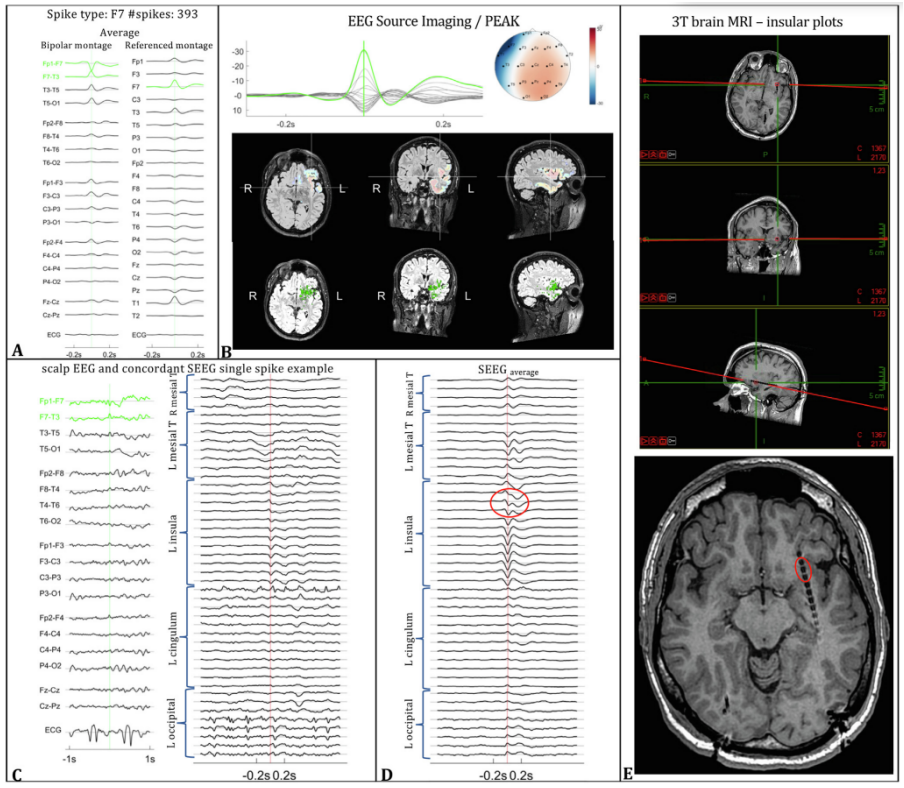

Figure 4.11: An example of a true positive case: Patient 23. A) Cluster F7 showing the averaged scalp EEG in both bipolar and referential montages, B) Topography of the averaged scalp EEG (top), followed by ESI outcome at the peak of the spike for the averaged spike (middle) and the single spikes (bottom), C) An example of an identical spike event observed in scalp EEG (left) and in sEEG (right), D) the averaged sEEG corresponding to the cluster F7 cluster. ESI and the averaged sEEG showing the fully concordant (red circle is the phase reversal on insular electrode), E) 3D view of deep electrode implantation and left insular electrode plots. Abbreviations: L – left, R – right, T – temporal. Adapted from [126].

4.4.3 Results

After reviewing the iEEG reports in the first level of assessment, it was discovered that out of 30 patients, 7 did not show any insular activities. PreOp identified 6 of these patients, which resulted in 1 false positive. Out of the remaining 23 patients, PreOp successfully localized the insular-IZ in 14 patients, resulting in true positive results. However, 9 cases led to false negatives. In the second level of assessment, by analyzing the outcomes of time-locked sEEG, PreOp identified 10 true positive cases, while 4 cases resulted in false negatives. This means that PreOp had conducted a sensitivity

and specificity of 53% (C.I. 29–76%) and 55% (C.I. 23–83%), respectively, to localize the epileptic insular zone. This resulted in an overall accuracy of 53% (C.I. 29–76%). Notably, those patients who experienced frequent and dominant interictal insular spikes exhibited higher levels of accuracy.

For further information on this study, please refer to [126].

4.5 Interictal ESI on MRI-negative patients; a prospective study

4.5.1 Introduction

This section aims to evaluate the efficacy of automated interictal ESI in locating the EZ on non-lesional patients, also referred to as MRI-negative cases, in a prospective study.

4.5.2 Methods

All patients undergoing presurgical evaluation at Saint-Luc Hospital (Brussels, Belgium) from January 2019 to December 2020 were recruited in this study. However, only 29 out of 132 patients were MRI-negative and were included in the performance evaluation. LD EEG was recorded using array of 25 electrodes, including 10-20 standard setup along with F9/10, T9/10, and P9/10. HD EEG was also recorded using 76 channels of 10-10 montage in nine patients. For all patients, automated interictal ESI was performed.

The multidisciplinary team (MDT) hypothesized the EZ twice at the sublobar level (25 sublobes per hemisphere) for further clinical management of the patients: 1) Without prior knowledge of ESI, and 2) after the ESI had been presented and clinically interpreted. Clinical decision-making was based on investigating multiple tests, including sEEG, MEG, ictal SPECT, fMRI, and WADA, as well as combinations of these (Fig. 4.12).

According to the MDT team, ESI results were considered contributive if they introduced new and non-duplicative information that led to a reevaluation of EZ hypothesis and a change in clinical management decision. Patients whose clinical management was adjusted based on ESI were monitored to determine if these modifications resulted in more contributive sEEG implementation or successful epilepsy surgery. For this reason, the concordance of the ESI solution was evaluated at the sublobar level with sEEG electrode placement or resection area. The ILAE classification standard was used to assess the operational outcome, and the patient was considered seizure-free, having an ILAE Class 1 outcome at one year of postoperative follow-up.

4.5.3 Results

Figure 4.13 provides an overview of the involved patients and the ESI results of this study.

In 12/29 (41%) of patients, the ESI results were contributive and the management plan was altered due to Interictal ESI. In 9/12 (75%), the significant modifications resulted in a change in the invasive recording plan, and ESI

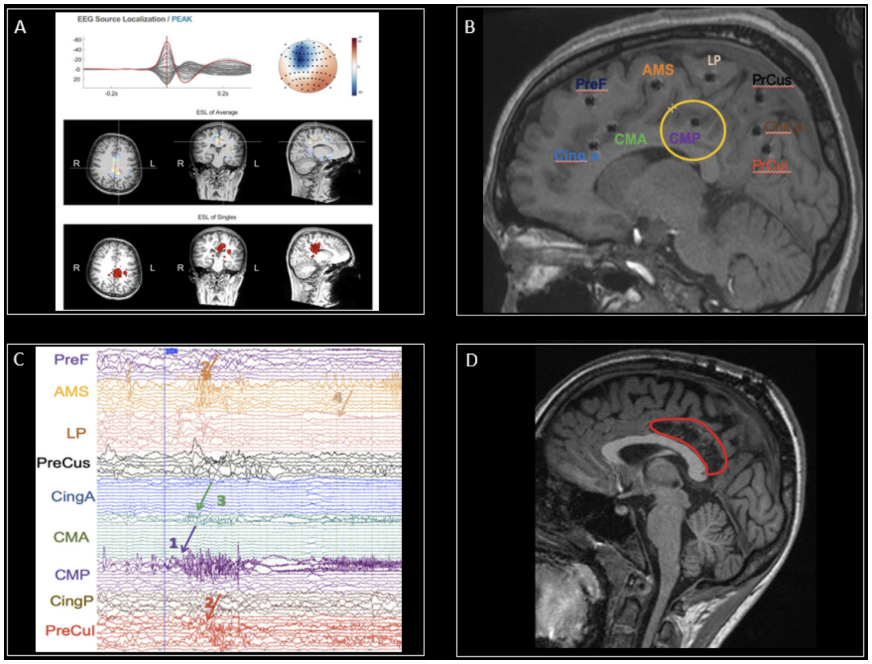

Figure 4.12: case study of the patient with ILAE class I surgical outcome at 2-year post-operative follow-up. A) The first cluster automated ESI results at the peak of the averaged spike and the single spikes in the group. The ESI outcome in the left middle/posterior cingulate cortex is concordant with the sEEG-SOZ and the resection area. B) sEEG plan: it is supported by ESI results to cover the middle/posterior cingulate cortex (yellow circle). C) sEEG recording: There is an onset of seizure discharges in the CMP electrode (violet arrow), which rapidly and multi-directionally propagate to AMS (dark yellow arrow), Precui (red arrow), and CMA (green arrow). D) Postoperative MRI: margins of resection are marked in red, and the ESI result is within the zone. Abbrivations: CingA: anterior cingular cortex; CMA: anterior/middle cingular cortex; CMP: middle/posterior cingular cortex; CingP: posterior cingular cortex; PreF: prefrontal; AMS: supplementary motor cortex; LP: paracentral lobule; PrCus: precuneus (superior part); PrCui: precuneus (inferior part). Adapted from [127].

changed the clinical management for the other 3/12 (%25) cases. Invasive recording was conducted in 8/9 (89%) patients. In 6/8 (75%) of this group, the intracranial EEG recording concorded with the ESI outcome at a sublobar level.

From the group ESI having contributive cooperation, 5/12 (%42) underwent surgical procedures and were followed up for at least one year. In all patients (5/5), the ESI solution was in the resected zone. Additionally, 4/5 (80%) are completely seizure-free, while one patient (1/5) has seizure reduction (ILAE 4).

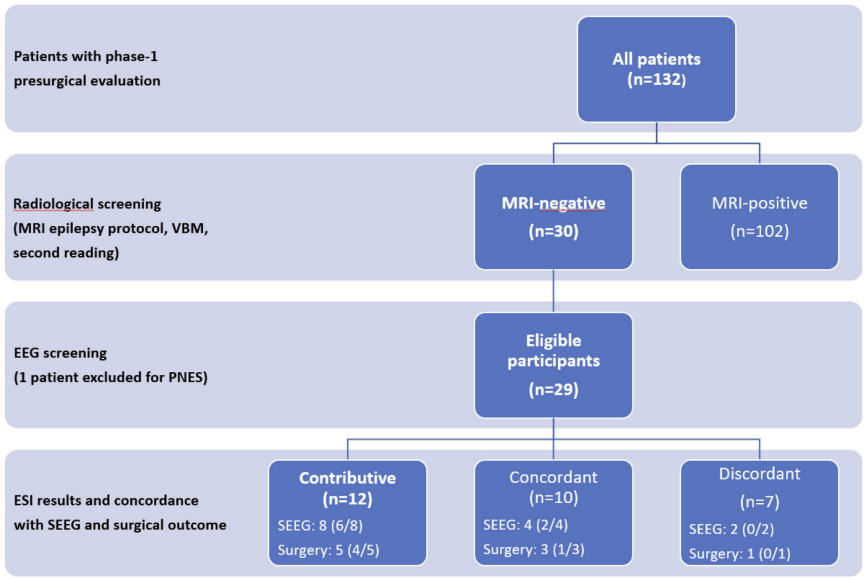

Figure 4.13: Study flowchart: recruiting 132 patients, including 29 for the ESI analysis, followed by classifying the ESI results into three groups as contributive, concordant and discordant. Adapted from [127].

4.5.4 Conclusion

This prospective study showed the added value of automated interictal ESI in the presurgical evaluation of MRI-negative patients. This technique helped plan sEEG depth electrode placement and localize the surgical resection zone.

For further information on this study, please read the article by Santalucia and et al [127].

4.6 Interictal ESI in a prospective single-center study

4.6.1 Introduction

In parallel with previous studies, we conducted a 4-year prospective to evaluate the PreOp pipeline in collaboration with HUG, Geneva, Switzerland.

4.6.2 Methods

Our study involved 122 patients with epilepsy between 2017 and 2021, out of which 40 cases qualified for our criteria. These cases involved patients with unifocal epilepsy who had undergone curative epilepsy surgery and had a minimum postoperative follow-up of two years. Scalp EEG recording was performed with 35 electrodes, including all standard 10-20 channels and some 10-10 electrodes (FP9/10, F9/10, Tp9/10, P9/10, FC1/2, FC5/6, CP1/2, and CP5/6) for all patients. Automated Interictal ESI was utilized to analyze all patients. Within this patient group, 15/40 (37.5%) cases were TLE patients,

13/40 (32.5%) had negative MRI results, and 20/40 (50%) individuals underwent subsequent invasive EEG monitoring.

4.6.3 Results

The performance of this technique is presented in Table 4.3, including the total and subgroup results.

	TLE (15)	ETLE (25)	MRI-Neg (13)	sEEG (20)	Total (40)
TP	11	14	9	12	26
FP	1	0	0	0	1
FN	2	8	2	5	9
TN	1	3	2	3	4
Sens	85%	64%	82%	71%	74%
Spec	50%	100%	100%	100%	80%
Acc	80%	68%	85%	75%	75%
PPV	92%	100%	100%	100%	96%
NPV	33%	27%	50%	38%	31%
OR	5.5	-	-	-	11.5

Table 4.3: The performance of the PreOp pipeline in a prospective study conducted by HUG in Geneva, Switzerland, including both total and subgroup results.

4.6.4 Conclusion

The study's findings are comparable to HD-ESI, likely due to increased signal-to-noise ratio because more spikes are detected and averaged compared to manual ESI. For more information about this study, please refer to article [128].

4.7 Interictal ESI in a prospective multi-center study

4.7.1 Introduction

The PreOp pipeline was a part of PROMAESIS, a prospective multi-center study investigating the accuracy and clinical usefulness of automated ESI in presurgical epilepsy evaluation.

4.7.2 Methods

A total of 392 consecutive patients were prospectively recruited from seventeen hospitals across Europe, including Austria(2), Czechia(2), Denmark(1), Italy(3), Germany(2), Portugal(3), Spain(3), and Romania(1). The patients underwent long-term video-EEG recording with 40 electrodes, and 71 had HD recordings. The low-density recording scalp EEG electrodes consist of 25 electrodes of IFCN standard, eight intermediate electrodes (FC1/2, FC5/6, CP1/2, CP5/6), and seven electrodes for better sampling of anterior, inferior, and posterior regions (AF11/12, AF1/2, PO1/2, and Iz). Additionally, HD recordings were performed using either 64 or 256 electrodes. The interictal ESI analysis has

been conducted on all the patients. For more information about the protocol of study, please refer to [129].

4.7.3 Results

The evaluation of PreOp's performance is pending and will be assessed once the results are available.

4.8 Integration of Interictal ESI in presurgical evaluation

4.8.1 Introduction

This prospective study investigated the time required to integrate Interictal ESI data into the clinical practice of a specialized epilepsy center using PreOp along with two other pipeline.

4.8.2 Methods

This research was carried out on 40 patients who underwent video EEG monitoring from 1 July 2021 to 30 June 2022 at the Epilepsy Center Berlin-Brandenburg. The number of scalp EEG electrodes varied between 33 and 45 based on the focus hypothesis. The study utilized three Interictal ESI analysis pipelines: Brainstorm and Cartool as academic free software packages and PreOp as a commercial pipeline. Figure 4.14 provides a detailed overview of the ESI workflow using these pipelines. EEG and MRI data were uploaded for three algorithms as the first step. The in-house ESI analysis, which uses Cartool and Brainstorm, started with software installation, troubleshooting, testing, and training in the first place. For each patient, the ESI analysis involved manually identifying genuine spikes in the EEG, averaging them, and possibly correcting the data, followed by MRI processing for the forward model and the inverse solution. On the other hand, the external ESI analysis only required data uploading. Finally, the interictal ESI solutions of these three pipelines were evaluated separately and then presented in the case conferences. The time spent on each step of these three pipelines was separately documented for further analysis.

4.8.3 Results

Of the 40 patients, 22 (55%) had sufficient interictal events to be used for interictal ESI analysis. The first third of the patients required a median of 4.7 hours for ESI analysis, whereas the remaining patients required only 2.0 hours. The infrastructural setup, troubleshooting, testing, and training of in-house ESI techniques required 68.5 working hours. Figure 4.15 provides more details of the time cost for each processing step to analyze the last eight patients per pipeline. The whole Interictal ESI analysis of PreOp was carried out by the external source, which accounts for the much shorter time spent than the other two pipelines.

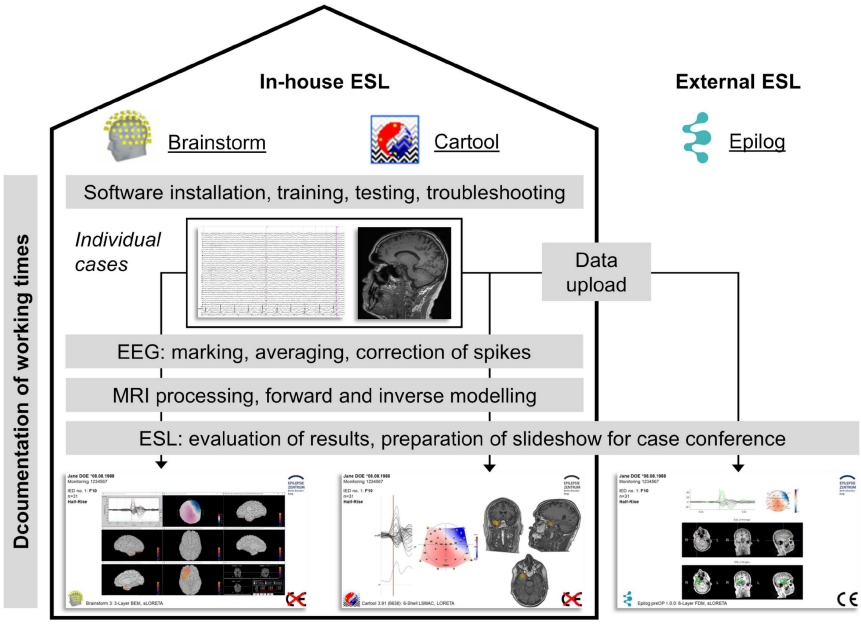

Figure 4.14: Illustration of interictal ESI workflow using in-house and external pipelines. The time spent implementing gray highlighted works were documents per case. Figure is adapted from [130].

4.8.4 Conclusion

This study discusses the integration of three interictal ESI pipelines into an epilepsy surgery program. The PreOp algorithm was found to have a shorter working time compared to the other ESI algorithms, and it did not require any time for digital infrastructure set-up, training, testing, or troubleshooting. For more information about this study, please refer to article [130].

4.9 Discussion

We thoroughly analyzed studies that utilized PreOp as an automated interictal ESI technique. Our evaluation focused on the performance of PreOp on patients who underwent surgical resection, where the localization accuracy of ESI was assessed for sublobar concordance with postoperative MRI. Additionally, we ensured that the study participants had a minimum of 1-year postoperative clinical follow-up available for review. The information provided in Table 4.4 summarizes the studies. The table includes the number of participants in each study, the total test indices statistics, the number of EEG electrodes utilized, and the study's highlights. Additionally, in Fig 4.16, you can find information on the sensitivity, specificity, and accuracy of each study and the overall performance of PreOp on this patient cohort.

Two studies ([132, 128]) have evaluated the performance of PreOp on ETLE cases. They reported that PreOp had a sensitivity, specificity, and accuracy of

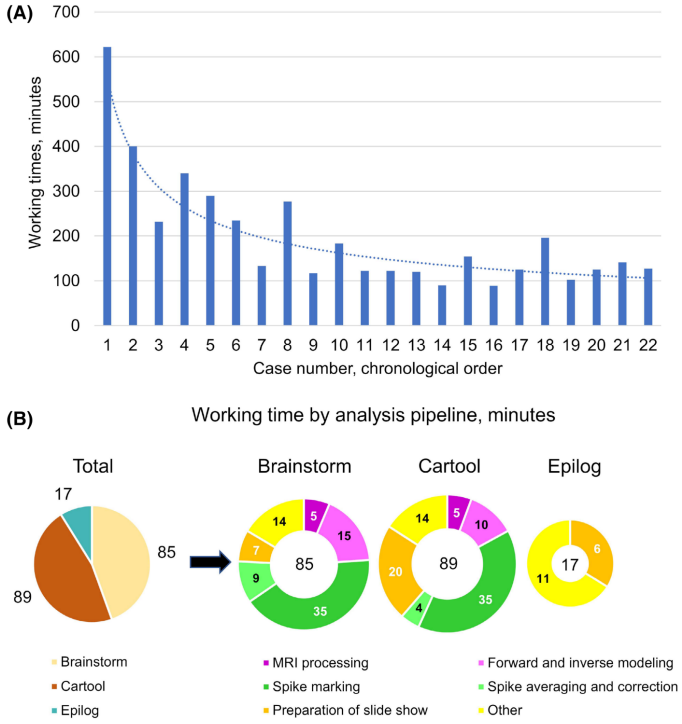

Figure 4.15: A: Interictal ESI time spent for each patient. B: The average time spent on each processing step for the analysis of the latest eight cases in the study has been recorded by the pipeline. Figure is adapted from [130].

58%&63%, 67%&100%, and 61%&68%, respectively, on these challenging cases. In addition, the efficacy of PreOp on negative MRI-negative patients was evaluated in two studies ([127, 128]). These studies showed that sensitivity was 82%&100%, specificity was 100%&0%, and accuracy was 80%&85% in this patient group. Overall, including all patients, PreOp yielded a sensitivity of 73%, specificity of 56%, and accuracy of 67%.

4.10 Conclusion

We have conducted several projects to evaluate the performance of automated interictal ESI, including a clinical validation, and some prospective projects. Additionally, we have tested the pipeline on patients with MRI-negative and extra-temporal lobe epilepsy, as well as on low-density and high-density EEG data. These studies have shown that automated interictal ESI has a similar accuracy level to neuroimaging methods previously reported to localize the epileptogenic focus. When it comes to HD EEG, automated HD ESI produces meaningful results. The diagnostic accuracy for both HD and LD EEG is comparable because of the numerous single detections in EEG data. LD EEG can be sufficient for ESI if many single spikes are available because of improvement in the signal-to-noise ratio of the averaged spike. Moreover, LD-ESI

PreOp Studies	N	TP	FN	FP	TN	Nr Ch.	Highlights
Baroumand et al. 2018 [131]	41	22	3	6	10	<=25	Validation study
Vespa et al. 2020 [132]	18	7	5	2	4	<=25	ETLE Cases
Vorderwülbecke et al. 2021 [125]	21	8	4	3	6	25	LD vs HD
	24	10	4	4	6	40	
	22	7	5	5	5	204	
	21	9	3	3	6	257	
Spinelli et al. 2023 [128]	40	26	9	1	4	35	Prospective study
Santalucia et al. 2023 [127]	5	4	0	1	0	25	MRI-negative ESI
Czarnetzki et al. 2023 [133]	33	12	5	11	5	35	Multi-modal comparison
Total: LD+HD	**225**	**105**	**38**	**36**	**46**	-	-
Total: LD	**182**	**89**	**30**	**28**	**35**	-	-
Total: HD	**43**	**16**	**8**	**8**	**11**	-	-

Table 4.4: Studies that used PreOp as the interictal ESI pipeline, along with some highlights of each study and the total number of processed cases.

precisely identifies the insular involvement in the IZ, which is unfeasible with traditional visual interictal scalp EEG interpretation. Additionally, we have shown that automated ESI can provide significant benefits in the presurgical assessment of cases with negative MRI results. This is especially helpful in guiding the placement of depth electrodes for sEEG. However, it is important to integrate ESI results into the overall multimodal evaluation and interpret them clinically for optimal outcomes.

4.11 The author's contributions

The automated interictal ESI pipeline has been featured in various studies and presented at multiple conferences [134, 135, 136, 137, 138, 139]. Additionally, these findings have been published in several journals[131, 125, 126, 127, 128]. Table 4.5 provides a comprehensive list of these studies and details the contributions of the author of this book to each study.

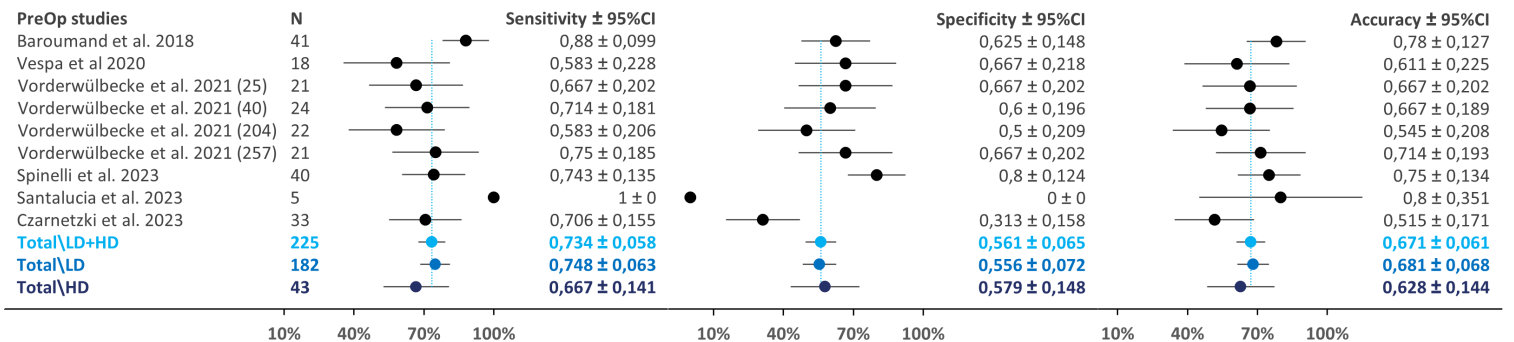

Figure 4.16: The results of PreOp's performance on patients are presented in Table 4.4, indicating sensitivity, specificity, and accuracy at both individual study and overall levels.

No	Article	Original contribution
1	Title: *Automated EEG source imaging: a retrospective, blinded clinical validation study* Authors: **Amir G. Baroumand**, Pieter van Mierlo, Gregor Strobbe, Lars H. Pinborg, Martin Fabricius, Guido Rubboli, Anne-Mette Leffers, Peter Uldall, Bo Jespersen, Jannick Brennum, Otto Mølby Henriksen, Sándor Beniczky	performing the analysis + writing the manuscripts
2	Title: *Automated interictal source localisation based on high-density EEG* Authors: Bernd J. Vorderwülbecke, **Amir G. Baroumand**, Laurent Spinelli, Margitta Seeck, Pieter van Mierlo, Serge Vulliemoz	performing the analysis + writing the draft of manuscripts (methods)
3	Title: *Automated electrical source imaging with scalp EEG to define the insular irritative zone: comparison with simultaneous intracranial EEG* Authors: Evelina Iachim, Simone Vespa, **Amir G. Baroumand**, Venethia Danthine, Pascal Vrielynck, Marianne de Tourtchaninoff, Alexane Fierain, Jose Geraldo Ribeiro Vaz, Christian Raftopoulos, Susana Ferrao Santos, Pieter van Mierlo, Riëm El Tahry.	performing the analysis
4	Title: *Clinical added value of interictal automated electrical source imaging in the presurgical evaluation of MRI-negative epilepsy: A real-life experience in 29 consecutive patients* Authors: Roberto Santalucia, Evelina Carapancea, Simone Vespa, Enrique Germany Morrison, **Amir G. Baroumand**, Pascal Vrielynck, Alexane Fierain, Vincent Joris, Christian Raftopoulos, Thierry Duprez, Susana Ferrao Santos, Pieter van Mierlo, Riëm El Tahry	performing the analysis
5	Title: *Semiautomatic interictal electric source localization based on long-term electroencephalographic monitoring: a prospective study* Authors: Laurent Spinelli, **Amir G. Baroumand**, Serge Vulliemoz, Shahan Momjian, Gregor Strobbe, Pieter van Mierlo, Margitta Seeck	performing the analysis

Table 4.5: Table of articles and author contributions using the automated interictal ESI pipeline.

Chapter 5

Automated Ictal ESI

Spread happiness across the earth, worry not for time keep your faith.

Barin

5.1 Introduction

In the previous chapter, we discussed the automated interictal ESI. This chapter focuses on the ESI of seizures, also known as ictal ESI. Section 5.2 covers the use of power ESI and functional connectivity as the core of the ESI pipeline. However, we encountered some limitations with this pipeline, which we fixed by developing and clinically validating a power ESI-based pipeline. We have submitted the complete manuscripts of this study in section 5.3. In section 5.4, we further improved this pipeline and discussed the details of the latest version of ictal ESI.

5.2 ESI power vs. ESI functional connectivity

5.2.1 Introduction

In a study by Staljanssens et al. [97], functional connectivity was established as a powerful tool for the localization of EZ using ictal EEG signals. The study compared two methods for identifying the SOZ. The first method, ESI power, involved identifying sources of the brain with high power during seizures in the time domain. The source with the highest power was then identified as the ESI solution. The second method, ESI power+connectivity, involved using a Granger causality-based algorithm to measure the outdegree of the high power sources. The source with the highest outdegree was then identified as the ESI solution. We tested this pipeline to localize the EZ on challenging cases with extra-temporal lobe epilepsy.

5.2.2 Method

The research involved 24 patients with drug-resistant focal ETLE (Saint Luc Hospital, Brussels, Belgium). EEG was recorded using electrodes from the 10-20 setup, and in some cases, additional channels such as T1/2, FT9/10, and TP9/10 were also utilized. However, T1/2 was incompatible with the standard IFCN montages, so it was excluded. We adopted the pipeline of Staljanssens's study but made modifications by measuring power in the frequency domain instead of the time domain. This alteration improved the pipeline's stability, particularly for noisy EEG data (Fig. 5.1).

This project was evaluated on two levels: at the seizure level (24 patients, 94 seizures) and at the patient level (18 patients). All ESI results were compared with the resected area and at the sublobar level by considering the surgical outcome after 1-year post-operative follow-up.

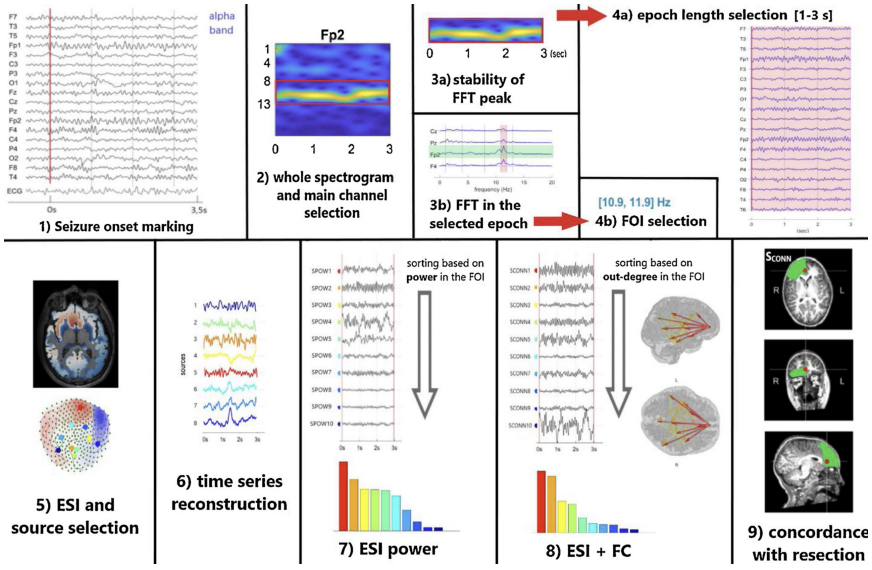

Figure 5.1: The pipeline of ESI power and ESI power+connectivity, 1) provided data before the analysis; marked seizure onset characterized by a rhythmical ictal activity between onset and +3s after, and frequency band of interest (BOI). 2) The spectrogram of the EEG channel that showing the BOI (alpha band in this example). 3a) Calculation of the length for epoch of interest (EOI) based on the length of ictal activity stability over time, and 3b) calculation of the frequency of interest (FOI) based on Fast Fourier transform (FFT) of EOI. 4a) Demonstration of EOI, which takes between 1s and 3s, and 4b) FOI. 5-6) ESI projects the activities of EOI at the source level, and the sources with the high power were included for further analysis. 7) Sources are sorted based on their power in the FOI. 8) Sources are sorted based on their outdegree in the FOI after functional connectivity calculation. 9) The solutions of ESI power and ESI power+connectivity are depicted in the post-operative MRI. Figure adapted from [132]

5.2.3 Results

When evaluating results at seizure level, ESI power achieved a sensitivity, specificity, and accuracy rates of 36%, 72%, and 45%. ESI power+connectivity resulted in higher rates of 52%, 84%, and 61%. However, when examining at patient level, ESI power had a sensitivity, specificity, and accuracy of 17%, 50%, and 28%, respectively. ESI power+connectivity improved these rates to 58%, 83%, and 67% for sensitivity, specificity, and accuracy, respectively. In addition, we evaluated these results in sub-groups. By excluding the hemispherotomy cases, the sensitivity for ESI power and ESI power+connectivity at seizure level was 29% and 43%, respectively. In this scenario, specificity was 54%, and 83% for ESI power and ESI power+connectivity, respectively. Table 5.1 provides an overview of ESI performance in various patient groups and at the seizure level.

For further information about the results and the whole study, please refer to [132].

Groups		Power	Power+Connectivity
All cases	Sensitivity	36%	52%
	Specificity	72%	84%
	Accuracy	45%	61%
Cor. & Les.	Sensitivity	29%	43%
	Specificity	54%	83%
Hem.	Sensitivity	56%	78%
	Specificity	80%	100%

Table 5.1: Diagnostic accuracy measures of ESI power and ESI power+connectivity at seizure level on ETLE patients. Abbreviations: Cor. = Cortectomy, Hem. = Hemispherotomy, Les. = Lesionectomy.

5.2.4 Discussion

In this research, it was again found that functional connectivity is a more useful tool than ESI power for identifying the epileptogenic zone. However, the performance of this method may not be as strong as in Staljanssens's study. This could be due to the fact that the participant pool in this research was limited to individuals with ETLE only, which are difficult to localize. Additionally, there are some underlying limitations in using functional connectivity for analyzing ictal ESI, such as:

1. The accuracy of connectivity analysis is dependent on choosing the correct seizure onset. Ideally, it should be applied at the very start of the seizure to achieve optimal results. However, this may not always be possible in clinical settings, as identifying the onset can be a difficult task for some seizures.

2. This method relies on another technique and cannot be applied solely for localization purposes. In our study, we utilized ESI power to create signals of the sources, which were then analyzed by connectivity. Therefore, connectivity could be blinded to some sources if ESI power could not pick up their activities in the EEG.

Using connectivity for daily clinical purposes also presents challenges. The computation speed of connectivity is dependent on various parameters, such as the number and length of time series on which connectivity is applied. This process can be time-consuming. Additionally, clinical interpretation of connectivity remains difficult and requires more improvements.

A potential solution for improving the performance of the ictal ESI pipeline is to focus on enhancing ESI power and refining the technique, instead of relying on ESI connectivity and power combined. The ESI engine could be upgraded by adjusting the ESI inverse solution. Additionally, a standardized methodology should be established for source selection. This can be achieved by selecting sources per sublobe, ensuring that all sublobes contribute to the ultimate ESI power analysis.

5.2.5 Conclusion

Although functional connectivity is a valuable tool for analyzing ictal ESI to locate the epileptogenic zone, its limitations prevent us from using this technique in our ictal ESI engine. Instead, we decided to improve the ESI power method. We will discuss the developed pipeline based on ictal power in the following section.

5.3 Automated Ictal ESI; clinical validation study

Title: "Automated ictal EEG source imaging: A retrospective, blinded clinical validation study"

5.3.1 Introduction

The delineation of the Epileptogenic Zone (EZ) is of utmost importance for patients with pharmaco-resistant focal epilepsy. Resective surgery of the presumed EZ is the treatment with the highest efficacy to render these patients seizure-free [140]. A multimodal approach is used in the presurgical work-up to decide whether resective surgery is a favorable treatment option for each individual case [33]. Among these techniques, EEG Source Imaging (ESI) of interictal epileptiform discharges (IEDs) and ictal EEG activity have high diagnostic value in the presurgical evaluation [141, 123, 124]. However, ESI requires special expertise, not available in all centers, and therefore this method is underutilized [142]. Using automated methods for ESI could circumvent this impediment [131, 99, 132].

Interictal ESI, performed by experts, has a moderate to high accuracy (57%–88%) to localize the EZ [30, 92, 141, 123]. In the presurgical evaluation, ESI provides non-redundant information in one third of the patients [143]. Despite these

encouraging results, ESI is only used in a limited number of centers world-wide. A study from the E-pilepsy consortium showed that only nine of the 25 centers used interictal ESI in the presurgical evaluation [31]. The limited use can be explained by several factors: (i) the manual analysis that entails marking the spikes and constructing the head models from MRI is time-consuming, (ii) it requires specific expertise. To overcome these, automated, standardized and objective interictal ESI analysis was recently developed and validated with a blinded study [131, 99]. The algorithm detects all IEDs in the long-term EEG recording, constructs a head model and delivers an easy to understand, concise report that, can be easily interpreted by the epileptologists.

Ictal ESI estimates the localization of the seizure onset zone (SOZ) [144]. However, this method faces additional challenges compared with interictal ESI: low signal-to-noise ratio during ictal epochs and rapid propagation of the activity during seizures [145]. In some patients, the irritative zone (IZ) and SOZ will overlap, while in others they can be discordant [123]. Therefore, ESI of ictal EEG signals is considered to be more informative to localize the EZ than the ESI of interictal signals. To overcome with these difficulties, we developed an automated ictal ESI workflow to localize the SOZ from rhythmic ictal EEG activity [132].

In this study, we report the clinical validation of the automated ictal ESI, in 50 consecutive patients with focal epilepsy who underwent resective surgery. The analysis was performed retrospectively. However, the operators of the automated ictal ESI were blinded to all other data and the operation outcome. We used the sublobar concordance with the resected area and one-year postoperative outcome as the reference standard ("gold standard"). The study is reported according to the STARD criteria (Standards for Reporting Diagnostic Accuracy Studies) [112].

5.3.2 Methods

I. Patients and analyzed data

De-identified EEG and MRI data, from consecutive patients were analyzed retrospectively. Inclusion criteria were: (1) patients with drug-resistant focal epilepsy, (2) admitted to the Epilepsy Monitoring Unit (EMU) at the Danish Epilepsy Centre, Filadelfia, as part of the presurgical evaluation, (3) who had rhythmic ictal EEG activity during the seizures recorded in the EMU, (4) patients who underwent resective surgery, (5) postoperative follow-up of at least one year. Exclusion criterion was the lack of MRI sequences necessary for constructing the Individual head model needed to perform ESI. Patients gave their informed consent prior to admission to the EMU.

EEG was recorded at the Danish Epilepsy Centre, using the standard 25-electrode array of the International Federation of Clinical Neurophysiology [40]. Besides the electrodes of the 10–20 system, it included six additional electrodes in the inferior temporal chain (F9/10, T9/10 and P9/10). Electrode impedance was kept below 5KΩ. EEG was recorded with a sampling frequency of 256 Hz, using the NicoletOne system. MRI examination was performed on a

3 T Siemens scanner, at the Department of Radiology, Hvidovre Hospital. The T1-3D-MPR-sequence was used for constructing the individual head models.

In the long-term EEG recordings, the seizure onset time-points were marked by an experienced epileptologist (AAA) at the beginning of the rhythmic ictal discharges for each seizure. Furthermore, the ictal frequency band of interest (BOI) was reported for each seizure by another author (SB), blinded at this step to the other data. Seizures with poor signal-to-noise ratio were excluded. Spectrograms were cross-checked with the EEG data, to identify frequencies that represented filtered muscle artifacts. Markers of seizure start time-point were adjusted on the spectrograms. To remove eye, muscle and cardiac artefacts independent component analysis (ICA) was applied. The data was first band-pass filtered and later ICA was applied. All ICA components were visually checked to identify which components contained only muscle, eye or cardiac artefacts. These components were then removed. In 13 patients we removed artefacts using ICA. In several seizures we were not able to remove the artefacts and therefore we had to exclude these seizures.

II. Automated ictal ESI pipeline

The automated ictal ESI pipeline is shown in Fig. 5.2. The analysis started by calculating the window of interest (WOI) for the analysis, within 0–3 s from the marked electrographic onset and BOI. Within this window, time–frequency analysis was performed in sensor level to define the WOI. The point with highest activity in the frequency band of interest was chosen and region growing was performed to set the time interval and frequency interval of interest. In practice the WOI had a duration of 1 s to 3 s in all patients. ESI was performed on the time-points inside the WOI, to reconstruct the neuronal activity in 50 sublobes in the brain (25 per hemisphere). Time-frequency analysis of the reconstructed sublobar time series was performed to assess which of the sublobes has the highest power in the WOI, and was identified as SOZ. The operators of the automated pipeline were blinded to all other data. A concise report of the ictal ESI of all seizures per patient was returned to the clinicians for evaluation.

III. The forward ESI model and the inverse solution

For each patient an individual head model was built with a 1x1x1mm resolution from the T1-weighted MRI. To this end, the MRI is segmented into six tissues, containing grey matter, white matter, cerebrospinal fluid, skull, scalp and air [113, 98] using the statistical parametric mapping software (SPM12). The estimated probability maps of tissues are then combined after smoothing to construct the head model. We used the conductivity values reported in literature. The skull conductivity was set to 0.0105 S/m according to [146] who calculated the optimal isotropic skull conductivity on the basis of the conductivity measurements of the spongy and hard bone compartments of [147]. The conductivities of gray and white matter were set to 0.333 S/m and 0.142 S/m [148], CSF to 1.785 S/m [149] and scalp to 0.327 S/m [150, 151].

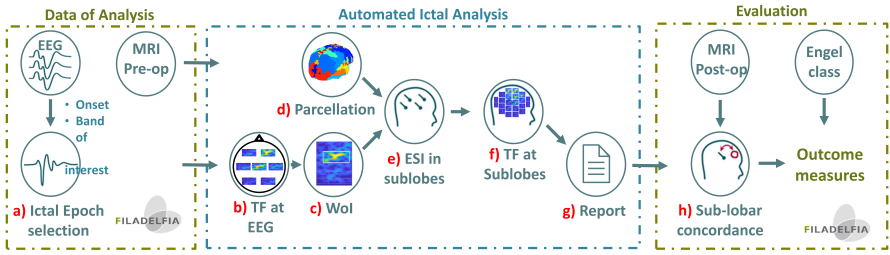

Figure 5.2: Ictal analysis pipeline: a) marking of the onset and indicating the frequency band of interest (done by experts as part of the clinical work-up), b) time–frequency (TF) analysis at sensor level, c) acquiring the window of interest (WOI) by a region growing procedure, d) parcellation of gray matter into 50 sublobes, e) applying EEG source imaging (ESI) and constructing electric time-series for each sublobe, f) time–frequency analysis at sublobe level and identifying the seizure onset zone, g) generating the ictal report, h) evaluating the analysis by measuring sensitivity and specificity based on the post-surgical outcome (calculated at the epilepsy center). The source imaging (i.e. steps b-g) was automated.

For positioning the EEG electrodes on the head, the position of the nasion, inion, electrodes T9/10, T7/8, and Tp9/10 are marked on the 3D model of scalp. The positions of all electrodes are then automatically identified by calculating the distances along the 3D scalp and placing the electrodes at their corresponding position. Positioning of all electrodes are checked visually and small correction are performed when needed.

For the forward ESI model, first more than 13.000 dipoles were distributed over the gray matter with 3 mm spacing. Then, the leadfield matrix is computed using the finite difference method [59, 114, 115]. It explains the relation between the recorded scalp EEG and the current dipoles in the gray matter. Additionally, the gray matter was parceled into 50 sublobes (25 per hemisphere) as defined in the SCORE guideline [116], meaning that every dipole was assigned to a specific sublobe.

As inverse solution, a modified version of LORETA was used. To this end, the spatial Laplacian operator was weighted according to the number of neighbors of each dipole to ensure solution in which multiple regions can be active simultaneously. As a result, there were some modifications in eq. (3.27) as follows:

$$X = average(neighbours)$$

$$[A_1]_{\gamma\beta} = \begin{Bmatrix} 1/X, & if||v_\gamma - v_\beta|| = d \\ 0, & otherwiose \end{Bmatrix}, \forall\gamma, \beta = 1, ..., M$$

IV. From EEG to SOZ localization

The spectrogram was calculated from the marked onset until 3 seconds after, for all EEG electrodes. Based on the BOI, the time– frequency window of

interest (WOI) was identified by the maximum power in the BOI over all channels and applying region growing until the power has dropped. Next, ESI was performed in the WOI to reconstruct the neuronal activity at each dipole. For each sublobe, the neuronal activity time series was reconstructed by applying principle component analysis to the time series of the dipoles and selecting the principle component that had most energy in the WOI. Finally, the sublobe with the time series that has the highest activity in the WOI was defined as SOZ.

V. Performance evaluation

The results of the automated ictal pipeline were summarized in a concise Ictal ESI report and were forwarded to the epileptologist (SB) who compared the SOZ localization with the resection site, at sublobar level.

The performance of the automated ESI was determined by calculating sensitivity, specificity, overall accuracy, positive predictive value (PPV) and negative predictive value (NPV). The resected area (RA) and the surgical outcome after one year were used as gold standard [116]. Patients with Engel class I outcome were considered as seizure-free. Results of the index test (automated ESI) were classified as True Positive (TP), False Positive (FP), True Negative (TN) and False Negative (FN) according to the definitions summarized in Table 1. Briefly: when all seizures were in the resected area, the results were considered positive. When at least one seizure localized outside the resected area, the results were negative. Cases in which ESI was non-localizable were considered negative. Depending on the one-year postoperative outcome, these were classified further as true or false results (Table 5.2).

True Positive (TP)	False Positive (FP)
All seizures localized inside the RA	All seizure localized inside the RA
+	+
seizure free outcome	not seizure free outcome
False Negative (FN)	True Negative (TN)
At least one seizure localized outside the RA	At least one seizure localized outside the RA
+	+
seizure free outcome	not seizure free outcome

Table 5.2: Defining the outcome of the automated ictal EEG source imaging. RA: resected area

5.3.3 Results

Fifty-one consecutive operated patients met the inclusion criteria. One patient was excluded because no MRI was available (Fig. 5.3). Data of all 50 eligible patients were analyzed (28 female; age: 12–66 years, median: 32.5 years).

Thirty-four patients (68%) had temporal and 16 patients (32%) had extra-temporal resections (9 frontal, 3 parietal, 2 occipital, one insular and one insular/frontal operculum). The pathology was hippocampal sclerosis in 23 patients, focal cortical dysplasia in 13 patients (with additional hippocampal sclerosis in two patients), periventricular nodular heterotopia in one patient, benign tumors in two patients. One patient had a temporo-polar encephalocele. Four patients showed non-specific findings (gliosis) and histopathology was normal in six patients. MRI showed a potentially epileptogenic lesion in 34 patients and it was normal in 16 patients. Thirty patients (60%) were seizure-free at one-year follow-up. Fig. 5.4 and Fig. 5.5 show the results of the automated ictal ESI for a temporal and an extra-temporal case.

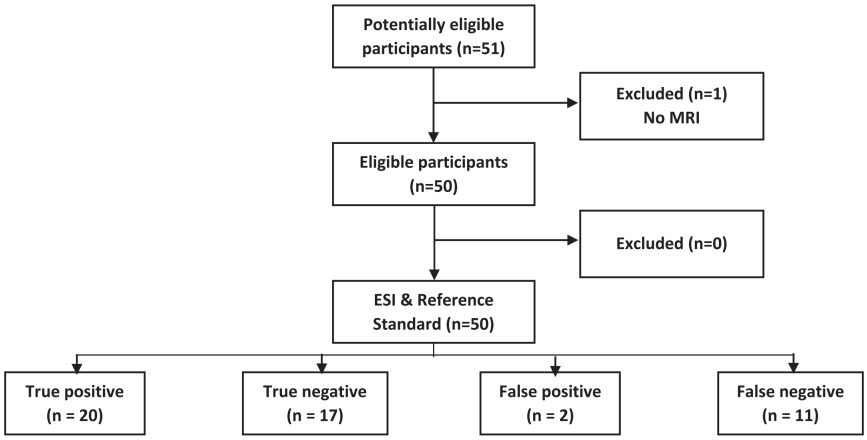

Figure 5.3: Flow diagram of the study.

We excluded 31 out of 111 seizures because they were too noisy or did not have rhythmic discharges. A total of 80 seizures (mean: 1.6 per patient) were analyzed using automated ESI. In six patients (11 seizures), the automated ESI did not result in localizable sources and were considered negative (TN: 2 patients; FN: 4 patients). The outcome of comparing the ESI results with the gold standard is shown in Fig. 5.3, and Table 5.3 summarizes the diagnostic accuracy measures. There was no difference between the diagnostic accuracy of the temporal cases (73.53%; 95% confidence interval: 55.64–87.12%) and extra-temporal cases (75.00% ; 95% confidence interval: 47.62–92.73%). In the subgroup of 16 patients with normal MRI, the accuracy of the automated ictal ESI was 87.50% (95% CI: 61.65–98.45%).

5.3.4 Discussion

In this study, we validated an automated ictal ESI pipeline, based on spectral analysis in source space. We analyzed 50 operated patients with focal epilepsy. Using concordance with the resection site and one-year postoperative outcome as gold standard, we found that automated ESI had high diagnostic accuracy, at sublobar level (74%), with high specificity (89.47%) and reasonable sensitivity

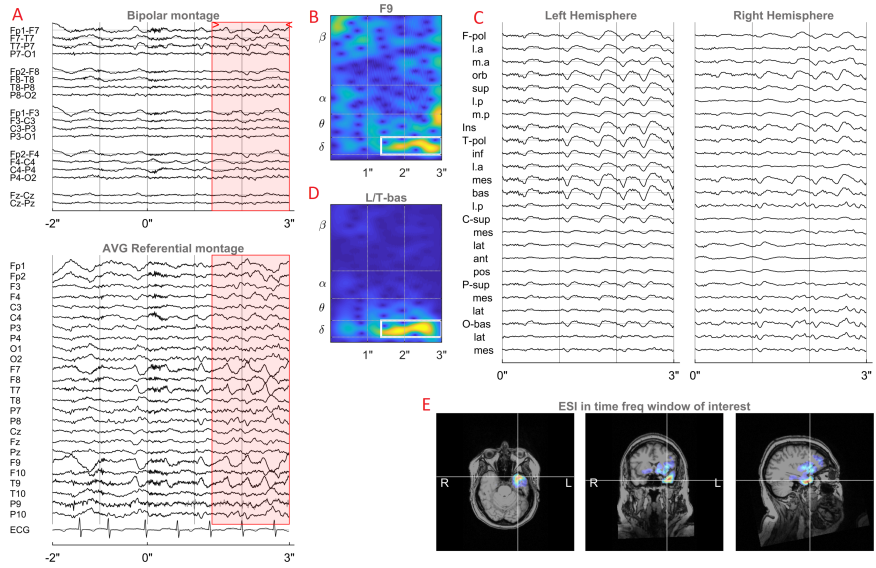

Figure 5.4: Ictal analysis of a patient with temporal lobe epilepsy. A) Ictal EEG epoch from 2 s before the marked onset and 3 s after in both bipolar and average referential montages. The EEG inside the red rectangle shows the epoch of interest, as determined from the spectrogram. B) Spectrogram of the channel with the highest power in the indicated band of interest. The white rectangle determines the time–frequency of interest. C) Source-space time-series in the 50 regions of interest, from the onset to 3 s after. D) Spectrogram of the region of interest with the highest power in the indicated band of interest in which the white rectangle demonstrates the time–frequency of interest. E) 3-dimensional localization of the source with the highest power in the region of interest. Note that automated ictal EEG source imaging (ESI) shows a source in the left basal-anterior temporal region, which is in concordance with the resection area. This patient was seizure-free (Engel I) at the one-year after a left anterior temporal resection.

Diagnostic measure	Percent (95% CI)
Sensitivity (95% CI)	64.52% (45.37–80.77%)
Specificity (95% CI)	89.47% (66.86–98.70%)
PPV (95% CI)	90.91% (72.43–97.44%)
NPV (95% CI)	60.71% (48.41–71.80%)
Accuracy (95% CI)	74.00% (59.66–85.37%)

Table 5.3: Diagnostic accuracy measures of the automated ictal EEG source imaging.

(64.52%). Similar accuracy has been achieved in the temporal and extra-temporal cases.

The automated method analyzes the ictal epoch identified by the clinicians in sensor-space. The pipeline uses spectral analysis in source-space to identify the region of interest with the highest power of the identified rhythmic ictal

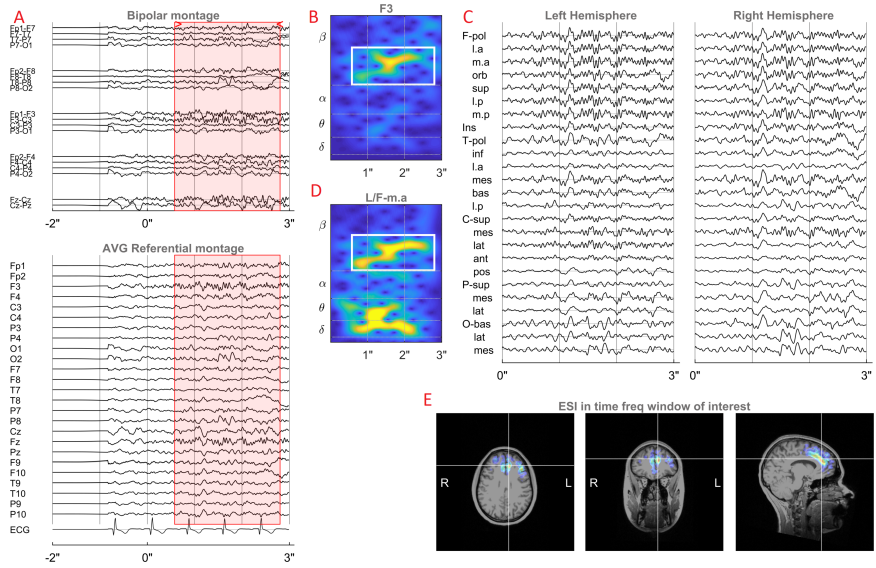

Figure 5.5: Ictal analysis of the patient with frontal focus. Ictal EEG epoch from 2 s before the marked onset and 3 s after in both bipolar and average referential montages. The EEG inside the red rectangle shows the epoch of interest, as determined from the spectrogram. B) Spectrogram of the channel with the highest power in the indicated band of interest. The white rectangle determines the time–frequency of interest. C) Source-space time-series in the 50 regions of interest, from the onset to 3 s after. D) Spectrogram of the region of interest with the highest power in the indicated band of interest in which the white rectangle demonstrates the time–frequency of interest. E) 3-dimensional localization of the source with the highest power in the region of interest. Note that the ictal EEG source imaging (ESI) localizes to the anterior mesial part of the left frontal lobe. This area has been resected and the patient was seizure-free (Engel I) at the one-year postoperative follow-up.

activity. As inverse solution, a modified version of LORETA is used, in a six-layer individual head model. The automated pipeline issues a report with the spectrograms and source images that the physicians easily can interpret in the clinical context. Hence, the clinicians are still in charge of the input and the output of the process, yet they are relieved form the time-consuming burden of the analysis.

Although our study was retrospective, the operators of the automated pipeline were blinded to all other data, to reduce the risk of bias. The pipeline used a pre-defined fixed algorithm, and it was validated on an independent dataset, different from what was used for developing the method [132].

A meta-analysis of ictal ESI done by experts has been recently published [141]. Based on data from 159 operated patients, from six clinical studies, the meta-analysis showed a diagnostic accuracy of 74.84% (68.1–81.59%), with a sensitivity of 89.9% (81.8–94.6%) and specificity of 46.9% (30.5–63.9%). Our

automated ictal ESI yielded a similar accuracy, yet with lower sensitivity, but higher specificity. However, it is difficult to compare the diagnostic performance across these studies, as the patient populations were different. Head-to-head comparison studies, using the same cohort are needed to reliably compare the performance of automated and expert-based ictal ESI.

An interesting finding in our study was the high specificity achieved. We only can speculate on why this occurred. When ESI is performed by experts, during the clinical evaluation of the patients, the numerous subjective decisions during the analysis can induce a strong bias, so that fewer patients would have the source estimated outside the resection area. However, in the automated pipeline, this potential bias is reduced, resulting in a higher number of negative cases. The fact that many of the negative cases were true negatives, suggests that the approach described in this paper has a potential clinical value, by raising a red flag in these cases.

An important cause of false negatives was the noisy ictal EEG segment, not allowing a precise localization. In 36% of the false negatives, the ictal ESI was not localizable, yet the patients were operated and became seizure-free. This highlights one of the limtations of the method: for accurate localization there is a need for an relatively good signal-to-noise ratio in the ictal recording, which is not always the case. In the remaining false negative cases, automated ESI localized to a sub-lobar region outside the resected area in patients who become seizure-free. This highlights the other major limitation of the method: ictal signals can be inconspicuous at scalp electrodes at the onset, and the first identifiable rhythm might already be generated in a distant area, where the ictal activity propagates to. There were only two false positives, so it is not possible to draw a clear conclusion in this subgroup. In both cases, the ESI localized to the antero-basal part of the temporal lobe. Both patients underwent anterior temporal lobectomy, and the sources were resected. In both patients, the histopathology showed hippocampal sclerosis, yet the patients did not become seizure-free (Engel class II).

Four patients underwent resective epilepsy surgery before the EEG (i.e. the analysis was done on EEG recorded in the evaluation for the second surgery). Automated ictal ESI provided accurate results in three of them. Although this number is too low to draw a definite conclusion, these results might suggest that using individual head models makes ESI feasible in previously operated patients. This is consistent with a previously published head-to-head comparison of EEG and MEG (Magnetoencephalography) source imaging of interictal epileptiform discharges, done by experts [152].

In the subgroup of 16 patients with normal MRI, the accuracy of the automated ictal ESI was somewhat higher than the accuracy in the whole cohort, but the difference was not significant. This finding raises the possibility that automated ESI contributes with valuable information to the decision-making process, in non-lesional cases. Further, prospective studies are needed to address directly the decision-changes based on the automated ESI data. Normal histopathology is a negative predictor of seizure freedom. In our

cohort, only one of the six patients with normal histopathology became seizure-free. The source of the automated ictal ESI was within the resected area in the single patient who became seizure-free in this subgroup, and was outside the resected area in the five patients who did not become seizure-free.

As our diagnostic accuracy study was retrospective, the results of the automated ictal ESI were not considered for the decision of the multidisciplinary epilepsy surgery team. Therefore, assessment of the clinical utility was beyond the scope and limitations of this study. A recently published prospective study on the clinical utility of ESI in presurgical evaluation showed, that it changed the decision of the multidisciplinary team in one third of the patients, and most often these changes were related to the strategy of planning the intracranial recordings [143].

Standard clinical analysis of ictal video EEG typically aims at localizing the peak negativity on the scalp. However, as electric currents flow in the tissue of the head, the peak negativity on the scalp might be at a distant location from the real source. ESI models the flow of the electric currents in the tissue of the brain, leading to more accurate results. In a previous study, the highest sensitivity achieved by experts who visually interpreted ictal signals was 63% [38]. Source imaging achieved a higher sensitivity (83%) in that study.

Our study has several limitations. The pipeline was developed to localize epochs with rhythmic ictal discharges. This means that the method is not suitable for localizing electrodecremental ictal changes or spike-waves / polyspike-waves. Additionally, the stability of the pipeline is limited for noisy data and due to that, we were not able to localize the ictal source in six patients. Nevertheless, these patients were included into calculating the performance of the automated pipeline. Further, prospective studies are needed to determine precisely the diagnostic accuracy and clinical utility of automated ESI. The large-scale, prospective multicenter study on automated ESI (PROMAESIS) is currently conducted, with the participation of the epilepsy centers of the European Reference Network – Epicare (Identifier: NCT04218812).

In conclusion, our retrospective, blinded clinical validation study suggests that automated ictal ESI could be a useful tool in the multimodal presurgical evaluation of patients with drug-resistant focal epilepsy.

5.4 ESI power with a sliding-window approach

5.4.1 Introduction

Although the ESI power method developed in previous section has shown relatively promising results in localizing the seizure onset zone, it does have certain limitations. The current pipeline only works if the ictal onset is within 0 seconds and +3s after the marked onset, and if the band of interest matches the marked band completely. In this section, we have addressed these limitations by updating the ESI engine and introducing the ESI power in a sliding window method, so called Sliding Ictal ESI, to make the pipeline more effective.

5.4.2 Method

I. ESI engine

As discussed in Section 5.3.2 Subsection IV., we used ESI in combination with PCA to generate signals for each dipole. Spectrogram analysis was then used to locate the source with the highest power during a seizure. Although PCA created a unique time series from the three signals of x-, y-, and z-directions, it may not always be the most accurate representation of the dipole's actual signal. Therefore, creating unique source signals using the PCA technique might not be the optimal technique to be used in this setting.. Instead, we propose conducting direct spectrogram analysis on sources. To achieve this, we conducted spectrogram analysis on each dipole's three Cartesian signals (x, y, and z), and then calculated their mean to introduce them as the dipole's spectrogram. Here, the source with the highest power in the WoI was again considered as the solution of the ESI pipeline.

To address the issue of inadequate onset marking, we extended the ESI range from -2 seconds to +5s after the marked onset. Additionally, to overcome the problem of insufficient BOI marking, we calculated the ESI findings for two time-frequency WOIs. This resulted in the development of a sliding-window ESI power pipeline known as Sliding Ictal ES. The pipeline uses a 2-second sliding window with a 1-second overlap and selects up to two WOI for each window using a growing region technique. At each sliding window, ESI is performed, and the source with the highest energy in the selected WOI is considered the ESI solution. This methodology allows the investigation of the temporal and spatial propagation of ictal activities and generally produces a set of ESI ictal solutions. These solutions can be evaluated based on the clinically meaningful window of interest. Figure 5.6 summarizes the pipeline of Sliding Ictal ES.

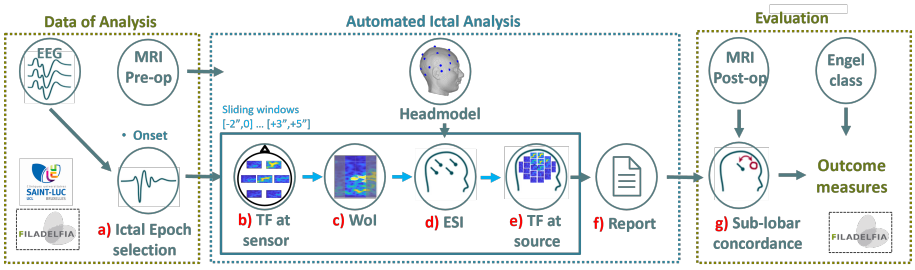

Figure 5.6: a) marking of the ictal EEG onset (by expert electrophysiologist), For each 2s sliding window between -2s and +5s with 1s overlap: b) performing spectrogram analysis at sensor level, c) acquiring up to 2 windows of interest (WoIs) by a region growing procedure selecting those with highest energy, d) applying ESI and mapping ictal waves to source space, e) performing spectrogram analysis at source level and identifying the source with the highest energy as SOZ, f) generating the ictal report, g) evaluating the analysis by measuring sensitivity, specificity and accuracy at seizure- and patient- level and based on the post-surgical outcome.

II. Patient cohort and evaluation

In order to evaluate the Sliding Ictal ESI pipeline, all the patients from the Danish Epilepsy Centre, Filadelfia, Denmark, discussed in Subsection 5.3.2 - Subsubsection I., were used. The evaluation was carried out at the seizure- and patient-level by calculating sensitivity, specificity, PPV, NPV, and overall accuracy. For assessing the patient level, the definition of TP, FP, FN, and TN is the same as discussed in table 5.2. The gold standard for the evaluation approach used in section 5.3 was also considered, which involves taking into account the resection area and surgical outcome after 1-year post-operative follow-up.

5.4.3 Results

The assessment included 89 seizures (57 from TLE and 32 from ETLE) from 50 patients (33 with TLE and 17 with ETLE). Only in one patient, which included two seizures, the Ictal ESI pipeline did not perform the analysis due to the quality of onset marking (TN: 1). Figure 5.7 shows the results of the pipeline for a patient with an extra temporal lobe epilepsy in the time window between -1s and +1s after the onset.

The results of the Sliding Ictal ESI were compared to the gold standard at the seizure and patient level. The test indices and diagnostic measures are summarized in table 5.4.

	Seizure-level			Patient-level		
	TLE	ETLE	Total	TLE	ETLE	Total
TP	26	6	32	16	2	18
FN	14	4	18	9	3	12
FP	6	2	8	3	1	4
TN	11	20	31	5	11	16
Sensitivity	65.0%	60.0%	64.0%	64.0%	40.0%	60.0%
Specificity	64.7%	90.9%	79.5%	62.5%	91.7%	80.0%
PPV	81.3%	75.0%	80.0%	84.2%	66.7%	81.8%
NPV	44.0%	83.3%	63.3%	35.7%	78.6%	57.1%
Accuracy	64.9%	81.3%	70.8%	63.6%	76.5%	68.0%

Table 5.4: The performance of Sliding Ictal ES at seizure- and patient-level. The results are categorized into three groups: TLE cases, ETLE cases, and total patients.

The results of the Total column show that there is not a significant difference between the diagnostic measures at the seizure and patient level. The sensitivity was 64% and 60%, specificity was 79.5% and 80%, and accuracy was 70.8% and 68% respectively.

At the seizure level, the sensitivity of TLE, ETLE, and Total cases are similar. However, the specificity and accuracy of ETLE cases are higher than those of TLE and Total cases. At the patient level, the sensitivity of ETLE patients is

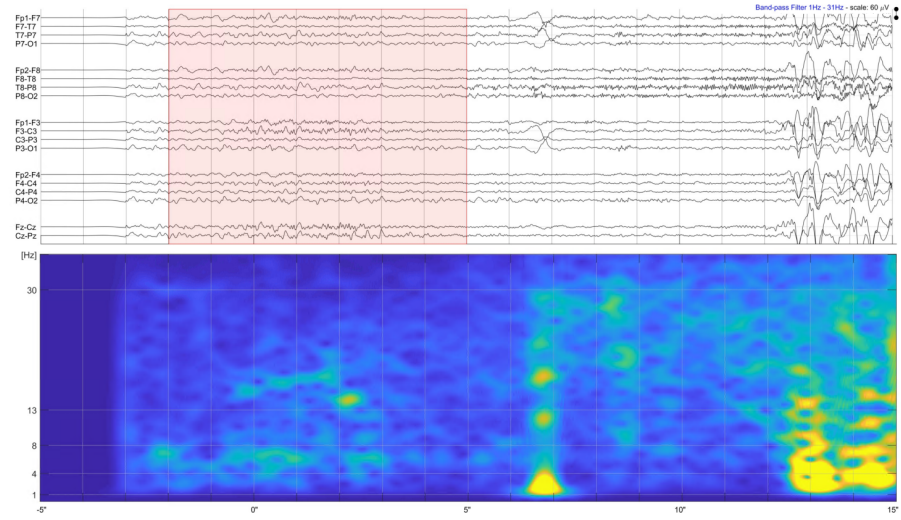
Band-pass Filter 1Hz - 31Hz - scale: 60 µV
Fp1-F7
F7-T7
T7-P7
P7-O1
Fp2-F8
F8-T8
T8-P8
P8-O2
Fp1-F3
F3-C3
C3-P3
P3-O1
Fp2-F4
F4-C4
C4-P4
P4-O2
Fz-Cz
Cz-Pz
[Hz]
30
13
8
4
1
-5"
0"
5"
10"
15"

(a)

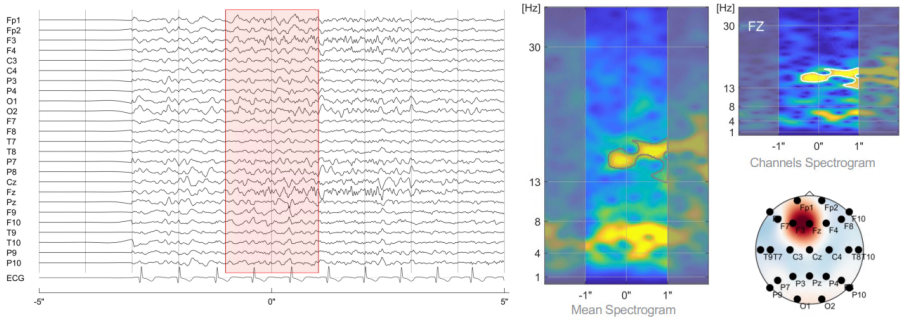
Fp1
Fp2
F3
F4
C3
C4
P3
P4
O1
O2
F7
F8
T7
T8
P7
P8
Cz
Fz
Pz
F9
F10
T9
T10
P9
P10
ECG
-5"
0"
5"
[Hz]
30
13
8
4
1
-1"
0"
1"
Mean Spectrogram
FZ
Channels Spectrogram

(b)

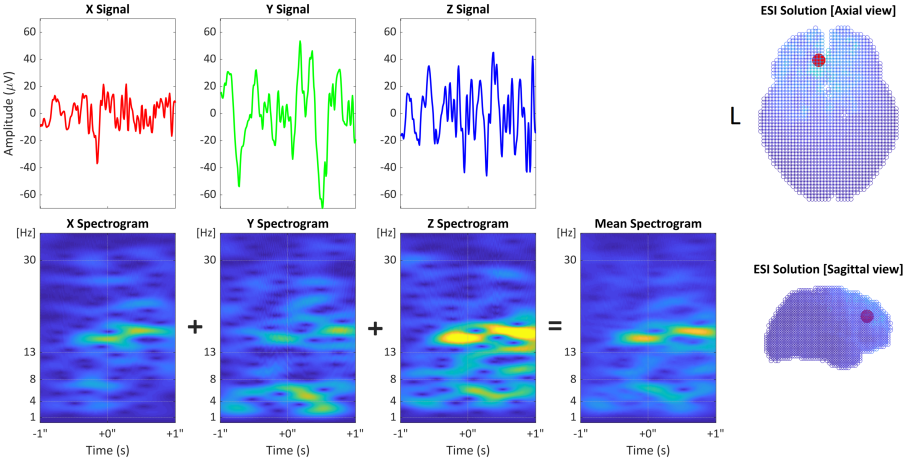
X Signal
Y Signal
Z Signal
Amplitude (µV)
60
40
20
0
-20
-40
-60
X Spectrogram
Y Spectrogram
Z Spectrogram
Mean Spectrogram
[Hz]
30
13
8
4
1
-1"
+0"
+1"
Time (s)
+
=
ESI Solution [Axial view]
L
ESI Solution [Sagittal view]

(c)

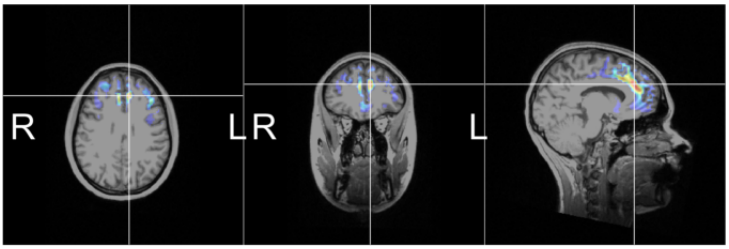

(d)

Figure 5.7: Siding Ictal ESI analysis of an ETLE patient, a) EEG signals in bipolar montage (top) and the mean spectrogram (bottom) generated using all EEG data from -5s to +15s after the seizure onset. b) Shorten EEG data in referential average montage between -5s and +5s after the onset and the sliding window of -1s to +1s in red box (left). Mean spectrogram; EEG of sliding window (middle). Spectrogram of the channel of interest (right-top), and corresponding topography generated by the choice of region growing WoI over all channels (right-bottom). c) The source with the highest energy in the WoI: the source signals of x, y, and z directions along with the corresponding spectrogram plots of the above-mentioned directions, and the mean spectrogram of the source. The location of this dipole is depicted in axial and sagittal views. d) ESI solution (SOZ) that is depicted in axial, coronal, and sagittal views in preoperative MRI slices. Note: The patient became seizure-free and achieved Engel class I status after undergoing resection in the specified region. The patient remained seizure-free during the one-year follow-up post-surgery.

lower than the TLE and Total cases (40% compared to 64% and 60%, respectively). However, the accuracy of TLE and Total cases is equivalent, and ETLE cases have relatively higher accuracy.

5.4.4 Discussion

At the seizure level, 10/18(55.5%) of false negative cases were localized near the resection zone but not inside. In 9/10 (90%) cases, our pipeline estimated the SOZ to be temporal polar (5), temporal posterior (2), and insula (2), even though the gold standard suggested that they should be localized in the Spencer region. In 1/10(10%), the SOZ was estimated to be in the insula, even though the resection area was frontal lateral (premotor). This is a limitation of our pipeline, which can estimate the localization reasonably close to the resection area but not necessarily in the same sub-lobe. However, in 6/18(33.3%) of false negative seizures, EEG findings were moderately far from the resection zone, and our pipeline's performance is poor for them. Figure 5.8 shows an example of one of these seizures. In 2/6 (33.3%) cases, the ictal activities were identified in the temporal electrodes despite the resection site being located in the occipital lobe. In contrast, ictal activities were localized in the posterior electrodes for 1/6 (16.7%), while the surgical site was located in the temporal mesial region. In 1/18(5.5%) of false negative seizures, MRI was with resection, and localization went wrong since no dipole existed in that region. This is another limitation of the pipeline that requires every sublobe

to have sufficient gray matter. Finally, in the last false negative seizure (1/18), the resection area was located in the left frontal mesial. However, the solution localized the frontal solution of both hemispheres depending on the choice of the sliding windows. This patient had two true positive seizures and one false negative seizure, and it was accordingly diagnosed as multifocal. This case can be categorized as one with high resolution in localization.

At the seizure level, eight cases were identified as false positives, making it difficult to draw a definite conclusion in this subgroup, similar to the previous ictal pipeline. However, the EEG findings suggest that these seizures may have been caused by the high resolution of the pipeline.

Sliding Ictal ESI has undergone performance testing in a few patient groups and studies, which may impact its performance metrics. Table 5.5 shows a list of these studies. In a recent project, researchers used Sliding Ictal ESI to investigate the impact of sphenoidal electrodes in EZ localization. These electrodes are minimally invasive channels that are inserted perpendicularly to the skin through the mandibular notch, just below the zygomatic process of the temporal bone [153]. The study involved analyzing EEG signals with and without the sphenoidal electrodes, and the results showed that including the electrodes increased the sensitivity from 49% to 73%, based on 169 out of 184 seizures. However, the performance of Sliding ESI was relatively poor when the sphenoidal electrodes were excluded. This could be due to poor recording of temporal activities because the lower temporal chain (F9/19, T9/10, TP9/10), F9/F!) was not used in the EEG setup. The manuscript of this study is currently being prepared for publication.

No	Study	Description	N	S.R.O.
1	[132]; Re-analysis	Ret.1; study ETLE cases	18	Knonw
2	[154]; Re-analysis	Ret.2	50	Knonw
3	[130]	Prs.1	40	Unknown
4	Minimally-invasive	Ret.3	40	Knonw

Table 5.5: The table of studies that Sliding Ictal ES was used as the ictal ESI tool. Abbreviation; S.R.O. = surgical resection outcome, Ret. = Retrospective study, Prs. = Prospective study.

Like the previous ictal pipeline, this pipeline also has a few limitations. The pipeline was created specifically to identify epochs with rhythmic ictal discharges. Therefore, this method is not appropriate for localizing electrodecremental ictal waves, spike-waves, and polyspike-waves. More investigations are required to evaluate the pipeline of different seizure types.

5.5 The author's contributions

In this chapter, three ictal ESI pipelines—ESI Power+Connectivity, Primary Ictal ESI, and Sliding-Window Ictal ESI—are presented. These algorithms have been incorporated into various studies and presented at multiple conferences

[155, 156, 157, 158]. Additionally, studies related to ESI Power+Connectivity and the clinical validation of ictal ESI have been published in academic journals [132, 154] (Table 5.6)

No	Article	Original contribution
1	Title: *Ictal EEG source imaging and connectivity to localize the seizure onset zone in extratemporal lobe epilepsy* Authors: Simone Vespa, **Amir G. Baroumand**, Susana Ferrao Santos, Pascal Vrielynck, Marianne de Tourtchaninoff, Odile Feys, Gregor Strobbe, Christian Raftopoulos, Pieter van Mierlo, Riëm El Tahry	performing the analysis + writing the manuscripts (methods)
2	Title: *Automated ictal EEG source imaging: a retrospective, blinded clinical validation study* Authors: **Amir G. Baroumand**, Anca A. Arbune, Gregor Strobbe, Vincent Keereman, Lars H. Pinborg, Martin Fabricius, Guido Rubboli, Camilla Gøbel Madsen, Bo Jespersen, Jannick Brennum, Otto Mølby Henriksen, Pieter van Mierlo, Sándor Beniczky	performing the analysis + writing the manuscripts

Table 5.6: Table of articles and author contributions using the automated ictal ESI Pipeline.

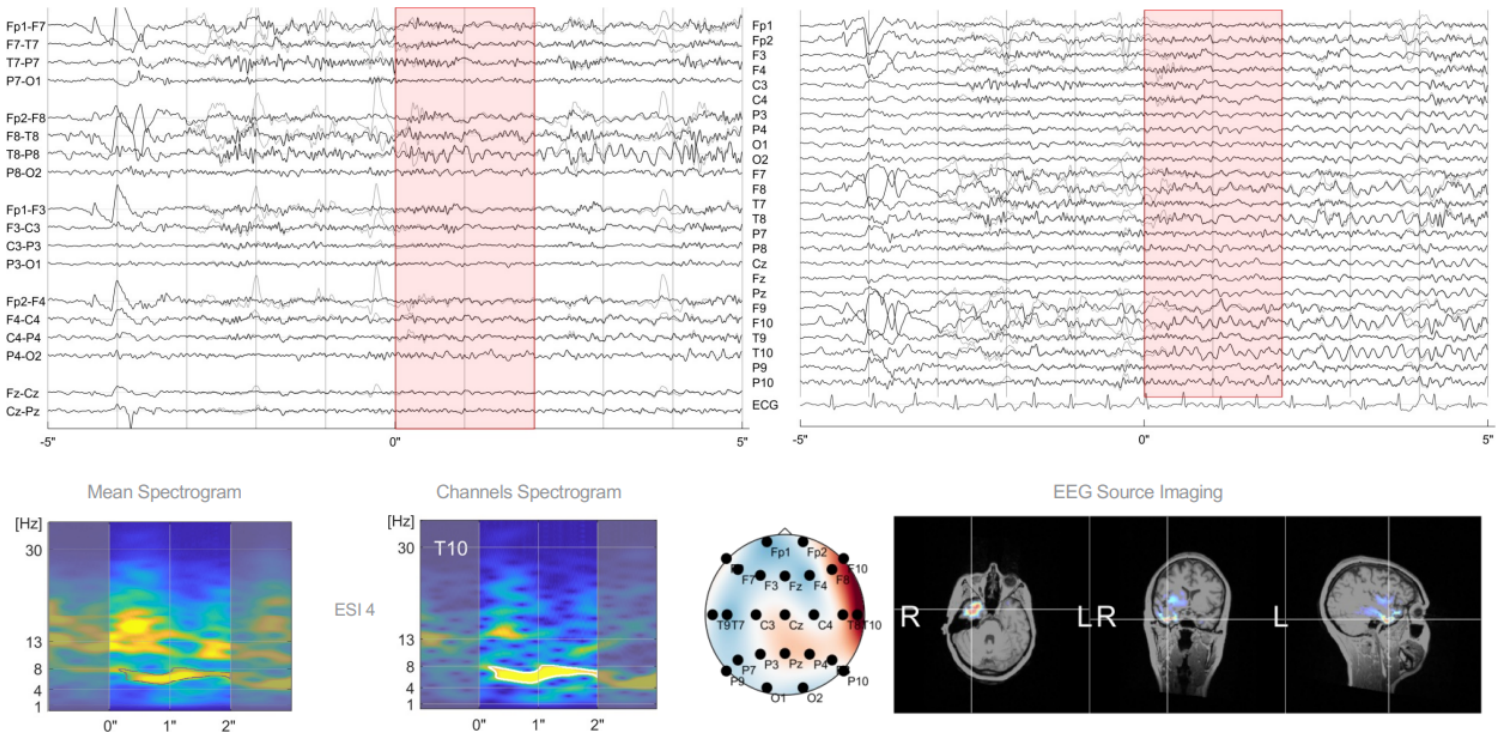

Figure 5.8: An example of a false negative outcome of Sliding Ictal ESI, where scalp EEG findings are not consistent with the resection zone. Theta is the frequency band of interest, which is visible in the right temporal chain electrodes, and the SOZ localization was found to be in the temporal lobe. However, this patient has an Engel Class 1 resection surgical outcome, and the gold standard is left occipital.

Chapter 6

Discussion

I hear and I forget. I see and I remember. I do and I understand.
Confucius

6.1 Introduction

The dissertation introduces two distinct ESI methods, with each method subject to individual evaluation within preceding chapters. The primary objective of this chapter is to conduct a comparative analysis, assessing the efficacy of these techniques both in relation to each other and in contrast to alternative modalities, particularly regarding their capability to pinpoint the epileptogenic zone.

6.2 Methods

A qualitative literature review was performed to assess the performance of ESI, magnetic source imaging (MSI) and other techniques used in the presurgical evaluation to localize the EZ. The clinical gold standard for diagnostic methodologies was established based on the resection area and post-surgical outcomes. The investigation entailed a comparative analysis of spatial solutions, representing 3D brain locations, against the postoperative outcomes at the sublobar level. Postoperative outcomes were determined through clinical follow-ups extending at least 12 months. To determine the correct localization of EZ, we considered the resection of the solution and seizure-freedom of the patients who had an Engel class 1 surgical outcome after one year of follow-up as the standard. In instances where sublobar outcome data was unavailable, the evaluation of performance relied on information extracted from the published article or supported documents, if accessible. We only included studies with a minimum of five participants, except for those that involved ictal MSI, and up to four cases were included since there were just a few studies. Among the chosen ESI or MSI papers, the evaluation

incorporated the outcomes derived from MRI, PET, and ictal SPECT, were also considered for their relevance and inclusion in the assessment process.

By including all data, the comparison among different modalities were presented as follows:

1. We analyzed each article and determined the test indices of the existing modalities using TP, FN, FP, and TN calculations. After this, we calculated the diagnostic accuracy measures, such as sensitivity, specificity, and accuracy, with a 95% confidence interval.

2. We computed TP, FN, FP, and TN for all available modality data, which we refer to as **overall**. Then, we calculated the sensitivity, specificity, and accuracy with a 95% confidence interval of each modality over overall.

3. Moreover, the sensitivity, specificity, and accuracy of existing review papers on ESI and MSI, namely **review paper**, were also included.

4. These measures were then compared over each modality and against the outcomes of PreOp and sliding ESI power, respectively.

5. Finally, the results of **overall** for each modality were compared to each other. Here, the outcome of PPV, NPV, odd ratio, positive likelihood ratio (PLR), and negative likelihood ratio (NLR) were also presented. PLR and NLR were calculated using the following formulas:

$$PLR = \frac{sensitivity}{1 - specificity}$$

$$NLR = \frac{1 - sensitivity}{specificity}$$

6.3 Results

We identified 63 articles, including [30, 92, 94, 99, 133, 152, 101, 123, 93, 111, 159, 160, 161, 162, 163, 164, 165, 166, 167, 168, 169, 170, 171, 172, 173, 174, 175, 176, 177, 178, 179, 180, 181, 182, 183, 184, 185, 186, 187, 188, 189, 190, 191, 192, 193, 194, 195, 196, 197, 198, 199, 200, 201, 202, 203, 204, 205, 206, 207, 208, 209], and one review paper ([141]) on ESI and MSI meeting our inclusion criteria, spanning the period from 1999 to 2023. Table 6.1 shows the number of articles and patients included in the literature review, review paper, and our in-house ESI pipeline evaluation studies.

The evaluation of the discussed modalities is presented in figures 6.1 to 6.5 through forest plots that display sensitivity, specificity, and accuracy. Each plot assesses the individual studies, followed by the overall findings. Then, it presents the outcome of the modality in the review study (if available), and finally, it reports the PreOp and Sliding Ictal ESI outcome. According to these plots:

No	Modality	Literature review		Review paper		In-house ESI	
		#Art.	#Pat.	#Art.	#Pat.	#Art.	#Pat.
1	Interictal ESI	27	717	19	515	-	-
2	Interictal MSI	25	745	19	440	-	-
3	Ictal ESI	12	259	6	159	-	-
4	Ictal MSI	7	64	4	36	-	-
5	MRI	7	519	-	-	-	-
6	PET	13	>535	-	-	-	-
7	Ictal SPECT	9	351	-	-	-	-
8	PreOp	-	-	-	-	6	225
9	Sliding Ictal ESI	-	-	-	-	1	50

Table 6.1: The chart comprised articles evaluating diverse modalities and the review paper information concerning the localization of the EZ in patients with drug-resistant epilepsy.

1. PreOp exhibited superior sensitivity compared to Sliding Ictal ESI while Sliding Ictal ESI demonstrated higher specificity than PreOp. Remarkably, both in-house techniques showcased nearly identical levels of accuracy.

2. The PreOp technique showed sensitivity, specificity, and accuracy measures that closely resemble the overall results obtained from Interictal ESI and Interictal MSI solutions, respectively. However, the Sliding Ictal ESI method displays reduced sensitivity compared to Ictal ESI and Ictal MSI; nevertheless, its specificity surpasses that of the aforementioned techniques. Notably, the accuracy of Sliding Ictal ESI aligns closely with both Ictal ESI and Ictal MSI methodologies.

3. The performance of PreOp was compared with Ictal ESI, Ictal MSI, MRI, PET, and Ictal SPECT. PreOp has lower sensitivity than Ictal MSI, higher sensitivity than Ictal SPECT, and sensitivity almost equal to the other techniques. The specificity of PreOp is almost similar to Ictal SPECT but higher than all other mentioned techniques. Finally, the accuracy of PreOp is comparable to all techniques except Ictal SPECT, which has lower accuracy.

4. A comparison was made between the performance of Sliding Ictal ESI and other techniques such as interictal ESI, interictal MSI, MRI, PET, and Ictal SPECT. The sensitivity of Sliding Ictal ESI was found to be lower than all techniques except Ictal SPECT, which had similar results. However, Sliding Ictal ESI outperformed all other techniques in terms of specificity. In the end, Sliding Ictal ESI showed the same level of accuracy as all other methods except for Ictal SPECT, where it had a higher accuracy.

The following text summarizes the overall findings of the study, which are presented in the figures of 6.6(a-d). They show different measures such as sensitivity, specificity, PPV, NPV, accuracy, OR, PLR, and NLR. They also allow for a comparison of the performance of the developed in-house ESI techniques to the overall results. Based on the findings presented in Fig. 6.6-a, it can be concluded that ictal MSI and interictal MSI are the most sensitive and specific modalities, respectively. On the other hand, Ictal SPECT and Ictal MSI have the lowest sensitivity and specificity, respectively. PreOp falls within the same range as the two interictal-based techniques and has a reasonable sensitivity-specificity balance. By considering the position of Sliding Ictal ESI in the plot, it can be inferred that Sliding Ictal ESI can complement PreOp to improve localization performance.

Although Ictal SPECT and Ictal MSI demonstrated the highest positive predictive value (PPV) and negative predictive value (NPV), respectively (as seen in Fig. 6.6-b), they had the poorest performance in the other metric. On the other hand, both interictal-based techniques showed better results due to a more balanced PPV-NPV ratio. It is worth noting that Sliding Ictal ESI had the highest PPV and NPV, while PreOp had an almost equivalent NPV.

Based on the findings presented in Fig. 6.6-c, it can be concluded that all techniques, except Ictal SPECT, have an accuracy rate ranging between 63% and 68%. Ictal SPECT, on the other hand, has the lowest accuracy rate. In addition, the interictal-based approaches have the highest OR, which is above 3. PreOp has the same accuracy rate and OR as the other two interictal methods. Moreover, Sliding Ictal ESI maintains the same accuracy rate as PreOp but has double the OR.

In addition to the clinical measures used, positive likelihood ratio and negative likelihood ratio were calculated for each modality's overall findings. As shown in Fig. 6.6-d, both interictal-based methods have the highest PLR and lowest NLR. PreOp and Sliding Ictal ESI also have low NLRs but only PreOp has the same PLR as the interictal methods. Meanwhile, Sliding Ictal ESI has almost twice the PLR of PreOp.

To better compare the outcomes of different modalities, a stacked bar chart in Fig. 6.7 was used to summarize the findings. This chart presents the sensitivity, PPV, NPV, and accuracy of the modalities. The chart shows that interictal MSI, interictal ESI, and MRI are the three best modalities for localizing the EZ when all the measures are considered. Both ictal-based techniques perform similarly, but PET and Ictal SPECT have lower performance. Among the in-house ESI techniques, PreOp works similarly to the interictal-based methods, and Sliding Ictal ESI has slightly better performance. The findings obtained through in-house ESI potentially corroborate the hypothesis formulated in the expert review concerning the localization of the epileptogenic zone. Furthermore, these results suggest that in-house ESI could yield a comparable level of performance to that of an expert.

6.4 Discussion

According to the overall findings, interictal-based pipelines exhibited similar performance to each other, and they generally have better performance compared to other imaging modalities. This could be attributed to the high signal-to-noise ratio and low amounts of noise or artifacts present in the EEG data. It is worth noting that most of the studies used in the literature review that the overall findings relied on were performed retrospectively. In the prospective studies, it was shown that ESI and MSI results can positively influence the patients' presurgical management [127, 201, 210]. Nevertheless, it is essential to investigate whether the choice of interictal solutions is independent and blinded to other data than EEG. Incidentally, identifying sufficient genuine spikes (at least five per type) in long-term EEG recordings, the analysis of ESI or(and) MSI, and accurate interpretation of the analysis remain challenging tasks that require expertise to be implemented in clinical practices. After these two techniques, MRI, which provides detailed structural images of the brain, had the highest performance. This is due to different reasons, including its high spatial resolution and ability to detect structural abnormalities. On the other hand, it was found that the performance of Ictal ESI was not as good as interictal ESI. This could be because ictal epochs have a low signal-to-noise ratio, and ictal activities propagate rapidly throughout the brain. To compensate for these, inverse solutions probably require lower electromagnetic tomography resolution and proper artifact removal is essential before ictal analysis. Pre-processing steps were enhanced to improve the Sliding Ictal ESI pipeline to ensure that fewer artifacts were involved in the analysis. Other findings are the lower performance of PET and Ictal SPECT. Some reasons explain this, including the lower temporal resolution of these techniques and the complexity of interpreting the results.

Besides the article we discussed earlier, there are other studies that have looked into the usefulness of ESI and MSI for presurgical evaluation. Staljanssens et al. found that combining functional connectivity with ESI can help identify the seizure onset zone in a non-invasive way with high accuracy [97]. In their study, they calculated the distance between the estimated ESI solutions and the resection border for each case. When using ESI alone, only 31% of the seizures were localized inside the resection zone. However, when ESI was combined with connectivity, the number increased to 72%. It's worth noting that the choice of seizure onset is a limiting factor because connectivity performance depends on it. In another study, Pellegrino et al. [95] conducted a study to determine the location of the seizure onset zone (SOZ) by using ictal EEG and MEG data. They applied "wavelet-based maximum entropy on the mean (wMEM)" as an inverse solution and compared the results with the clinical SOZ, which was obtained through intracranial EEG or lesion topography. The study included 46 MEG EEG seizures from 13 individual patients. The researchers found that the estimated SOZ derived from MSI and ESI were in agreement with the clinical SOZ in 81% of the seizures. Additionally, MSI was found to be more accurate than ESI in localizing the

sources close to the clinical SOZ. Although this study proposed a novel pipeline for ESI and MSI localization, further testing with a larger sample is necessary to draw a more concrete conclusion regarding ESI/MSI comparison. The surgical outcome was known for four individuals in the study, with one patient being seizure-free after one year of postoperative follow-up.

Sohrabpour et al. [211] and Jiang et al. [212] have validated the FAST-IRES technique, which is a fast spatiotemporal iteratively reweighted edge sparsity minimization method, for ESI and MSI. This technique helps to address the issue with conventional localization approaches in determining the spatial extent of the source. As a result, it has the potential to differentiate between relevant brain activity and the background, enabling better analysis of interictal and ictal data. ESI was assessed on 16 patients, and the mean localization error in seizure-free (n=9, Engle 1-2) and non-seizure-free (n=7, Engel 3-6) cases was 13.9±11.96 mm and 23.5±15.7 mm, respectively. Meanwhile, the mean localization error to the resection area for MSI evaluation was 12.4±20.6 mm.

Various algorithms have been developed by research groups for ESI/MSI. Additionally, commercial software such as BESA (BESA GmbH, Grafeling, Germany) and Curry (Compumedics Neuroscan, Hamburg, Germany) have been evaluated for their performance in localizing EEG and MEG data [152, 174, 123, 101]. Rampp et al. [213] conducted a retrospective study of 1000 patients and demonstrated the added value of MSI analysis using BESA and Curry. They showed that complete MEG resection in patients with ETLE (n=67), TLE (n=86), and mesial-TLE (n=49) resulted in the sensitivity of 84%, 56%, and 64%, respectively. While specificity was 89%, 77%, and 69% in these patients group. In the study, the assessment of MSI results was not performed at the sublobar level but at the lobar level, in concordance with the presurgical workup.

The evaluation of each imaging modality has been discussed, and it is also found that the performance of each individual technique is limited. For instance, MRI shows reasonable performance when used for presurgical evaluation, but it does not help in cases where the lesion is absent. This means that relying on only one modality does not necessarily lead to promising surgical outcomes. Therefore, it is necessary to combine results from different imaging modalities to obtain a more comprehensive assessment for presurgical evaluation. A recent study by Czarnetzki et al [133]. investigated the optimal combination of available imaging techniques to achieve a positive outcome in patients with MRI-negative focal epilepsy. To achieve this, the study used morphometric MRI analysis (MAP), PET, Ictal SPECT, and ESI techniques on the patients. It evaluated the results of each modality and the combination of them. On an individual level, none of the techniques exceeded an odds ratio (OR) greater than 0.5, except for patients with interictal discharges, where the OR reached 3.2. On a combination level, the results improved when the ESI results of patients with only a spike were combined with other techniques. The study found that a combination of Ictal SPECT, ESI, and PET had the highest

performance, and OR increased to 11. Figure 6.8 provides more information about the measures of modalities at both individual and combination phases.

These findings demonstrate the potential of combining results from various modalities to form a more concrete hypothesis regarding the epileptogenic zone in drug-resistant epilepsy patients. In this perspective, PreOp had demonstrated similar accuracy to previously reported neuroimaging techniques in the presurgical evaluation of epilepsy patients. It has defined good accuracy for insular implication in the irritative zone, which is challenging with classical interictal scalp EEG interpretation. Prospective studies using PreOp have shown excellent localizing information and a high yield even in complex patient groups. This is compared favorably to high-density ESI. Furthermore, it confirmed that automated ESI can be helpful in the presurgical assessment of cases where MRI scans show no abnormalities, particularly when planning the implantation of depth electrodes for sEEG. It's important to integrate the results of ESI into the entire multimodal evaluation and interpret them clinically. There was a single retrospective study done on Sliding Ictal ESI, which showed its effectiveness in accurately localizing the seizure onset zone. To gain more understanding of the outcome of this in-house method, it would be beneficial to evaluate it in a larger patient group.

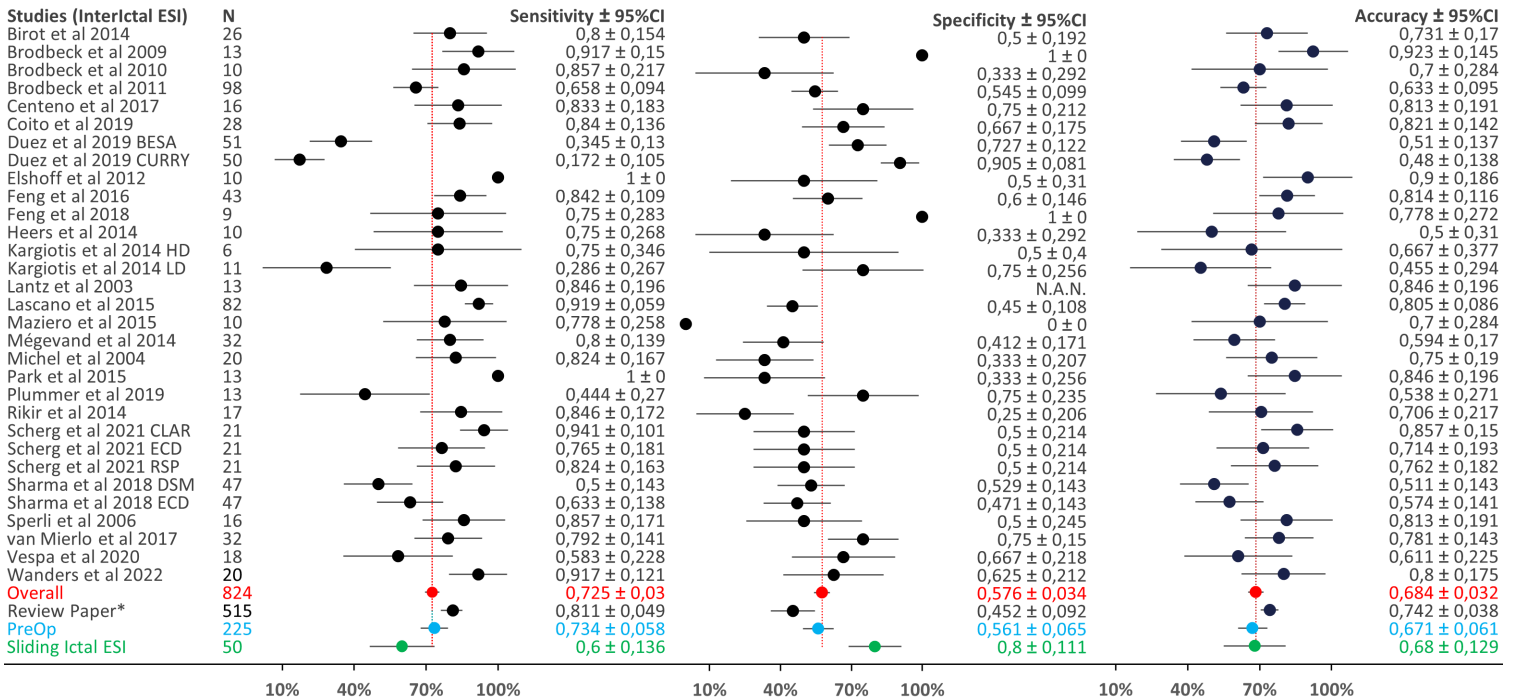

Figure 6.1: Forest plots illustrating the sensitivity, specificity, and accuracy of the **interictal ESI**; individual study results compared to overall findings, review paper outcome, and in-house ESI results. Abbreviation; N.A.N.: not a number.

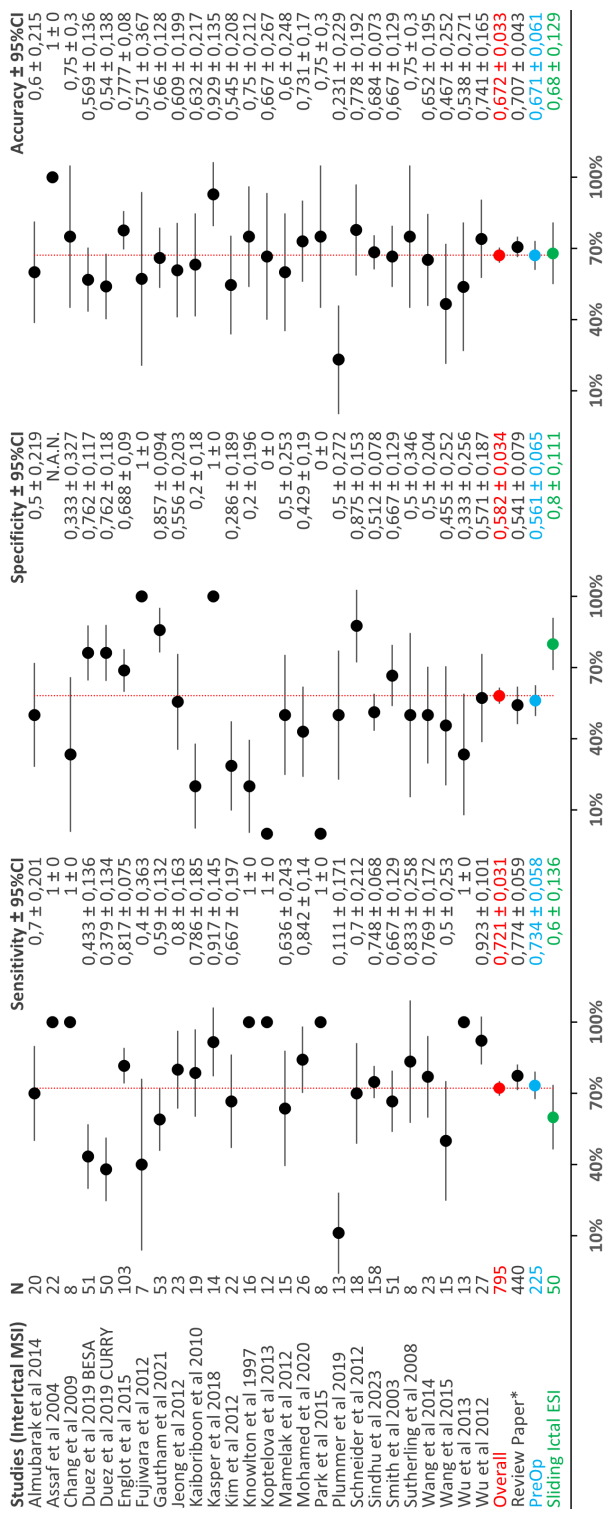

Figure 6.2: Forest plots illustrating the sensitivity, specificity, and accuracy of the **interictal MSI**; individual study results compared to overall findings, review paper outcome, and in-house ESI results. Abbreviation; N.A.N.: not a number.

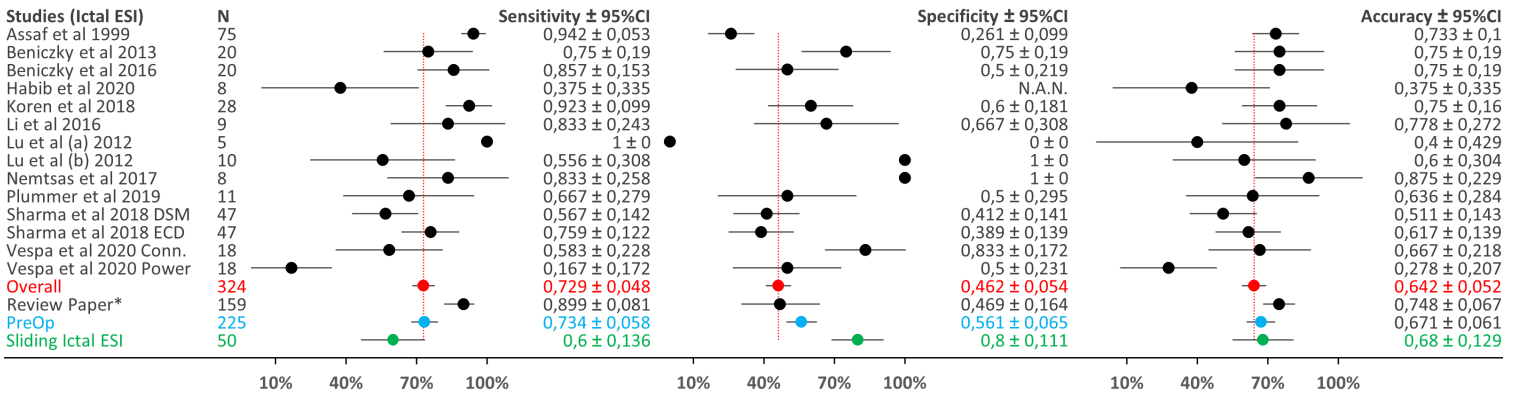

Figure 6.3: Forest plots illustrating the sensitivity, specificity, and accuracy of the **ictal ESI**; individual study results compared to overall findings, review paper outcome, and in-house ESI results. Abbreviation; N.A.N.: not a number.

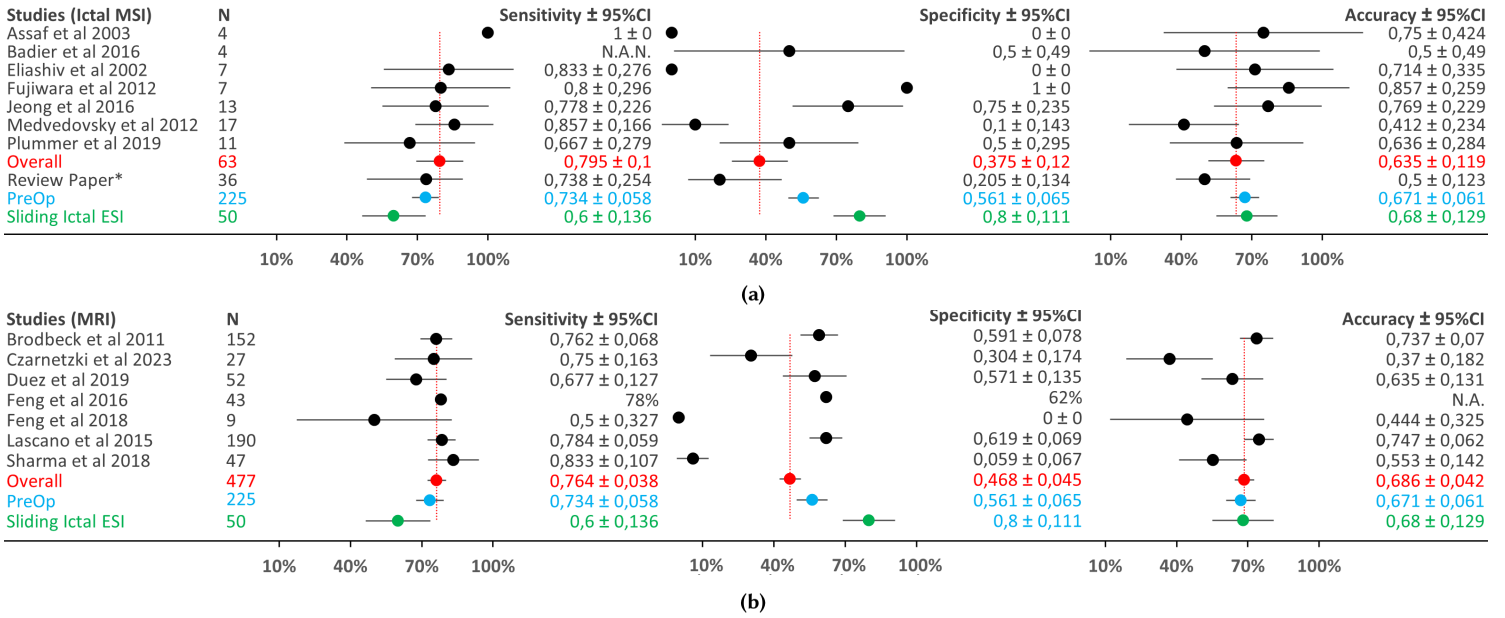

Figure 6.4: Forest plots illustrating the sensitivity, specificity, and accuracy of the a: **ictal MSI**, and b: **MRI**; individual study results compared to overall findings, review paper outcome, and in-house ESI results. Abbreviation; N.A.N.: not a number.

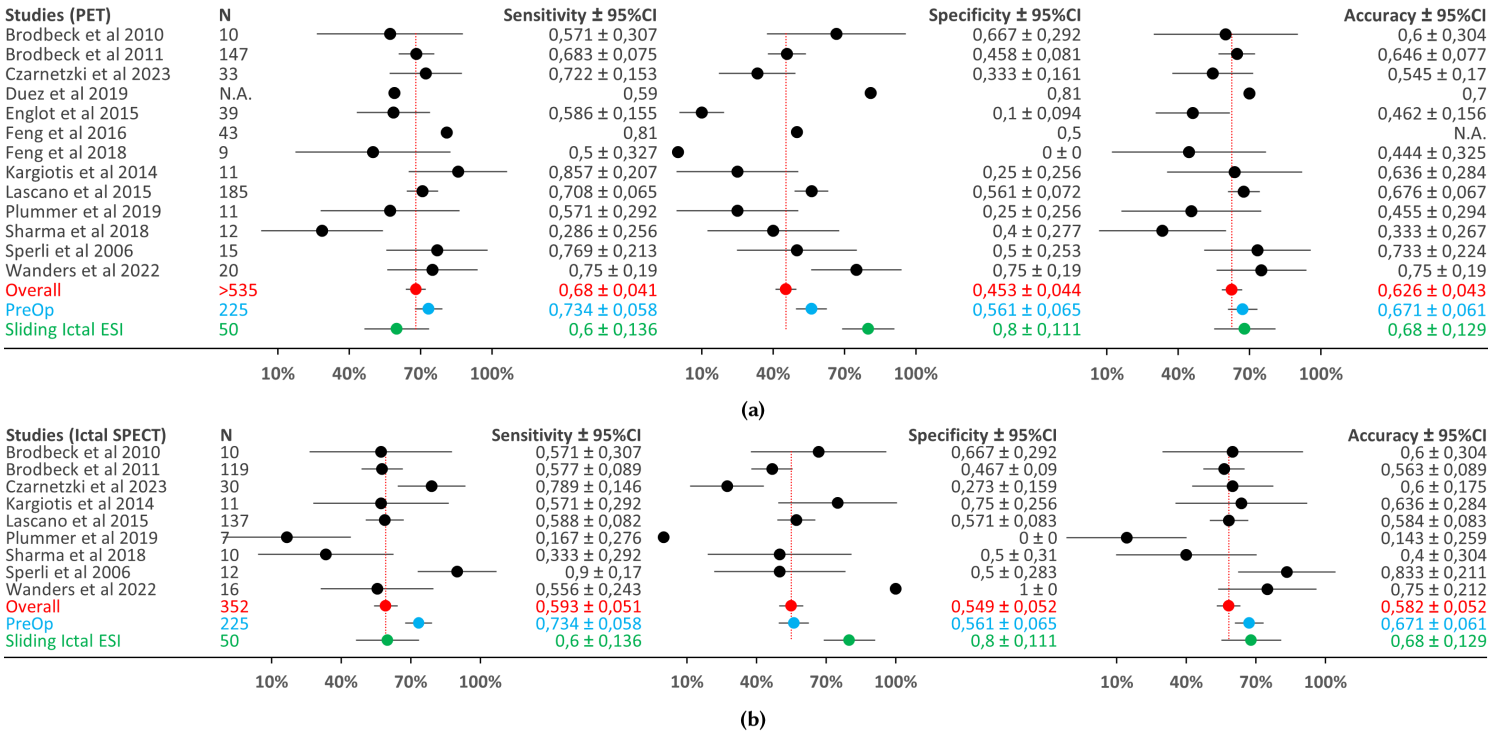

Figure 6.5: Forest plots illustrating the sensitivity, specificity, and accuracy of the a: **PET**, and b: **Ictal SPECT**; individual study results compared to overall findings, review paper outcome, and in-house ESI results. Abbreviation; N.A.N.: not a number.

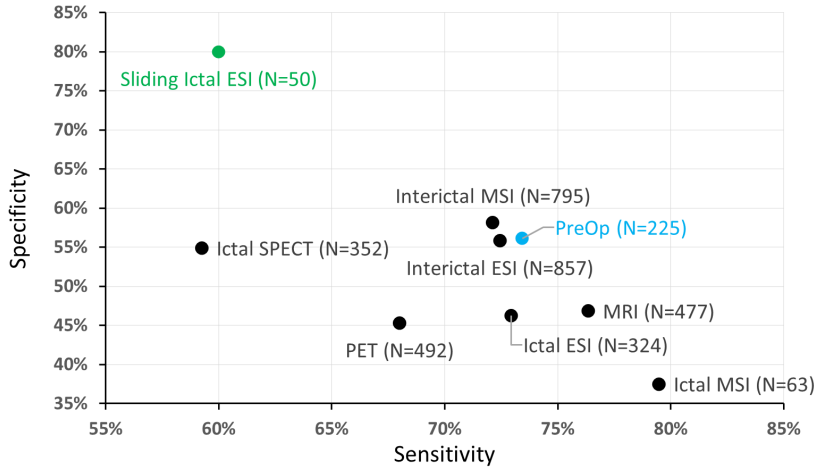
Specificity
Sensitivity
85%
80%
75%
70%
65%
60%
55%
50%
45%
40%
35%
55%
60%
65%
70%
75%
80%
85%
Sliding Ictal ESI (N=50)
Interictal MSI (N=795)
PreOp (N=225)
Ictal SPECT (N=352)
Interictal ESI (N=857)
MRI (N=477)
PET (N=492)
Ictal ESI (N=324)
Ictal MSI (N=63)

(a)

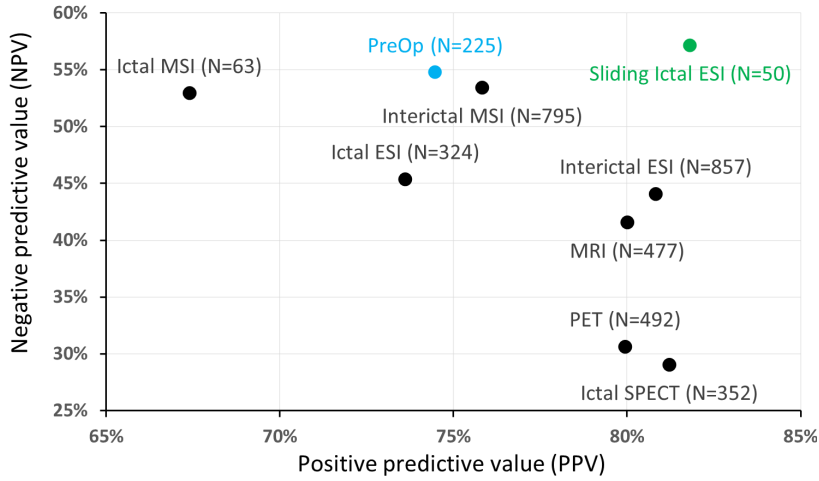
Negative predictive value (NPV)
Positive predictive value (PPV)
60%
55%
50%
45%
40%
35%
30%
25%
65%
70%
75%
80%
85%
Ictal MSI (N=63)
PreOp (N=225)
Sliding Ictal ESI (N=50)
Interictal MSI (N=795)
Ictal ESI (N=324)
Interictal ESI (N=857)
MRI (N=477)
PET (N=492)
Ictal SPECT (N=352)

(b)

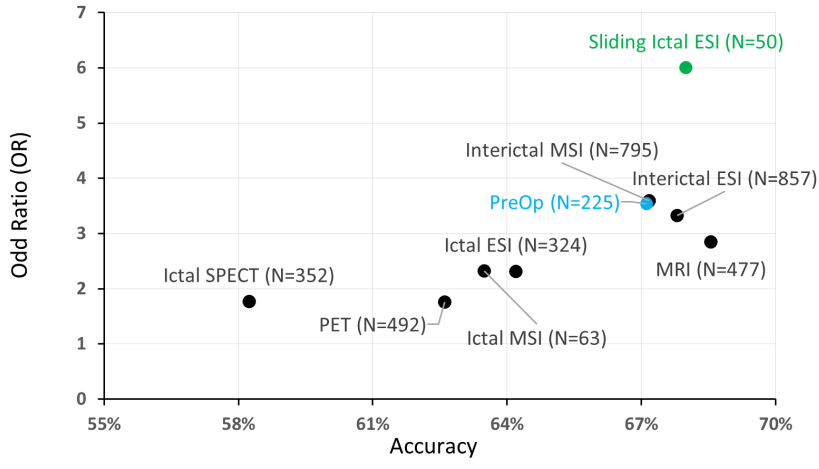
Odd Ratio (OR)
Accuracy
7
6
5
4
3
2
1
0
55%
58%
61%
64%
67%
70%
Sliding Ictal ESI (N=50)
Interictal MSI (N=795)
Interictal ESI (N=857)
PreOp (N=225)
Ictal ESI (N=324)
MRI (N=477)
Ictal SPECT (N=352)
PET (N=492)
Ictal MSI (N=63)

(c)

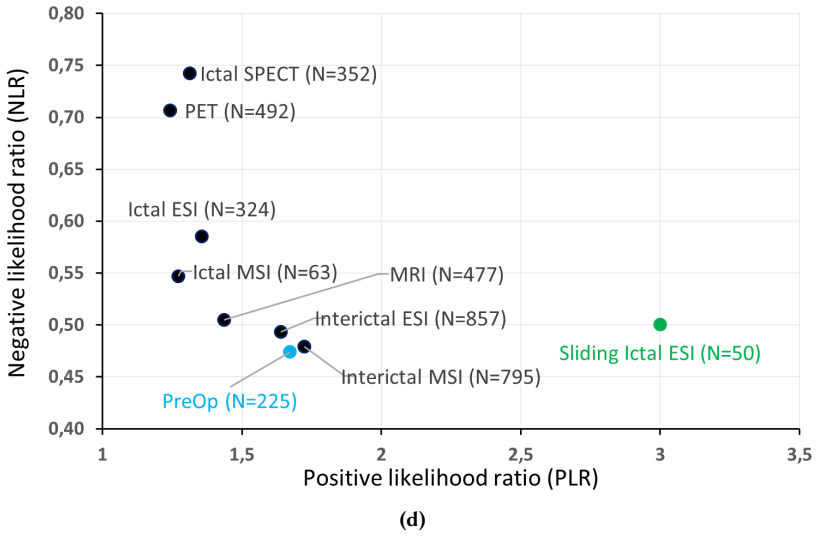

(d)

Figure 6.6: Comparative analysis across seven modalities versus the overall findings of our in-house ESI pipelines, a: Sensitivity-Specificity, b: PPV-NPV, c: Accuracy-OR, d: PLR-NLR.

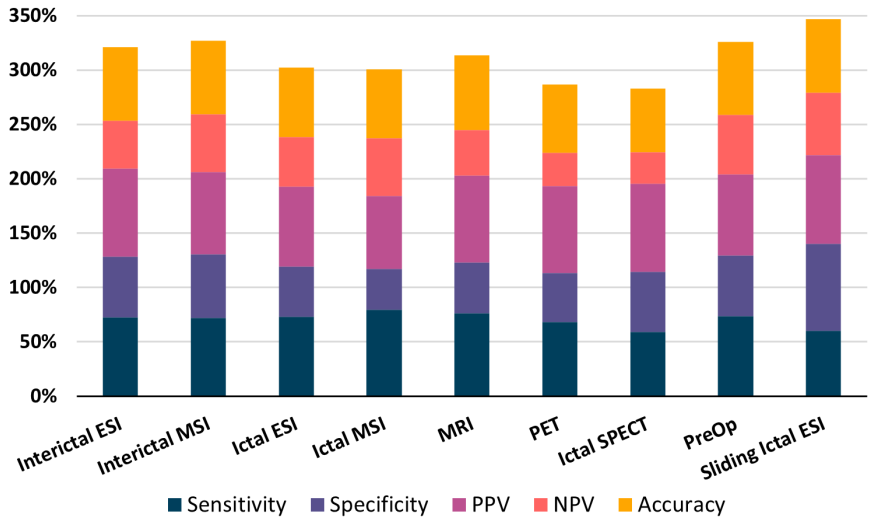

Figure 6.7: The stacked bar graphs illustrating the compositions and comparative analyses of sensitivity, specificity, PPV, NPV, and accuracy across all modalities, including in-house developed ESI techniques.

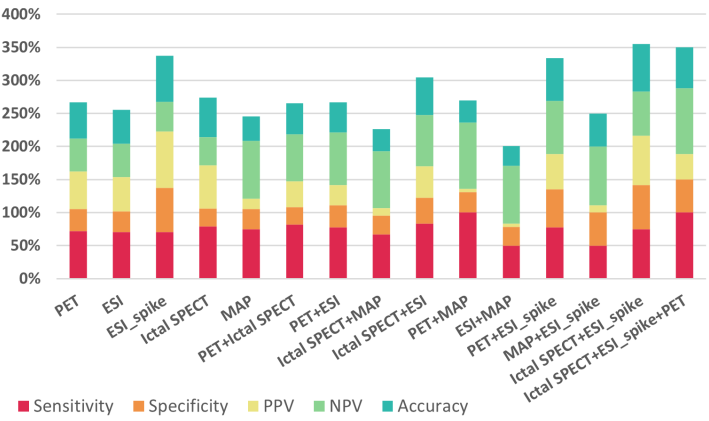

Figure 6.8: The stacked bar graphs showing the outcome of study conducted by Czarnetzki et al [133].

Chapter 7

Conclusions and future options

Be happy for this moment. This moment is your life.

Khayyam

In the final chapter, we recapitulate the main findings presented in this dissertation, explore the potential topics for future research, and draw final conclusions.

7.1 Summary

The purpose of the dissertation was to develop automated pipelines to localize the epileptogenic zone in patients suffering from drug-resistant epilepsy using interictal and ictal EEG data. Automated interictal ESI, PreOp, was validated in multiple retrospective and prospective studies. Additionally, Ictal ESI was developed and the performance to localize the SOZ was assessed. These two pipelines underwent retrospective and prospective studies. Our approach to make this happen consisted of the following steps.

In Chapter 2, we inquired about the subject of epilepsy and provided a comprehensive overview of the issues that afflict patients. We began by discussing the various classifications, statistics, and definitions of seizures and epilepsy, and then explored the different diagnostic options and conventional treatment methods. As a result of this analysis, we were able to examine the concept of drug-resistant epilepsy in more depth. Finally, we examined the various structural and functional neuroimaging techniques used in the presurgical evaluations of refractory epilepsy patients.

In Chapter 3, we explored the details of EEG and ESI. In the EEG section, we introduced the source of EEG signals in the brain, the different rhythms and artifacts that can be present in scalp EEG signals, and the commonly

used montages for recording them using both low- and high-density electrode setups. Moving on to ESI, we began by introducing the head model and discussing how to generate it based on an individual patient's MRI. We then delved into forward models and leadfields matrix, providing detailed explanations of their mathematical and physical aspects. Finally, we provided an overview of conventional inverse techniques in the literature.

Chapter 4 investigated the automated interictal ESI pipeline. This chapter began with the retrospective, blinded clinical validation study of this technique that elaborated via the full article about it. Then, we discussed the studies we performed using PreOp. One study compared the accuracy of automated interictal ESI on high-density and low-density EEG in 30 patients. It was shown that there were no significant differences between low- and high-density ESI results with 25 to 257 electrodes. It concluded that the low-density EEG setup could be sufficient for interictal ESI, especially if enough spikes are detected. The performance of PreOp to localize the epileptogenic zone in patients with insular epilepsy was assessed. ESI findings were compared with the simultaneous sEEG interictal activities. This study showed that LD-ESI accurately defines the insular implication in the IZ. PreOp was also evaluated in two prospective projects. In one of them, it was used in a patient group with 29 subjects with MRI-negative epilepsy. The results showed the added value of automated interictal ESI, especially in better planning for depth electrode implementation of sEEG recordings. PreOp also analyzed data from 122 patients in a 5-year prospective study started in 2017. Based on the results of 40 cases with subsequent epilepsy surgery, Preop had excellent localization findings with a high yield, even in complex patient groups. PreOp participated in a multi-center project called PROMAESIS alongside 17 European epilepsy centers. The project aimed to evaluate the accuracy and clinical relevance of automated ESI in presurgical epilepsy assessment. The project was the third prospective study of its kind. In the last study, PreOp, along with two other ESI pipelines, were used to evaluate the time required for integrating interictal ESI data into the clinical workflow of a specialized epilepsy center. The study revealed that PreOp algorithm requires significantly less working time compared to the other two ESI algorithms. Finally, we conducted a comprehensive evaluation of PreOp across multiple studies.

Chapter 5 primarily focused on developing an automated technique for localizing the SOZ. We devised an algorithm that utilized the power of EEG signals in the frequency domain along with functional connectivity measures. Our approach outperformed the conventional ESI power technique in a group of 18 patients with Epilepsy-related Temporal Lobe Epilepsy (ETLE). However, we found that ESI power still had the potential to be utilized in further developments. Consequently, we made some improvements to the ESI power method and generated an automated ictal ESI algorithm based on time-frequency content in source space. To assess its performance, we analyzed EEG signals from 50 patients, and our technique proved to be effective. We further enhanced the pipeline and addressed its limitations, which led to the

development of sliding-window ictal ESI. We evaluated its performance using the same dataset used for validating the previous ictal ESI pipeline.

In Chapter 6, we compared the performance of PreOp and Sliding Ictal ESI techniques with each other and with the other presurgical modalities for EZ localization. The analysis was carried out by collecting relevant articles from the literature that focused on EZ localization using interictal-ESI/MSI and ictal-ESI/MSI techniques. We extracted the performance metrics and cross-referenced them with results from other modalities such as MRI, PET, and ictal-SPECT. A comprehensive performance table was generated to facilitate intermodality comparison, and it involved the outcome of 7 different modalities.

7.2 Future research possibilities

The future trajectories of this study hinge on the resolution of the following research inquiries:

1. How to optimize the performance of our in-house pipelines?
2. How to enhance the interpretation of clinical data by providing additional insights and findings beyond the standard analysis?
3. How to effectively integrate these pipelines into the clinical workflow?
4. How to extract other informative clinical findings using our in-house pipelines?
5. In what ways can we integrate the outcomes of this research into other related domains?

To enhance the pipeline's performance, upgrading the head model and utilizing more sophisticated forward models or/and inverse solutions can be beneficial. For improving the head model, certain quality assurance procedures are necessary to guarantee the reliability of the segmentations and the ultimate head model. Moreover, evaluating alternative forward models, such as FEM, enables the comparison of its performance with FDM. One potential option to enhance the inverse solution in Ictal ESI analysis is to decrease the electromagnetic tomography resolution of the modified LORETA algorithm currently used. This can lead to a smoother inverse solution and consequently could be a helpful approach to consider.

The PreOp and Sliding Ictal ESI pipelines are used to analyze data without any interpretation of the results. Though these pipelines are beneficial, the interpretation of ESI results is still unresolved, and further research is needed in this regard. The PreOp pipeline applies ESI on the automatically detected events and provides results for up to 4 clusters, without verifying whether they are genuine spike clusters. However, it has been observed that this pipeline fails to provide ESI in some cases because no genuine spikes clusters

are within the first four clusters, or EEG data are not spiky. In a recent study of 33 patients, PreOp failed to provide ESI on spiky data in 30% of the cases [133], indicating the need for an additional algorithm to distinguish genuine interictal activities from other data. The high-frequency oscillations could serve as a potential biomarker. To confirm the genuineness of automated detected events, the concordance of these oscillations with the detected events can be examined [214]. This will help in providing more insights into the epileptogenic zone, especially in cases where the results of interictal and ictal are not identical.

The integration of an algorithm into clinical practice requires careful consideration to ensure its safe and effective use. For instance, essential requirements such as "Clinical Validation and Evidence" and "Regulatory Approval and Compliance" must be met. PreOp has already undergone clinical validation studies and regulatory approval, including the CE label and FDA approval, making it a reliable pipeline for clinical workups. However, before Sliding Ictal ESI can be implemented in clinical practice, some essential steps need to be taken. First, the pipeline should be standardized to work more objectively, with minimal manual interaction. Algorithms for automated artifact reduction and identifying the ictal onset and frequency band of interest are necessary. Second, validation studies are required to verify the Ictal pipeline for other seizure types, including spasm, spike waves, and polyspike waves. Apart from these notes, head model generations have been performed on specific patient MRIs, but further studies are necessary to verify their performance on template MRIs. Moreover, the estimation of epileptogenic zone localization in the pipeline requires improvement. Currently, it is a point estimation, but using Maximum Entropy on the Mean (MEM) [95] or Source Imaging based on Structured Sparsity (SISSY) techniques [215] can provide an area and make the analysis more realistic . This could enable more precise resection planning.

Performing analysis of EEG data using in-house ESI pipelines can produce more informative results. A study by Jeong et al. found that localization of the gamma band activities during Pre-Ictal epochs in MEG data had the highest concordance with the resection cavity among the frequencies and time windows [209]. Sliding Ictal ESI can be applied to the Pre-Ictal data in EEG to validate if it produces the same results. It is also worth conducting further research to explore whether these gamma band activities could potentially serve as a biomarker for the EZ.

There is the potential to assess the usefulness of our in-house ESI pipelines in epilepsy and some other diseases. Depending on the need for localization in a sample time or an epoch of data, PreOp and Ictal ESI could be performed. One potential area of research involves the diagnosis of epilepsy and the verification of its specific type. Utilizing PreOp analysis and the identification of corresponding source localizations, it may be possible to accurately identify and classify epileptic events, shedding light on critical diagnostic questions. PreOp also has the potential to be a valuable tool in evaluating the effectiveness of AED therapy in patients with confirmed

epilepsy. However, further research is needed to determine its usefulness by analysis of both focal and generalized spikes. A recent study utilized PreOp to assess the effectiveness of EEG (low density and high density) and MEG in detecting epileptiform activity in Alzheimer's disease (AD). The study found that AD patients with epileptiform activity exhibited greater cognitive deficits compared to those without. However, further research with a larger sample size is necessary to gain a better understanding of the phenomenon. An area of further exploration in seizure prediction involves using Ictal ESI. This process allows for monitoring of brain activity at the source level, particularly in the region where previous seizures have been localized. By extracting relevant features from this data, there is potential for inputting this information into an artificial intelligence model for forecasting future seizures.

7.3 Final conclusions

The dissertation discusses two in-house ESI pipelines that can be used to localize the EZ using interictal and ictal data in an automated, objective, and standardized manner. PreOp has already been incorporated into clinical practices and is currently used in presurgical evaluations. It has been shown to perform similarly for both low- and high-density electrode setups and has demonstrated consistent performance in cases of TLE and ETLE. Furthermore, it is applicable even in challenging cases with negative MRIs. Additionally, a clinical validation study was carried out for Sliding Ictal ESI. The ESI process is already automated, but further research could automate the entire pipeline. PreOp has shown higher sensitivity, and Sliding Ictal ESI has shown a higher specificity. Combining the results of PreOp and Ictal evaluations can provide complementary information, which can be advantageous in improving the presurgical workup and enhancing clinical decision-making in patients with epilepsy who are being considered for surgical intervention.

References

[1] R. S. Fisher et al. “Epileptic seizures and epilepsy: definitions proposed by the International League Against Epilepsy (ILAE) and the International Bureau for Epilepsy (IBE)”. In: *Epilepsia* 46.4 (2005), pp. 470–472. DOI: https://doi.org/10.1111/j.0013-9580.2005.66104.x.

[2] R. S. Fisher et al. “ILAE official report: a practical clinical definition of epilepsy”. In: *Epilepsia* 55.4 (2014), pp. 475–482. DOI: https://doi.org/10.1111/epi.12550.

[3] URL: https://www.who.int/news-room/fact-sheets/detail/epilepsy.

[4] K. M. Fiest et al. “Prevalence and incidence of epilepsy: A systematic review and meta-analysis of international studies”. In: *Neurology* 88.3 (2017), pp. 296–303. DOI: https://doi.org/10.1212/WNL.0000000000003509.

[5] I. E. Scheffer et al. “ILAE classification of the epilepsies: Position paper of the ILAE Commission for Classification and Terminology”. In: *Epilepsia* 58.4 (2017), pp. 512–521. DOI: https://doi.org/10.1111/epi.13709.

[6] R. S. Fisher et al. “Operational classification of seizure types by the International League Against Epilepsy: Position Paper of the ILAE Commission for Classification and Terminology”. In: *Epilepsia* 58.4 (2017), pp. 522–530. DOI: https://doi.org/10.1111/epi.13670.

[7] N. Kane et al. “A revised glossary of terms most commonly used by clinical electroencephalographers and updated proposal for the report format of the EEG findings. Revision 2017”. In: *Clin Neurophysiol Pract* 2 (2017), pp. 170–185. DOI: https://doi.org/10.1016/j.cnp.2017.07.002.

[8] S.R. Benbadis et al. *Handbook of EEG Interpretation.* . Springer Publishing Company, 2007. ISBN: 9781934559598. URL: https://books.google.be/books?id=_DQCQ6_ZtIYC.

[9] B. Galindo-Mendez et al. “Failure of antiepileptic drugs in controlling seizures in epilepsy: What do we do next?” In: *Epilepsy Behav Case Rep* 4 (2015). [DOI:10.1016/j.ebcr.2015.03.004], pp. 6–8.

[10] Z. Chen et al. “Treatment Outcomes in Patients With Newly Diagnosed Epilepsy Treated With Established and New Antiepileptic Drugs: A 30-Year Longitudinal Cohort Study”. In: *JAMA Neurol* 75.3 (2018). [PubMed Central:PMC3996117] [DOI:10.1001/jamaneurol.2017.3949] [PubMed:24492975], pp. 279–286.

[11] P. Kwan et al. “Definition of drug resistant epilepsy: consensus proposal by the ad hoc Task Force of the ILAE Commission on Therapeutic Strategies”. In: *Epilepsia* 51.6 (2010). [DOI:here], pp. 1069–1077.

[12] A. Geerts et al. “Course and outcome of childhood epilepsy: a 15-year follow-up of the Dutch Study of Epilepsy in Childhood”. In: *Epilepsia* 51.7 (2010). [DOI:10.1111/j.1528-1167.2010.02546.x] [PubMed:20557350], pp. 1189–1197.

[13] J. F. Annegers, W. A. Hauser, and L. R. Elveback. “Remission of seizures and relapse in patients with epilepsy”. In: *Epilepsia* 20.6 (Dec. 1979). [DOI:10.1111/j.1528-1157.1979.tb04857.x] [PubMed:499118], pp. 729–737.

[14] R. Dwivedi et al. “Surgery for Drug-Resistant Epilepsy in Children”. In: *N Engl J Med* 377.17 (Oct. 2017). [DOI:10.1056/NEJMoa1615335] [PubMed:29069568], pp. 1639–1647.

[15] J. Engel et al. “Early surgical therapy for drug-resistant temporal lobe epilepsy: a randomized trial”. In: *JAMA* 307.9 (Mar. 2012). [PubMed Central:PMC2077525] [DOI:10.1001/jama.2012.220] [PubMed:12609224], pp. 922–930.

[16] S. Wiebe et al. “A randomized, controlled trial of surgery for temporal-lobe epilepsy”. In: *N Engl J Med* 345.5 (Aug. 2001). [DOI:here], pp. 311–318.

[17] W.H. Theodore. *Surgical Treatment of Epilepsy*. Developments in Marine Technology. Elsevier, 1992. ISBN: 9780444894748. URL: https://books.google.be/books?id=9GtsAAAAMAAJ.

[18] F. Rosenow and H. ders. “Presurgical evaluation of epilepsy”. In: *Brain* 124.Pt 9 (Sept. 2001). [DOI:10.1093/brain/124.9.1683] [PubMed:11522572], pp. 1683–1700.

[19] Ajith Cherian et al. “Do sphenoidal electrodes aid in surgical decision making in drug resistant temporal lobe epilepsy?” In: *Clinical Neurophysiology* 123.3 (2012), pp. 463–470. ISSN: 1388-2457. DOI: https://doi.org/10.1016/j.clinph.2011.07.041.

[20] T. R. Velasco et al. “Foramen ovale electrodes can identify a focal seizure onset when surface EEG fails in mesial temporal lobe epilepsy”. In: *Epilepsia* 47.8 (Aug. 2006). [DOI:10.1111/j.1528-1167.2006.00547.x] [PubMed:16922874], pp. 1300–1307.

[21] Anders Bach Justesen et al. “Added clinical value of the inferior temporal EEG electrode chain”. In: *Clinical Neurophysiology* 129.1 (2018), pp. 291–295. ISSN: 1388-2457. DOI: https://doi.org/10.1016/j.clinph.2017.09.113.

[22] E. Boto et al. “Moving magnetoencephalography towards real-world applications with a wearable system”. In: *Nature* 555.7698 (Aug. 2018). [PubMed Central:PMC1863498] [DOI:here], pp. 657–661.

[23] R. Kuzniecky et al. “Magnetic resonance imaging in temporal lobe epilepsy: pathological correlations”. In: *Ann Neurol* 22.3 (Sept. 1987). [DOI:10.1002/ana.410220310] [PubMed:3674799], pp. 341–347.

[24] F. Bonini et al. “Predictive Factors of Surgical Outcome in Frontal Lobe Epilepsy Explored with Stereoelectroencephalography”. In: *Neurosurgery* 83.2 (Aug. 2018). [DOI:here], pp. 217–225.

[25] J. Wellmer et al. “Proposal for a magnetic resonance imaging protocol for the detection of epileptogenic lesions at early outpatient stages”. In: *Epilepsia* 54.11 (Nov. 2013). [DOI:10.1111/epi.12375] [PubMed:24117218], pp. 1977–1987.

[26] M. Goyal et al. “High-resolution MRI enhances identification of lesions amenable to surgical therapy in children with intractable epilepsy”. In: *Epilepsia* 45.8 (Aug. 2004). [DOI:10.1111/j.0013-9580.2004.39403.x] [PubMed:15270762], pp. 954–959.

[27] J. S. Ebersole and P. B. Wade. “Spike voltage topography and equivalent dipole localization in complex partial epilepsy”. In: *Brain Topogr* 3.1 (1990). [DOI:10.1007/BF01128858] [PubMed:6185310], pp. 21–34.

[28] P. Boon and M. é. “Interictal and ictal dipole modelling in patients with refractory partial epilepsy”. In: *Acta Neurol Scand* 92.1 (July 1995). [DOI:10.1111/j.1600-0404.1995.tb00460.x] [PubMed:7572065], pp. 7–18.

[29] J. S. Ebersole. “Magnetoencephalography/magnetic source imaging in the assessment of patients with epilepsy”. In: *Epilepsia* 38 Suppl 4 (1997). [DOI:10.1111/j.1528-1157.1997.tb04533.x] [PubMed:9240234], pp. 1–5.

[30] V. Brodbeck et al. “Electroencephalographic source imaging: a prospective study of 152 operated epileptic patients”. In: *Brain* 134.Pt 10 (Oct. 2011). [PubMed Central:PMC2760070] [DOI:10.1093/brain/awr243] [PubMed:16427355], pp. 2887–2897.

[31] Brian E Mouthaan et al. “Current use of imaging and electromagnetic source localization procedures in epilepsy surgery centers across Europe”. In: *Epilepsia* 57.5 (2016), pp. 770–776.

[32] Diego Jiménez-Jiménez et al. “Prognostic value of intracranial seizure onset patterns for surgical outcome of the treatment of epilepsy”. In: *Clinical Neurophysiology* 126.2 (2015), pp. 257–267. ISSN: 1388-2457. DOI: https://doi.org/10.1016/j.clinph.2014.06.005.

[33] M. Zijlmans, W. Zweiphenning, and N. van Klink. "Changing concepts in presurgical assessment for epilepsy surgery". In: *Nat Rev Neurol* 15.10 (Oct. 2019). [DOI:10.1038/s41582-019-0224-y] [PubMed:31341275], pp. 594–606.

[34] E.R. Kandel et al. *Principles of Neural Science, Fifth Edition*. McGraw Hill LLC, 2012. ISBN: 9780071810012. URL: https://books.google.be/books?id=Z2yVUTnlIQsC.

[35] In: (). URL: https://www.youtube.com/watch?v=0_boSag4f8g.

[36] Alexander J. Steiner et al. "Neurobiological Sciences: Neuroanatomy, Neurophysiology, and Neurochemistry". In: *Atlas of Psychiatry*. Ed. by Waguih William IsHak. Cham: Springer International Publishing, 2023, pp. 91–146. ISBN: 978-3-031-15401-0. DOI: 10.1007/978-3-031-15401-0_4. URL: https://doi.org/10.1007/978-3-031-15401-0_4.

[37] In: (). URL: https://www.youtube.com/watch?v=rzgDOaGjjOs&t=11s.

[38] Rosenzweig I Fogarasi A Johnsen B Alving J Fabricius ME Scherg M Neufeld MY Pressler R Kjaer TW van Emde Boas W Beniczky S. "Beyond the Double Banana: Improved Recognition of Temporal Lobe Seizures in Long-Term EEG". In: *Journal of Clinical Neurophysiology* 31.1 (2014), pp. 1–9. DOI: https://doi.org/10.1097/WNP.0000000000000019.

[39] Laurent Koessler et al. "Catching the Invisible: Mesial Temporal Source Contribution to Simultaneous EEG and SEEG Recordings". In: *Brain Topography* 28.1 (Jan. 2015), pp. 5–20. ISSN: 1573-6792. DOI: 10.1007/s10548-014-0417-z. URL: https://doi.org/10.1007/s10548-014-0417-z.

[40] Margitta Seeck et al. "The standardized EEG electrode array of the IFCN". In: *Clinical Neurophysiology* 128.10 (2017), pp. 2070–2077. ISSN: 1388-2457. DOI: https://doi.org/10.1016/j.clinph.2017.06.254.

[41] Gayaneh Petrossian et al. "Advances in Electrode Materials for Scalp, Forehead, and Ear EEG: A Mini-Review". In: *ACS Applied Bio Materials* 6.8 (2023). PMID: 37493408, pp. 3019–3032. DOI: 10.1021/acsabm.3c00322.

[42] Sörnmo L Laguna P. *Bioelectrical signal processing in cardiac and neurological applications*. Vol. 8. Academic press, 2005. DOI: https://doi.org/10.1186/1475-925X-6-27.

[43] Strobbe, Gregor. "Advanced forward models for EEG source imaging". eng. PhD thesis. Ghent University, 2015, XXVIII, 186. ISBN: 9789085787853.

[44] Tzyy-Ping Jung et al. “Extended ICA removes artifacts from electroencephalographic recordings”. In: *Advances in neural information processing systems* 10 (1997).

[45] Oostenveld R Fries P Maris E Schoffelen JM. “FieldTrip: Open source software for advanced analysis of MEG, EEG, and invasive electrophysiological data”. In: *Computational Intelligence and Neuroscience* 2011 (2011), p. 156869. DOI: https://doi.org/10.1155/2011/156869.

[46] T.F. Oostendorp, J. Delbeke, and D.F. Stegeman. “The conductivity of the human skull: results of in vivo and in vitro measurements”. In: *IEEE Transactions on Biomedical Engineering* 47.11 (2000), pp. 1487–1492. DOI: 10.1109/TBME.2000.880100.

[47] Victoria Montes-Restrepo et al. “Influence of Skull Modeling Approaches on EEG Source Localization”. In: *Brain Topography* 27.1 (Jan. 2014), pp. 95–111. ISSN: 1573-6792. DOI: 10.1007/s10548-013-0313-y. URL: https://doi.org/10.1007/s10548-013-0313-y.

[48] Johannes Vorwerk et al. “A guideline for head volume conductor modeling in EEG and MEG”. In: *NeuroImage* 100 (2014), pp. 590–607. ISSN: 1053-8119. DOI: https://doi.org/10.1016/j.neuroimage.2014.06.040.

[49] Laurent Koessler et al. “In-vivo measurements of human brain tissue conductivity using focal electrical current injection through intracerebral multicontact electrodes”. In: *Human Brain Mapping* 38.2 (2017), pp. 974–986. DOI: https://doi.org/10.1002/hbm.23431.

[50] Poßner L Seebeck L Laukner M Wilhelmy F Lindner D Pliquett U Petkovic B Ziolkowski M Knösche TR Weise K. *A four-point measurement probe for brain tissue conductivity and permittivity characterization.* 2021. DOI: https://doi.org/10.1101/2021.04.29.441988.

[51] Stefano Mandija et al. “Brain tissue conductivity measurements with MR-Electrical Properties Tomography: An in vivo study”. en. In: *Brain Topography* 34.1 (Jan. 2021), pp. 56–63. DOI: https://doi.org/10.1007/s10548-020-00813-1.

[52] Adib A. Becker. “The Boundary Element Method in Engineering: A Complete Course”. In: 1992.

[53] A.S. Ferguson and G. Stroink. “Factors affecting the accuracy of the boundary element method in the forward problem. I. Calculating surface potentials”. In: *IEEE Transactions on Biomedical Engineering* 44.11 (1997), pp. 1139–1155. DOI: 10.1109/10.641342.

[54] J.C. Mosher, R.M. Leahy, and P.S. Lewis. "EEG and MEG: forward solutions for inverse methods". In: *IEEE Transactions on Biomedical Engineering* 46.3 (1999), pp. 245–259. DOI: 10.1109/10.748978.

[55] M. Rosenfeld, R. Tanami, and S. Abboud. "Numerical solution of the potential due to dipole sources in volume conductors with arbitrary geometry and conductivity". In: *IEEE Transactions on Biomedical Engineering* 43.7 (1996), pp. 679–689. DOI: 10.1109/10.503175.

[56] H.I. Saleheen and K.T. Ng. "New finite difference formulations for general inhomogeneous anisotropic bioelectric problems". In: *IEEE Transactions on Biomedical Engineering* 44.9 (1997), pp. 800–809. DOI: 10.1109/10.623049.

[57] H.I. Saleheen and K.T. Ng. "A new three-dimensional finite-difference bidomain formulation for inhomogeneous anisotropic cardiac tissues". In: *IEEE Transactions on Biomedical Engineering* 45.1 (1998), pp. 15–25. DOI: 10.1109/10.650347.

[58] Vanrumste B Van Hoey G Van de Walle R D'Havè MRP Lemahieu IA Boon PAJM. "The Validation of the Finite Difference Method and Reciprocity for Solving the Inverse Problem in EEG Dipole Source Analysis". In: *Brain Topography* 14.2 (Dec. 2001), pp. 83–92. ISSN: 1573-6792. DOI: 10.1023/A:1012909511833. URL: https://doi.org/10.1023/A:1012909511833.

[59] Hallez, Hans and Vanrumste, Bart and Van Hese, Peter and D'Asseler, Yves and Lemahieu, Ignace and Van de Walle, Rik. "A finite difference method with reciprocity used to incorporate anisotropy in electroencephalogram dipole source localization". eng. In: *PHYSICS IN MEDICINE AND BIOLOGY* 50.16 (2005), 3787–3806. ISSN: 0031-9155. DOI: 10.1088/0031-9155/50/16/009.

[60] M. V. K. Chari and 1935-1996 (viaf)66542623 Silvester Peter Peet. *Finite elements in electrical and magnetic field problems*. eng. Repr. Chichester : Wiley, 1984. ISBN: 0471275786. URL: http://lib.ugent.be/catalog/rug01:000213259.

[61] S. P. van den Broeh, H. Zhou, and M. J. Peters. "Computation of neuromagnetic fields using finite-element method and Biot-Savart law". In: *Medical and Biological Engineering and Computing* 34.1 (Jan. 1996), pp. 21–26. ISSN: 1741-0444. DOI: 10.1007/BF02637018. URL: https://doi.org/10.1007/BF02637018.

[62] K.A. Awada et al. "Computational aspects of finite element modeling in EEG source localization". In: *IEEE Transactions on Biomedical Engineering* 44.8 (1997), pp. 736–752. DOI: 10.1109/10.605431.

[63] Helmut Buchner et al. "Inverse localization of electric dipole current sources in finite element models of the human head". In: *Electroencephalography and Clinical Neurophysiology* 102.4 (1997), pp. 267–278. ISSN: 0013-4694. DOI: https://doi.org/10.1016/S0013-4694(96)95698-9.

[64] C. H. Wolters et al. “A parallel algebraic multigrid solver for finite element method based source localization in the human brain”. In: *Computing and Visualization in Science* 5.3 (Dec. 2002), pp. 165–177. ISSN: 1432-9360. DOI: 10.1007/s00791-002-0098-0. URL: https://doi.org/10.1007/s00791-002-0098-0.

[65] Hallez H Vanrumste B Grech R Muscat J De Clercq W Vergult A DAsselerY Camilleri KP Fabri SG Van Huffel S Lemahieu I. “Review on solving the forward problem in EEG source analysis”. In: *Journal of NeuroEngineering and Rehabilitation* 4.1 (Nov. 2007), p. 46. ISSN: 1743-0003. DOI: 10.1186/1743-0003-4-46. URL: https://doi.org/10.1186/1743-0003-4-46.

[66] F.J Asencor and M Panizo. “Finite-difference operators in anisotropic inhomogeneous dielectrics: General case”. In: *Journal of Computational Physics* 95.2 (1991), pp. 387–399. ISSN: 0021-9991. DOI: https://doi.org/10.1016/0021-9991(91)90282-P.

[67] Stanley Rush and Daniel A. Driscoll. “EEG Electrode Sensitivity-An Application of Reciprocity”. In: *IEEE Transactions on Biomedical Engineering* BME-16.1 (1969), pp. 15–22. DOI: 10.1109/TBME.1969.4502598.

[68] Vanrumste, Bart. “EEG dipole source analysis in a realistic head model”. dut. PhD thesis. Ghent University, 2002. URL: http://dx.doi.org/1854/362.

[69] Bart Vanrumste. “EEG dipole source analysis in a realistic head model”. In: 2002. URL: https://api.semanticscholar.org/CorpusID:124223514.

[70] J.C. De Munck. “The estimation of time varying dipoles on the basis of evoked potentials”. In: *Electroencephalography and Clinical Neurophysiology/Evoked Potentials Section* 77.2 (1990), pp. 156–160. ISSN: 0168-5597. DOI: https://doi.org/10.1016/0168-5597(90)90032-9.

[71] Scherg M Bast T Berg P. “Multiple source analysis of interictal spikes: goals, requirements, and clinical value.” In: *Journal of Clinical Neurophysiology* 16.3 (1999), pp. 214–224. DOI: https://doi.org/10.1097/00004691-199905000-00003.

[72] Aine C Huang M Stephen J Christner R. “Multistart algorithms for MEG empirical data analysis reliably characterize locations and time courses of multiple sources.” In: *NeuroImage* 12.2 (2000), pp. 159–172. DOI: https://doi.org/10.1006/nimg.2000.0616.

[73] Hamalainen MS Ilmoniemi R. “Interpreting magnetic fields of the brain: minimum norm estimates.” In: *Medical & Biological Engineering & Computing* 32 (1994), pp. 35–42. DOI: https://doi.org/10.1007/BF02512476.

[74] Pascual Marqui RD Lehmann D Koenig T Kochi K Merlo MC Hell D Koukkou M. "Low resolution brain electromagnetic tomography (LORETA) functional imaging in acute, neuroleptic-naive, first-episode, productive schizophrenia." In: *Psychiatry Research: Neuroimaging* 90.2 (1999), pp. 169–179. DOI: https://doi.org/10.1016/s0925-4927(99)00013-x.

[75] Uutela K Hamalainen M Somersalo E. "Visualization of Magnetoencephalographic Data Using Minimum Current Estimates." In: *NeuroImage* 10.2 (1999), pp. 173–180. DOI: https://doi.org/10.1006/nimg.1999.0454.

[76] Michel CM Murray MM Lantz G Gonzalez S Spinelli L Grave de Peralta R. "EEG source imaging." In: *Clinical Neurophysiology* 115.10 (2004), pp. 2195–2222. DOI: https://doi.org/10.1016/j.clinph.2004.06.001.

[77] Grech R Cassar T Muscat J Camilleri KP Fabri SG Zervakis M Xanthopoulos P Sakkalis V Vanrumste B. "review on solving the inverse problem in EEG source analysis." In: *journal of neuroEngineering and rehabilitation* (2008), pp. 5–25. DOI: https://doi.org/10.1186/1743-0003-5-25.

[78] M.S. Hämäläinen and R.J. Ilmoniemi. *Interpreting Measured Magnetic Fields of the Brain: Estimates of Current Distributions*. Report TKK-F-A. Helsinki University of Technology, 1984. ISBN: 9789517533621. URL: https://books.google.be/books?id=tdE-AAAACAAJ.

[79] Greenblatt R. "Probabilistic reconstruction of multiple sources in the bioelectromagnetic inverse problem." In: *Inverse Problems* 9 (1993), pp. 271–284. DOI: https://doi.org/10.1088/0266-5611/9/2/008.

[80] Irina F. Gorodnitsky, John S. George, and Bhaskar D. Rao. "Neuromagnetic source imaging with FOCUSS: a recursive weighted minimum norm algorithm". In: *Electroencephalography and Clinical Neurophysiology* 95.4 (1995), pp. 231–251. ISSN: 0013-4694. DOI: https://doi.org/10.1016/0013-4694(95)00107-A.

[81] Gonzalez-Andino SL. Grave de Peralta-Menendez R. "A critical analysis of linear inverse solutions to the neuroelectromagnetic inverse problem." In: *IEEE Transactions on Biomedical Engineering* 45.4 (1998), pp. 440–448. DOI: https://doi.org/10.1109/10.664200.

[82] R.D. Pascual-Marqui, C.M. Michel, and D. Lehmann. "Low resolution electromagnetic tomography: a new method for localizing electrical activity in the brain". In: *International Journal of Psychophysiology* 18.1 (1994), pp. 49–65. ISSN: 0167-8760. DOI: https://doi.org/10.1016/0167-8760(84)90014-X.

[83] Roberto D. Pascual-Marqui. “Standardized low-resolution brain electromagnetic tomography (sLORETA): technical details.” In: *Methods and findings in experimental and clinical pharmacology* 24 Suppl D (2002), pp. 5–12. URL: https://api.semanticscholar.org/CorpusID:1529384.

[84] Anders M. Dale et al. “Dynamic Statistical Parametric Mapping: Combining fMRI and MEG for High-Resolution Imaging of Cortical Activity”. In: *Neuron* 26.1 (2000), pp. 55–67. ISSN: 0896-6273. DOI: https://doi.org/10.1016/S0896-6273(00)81138-1.

[85] P. Kwan and M. J. Brodie. “Early identification of refractory epilepsy”. In: *N Engl J Med* 342.5 (Feb. 2000). [DOI:10.1056/NEJM200002033420503] [PubMed:10660394], pp. 314–319.

[86] Rekha Dwivedi et al. “Surgery for Drug-Resistant Epilepsy in Children”. In: *New England Journal of Medicine* 377.17 (2017), pp. 1639–1647. DOI: 10.1056/NEJMoa1615335.

[87] Felix Rosenow and Hans Lüders. “Presurgical evaluation of epilepsy”. In: *Brain* 124.9 (Sept. 2001), pp. 1683–1700. ISSN: 0006-8950. DOI: 10.1093/brain/124.9.1683.

[88] John W Miller and Shahin Hakimian. “Surgical treatment of epilepsy”. In: *Continuum: Lifelong Learning in Neurology* 19.3 Epilepsy (2013), p. 730.

[89] M. Thom et al. “Mesial temporal lobe epilepsy: How do we improve surgical outcome?” In: *Ann Neurol* 68.4 (Oct. 2010). [PubMed Central:PMC2804395] [DOI:10.1002/ana.22142] [PubMed:19400880], pp. 424–434.

[90] B. A. Assaf and J. S. Ebersole. “Continuous source imaging of scalp ictal rhythms in temporal lobe epilepsy”. In: *Epilepsia* 38.10 (Oct. 1997). [DOI:10.1111/j.1528-1157.1997.tb01201.x] [PubMed:9579958], pp. 1114–1123.

[91] G. Lantz et al. “Frequency domain EEG source localization of ictal epileptiform activity in patients with partial complex epilepsy of temporal lobe origin”. In: *Clin Neurophysiol* 110.1 (Jan. 1999). [PubMed:here], pp. 176–184.

[92] Agustina M. Lascano et al. “Yield of MRI, high-density electric source imaging (HD-ESI), SPECT and PET in epilepsy surgery candidates”. In: *Clinical Neurophysiology* 127.1 (2016), pp. 150–155. ISSN: 1388-2457. DOI: https://doi.org/10.1016/j.clinph.2015.03.025.

[93] Yunfeng Lu et al. “Dynamic imaging of seizure activity in pediatric epilepsy patients”. In: *Clinical Neurophysiology* 123.11 (2012), pp. 2122–2129. ISSN: 1388-2457. DOI: https://doi.org/10.1016/j.clinph.2012.04.021.

[94] Pierre Mégevand et al. “Electric source imaging of interictal activity accurately localises the seizure onset zone”. In: 85.1 (2014), pp. 38–43. DOI: 10.1136/jnnp-2013-305515.

[95] G. Pellegrino et al. “Source localization of the seizure onset zone from ictal EEG/MEG data”. In: *Hum Brain Mapp* 37.7 (July 2016). [PubMed Central:PMC2292756] [DOI:10.1002/hbm.23191] [PubMed:11001337], pp. 2528–2546.

[96] W. Staljanssens et al. “Seizure Onset Zone Localization from Ictal High-Density EEG in Refractory Focal Epilepsy”. In: *Brain Topogr* 30.2 (Mar. 2017). [DOI:10.1007/s10548-016-0537-8] [PubMed:27853892], pp. 257–271.

[97] W. Staljanssens et al. “EEG source connectivity to localize the seizure onset zone in patients with drug resistant epilepsy”. In: *Neuroimage Clin* 16 (2017). [PubMed Central:PMC3359824] [PubMed:21453776], pp. 689–698.

[98] G. Strobbe et al. “Electrical source imaging of interictal spikes using multiple sparse volumetric priors for presurgical epileptogenic focus localization”. In: *Neuroimage Clin* 11 (2016). [PubMed Central:PMC2907216] [DOI:10.1016/j.nicl.2016.01.017] [PubMed:17029950], pp. 252–263.

[99] P. van Mierlo et al. “Automated long-term EEG analysis to localize the epileptogenic zone”. In: *Epilepsia Open* 2.3 (Sept. 2017). [PubMed Central:PMC2907216] [DOI:10.1002/epi4.12066] [PubMed:19780794], pp. 322–333.

[100] R. Wennberg, T. Valiante, and D. Cheyne. “EEG and MEG in mesial temporal lobe epilepsy: where do the spikes really come from?” In: *Clin Neurophysiol* 122.7 (July 2011). [DOI:10.1016/j.clinph.2010.11.019] [PubMed:21292549], pp. 1295–1313.

[101] S. Beniczky et al. “Ictal EEG source imaging in presurgical evaluation: High agreement between analysis methods”. In: *Seizure* 43 (Dec. 2016). [PubMed Central:PMC1072872] [DOI:10.1016/j.seizure.2016.09.017] [PubMed:16858632], pp. 1–5.

[102] R. Wennberg and D. Cheyne. “EEG source imaging of anterior temporal lobe spikes: validity and reliability”. In: *Clin Neurophysiol* 125.5 (May 2014). [DOI:10.1016/j.clinph.2013.09.042] [PubMed:24210516], pp. 886–902.

[103] L. Yang et al. “Dynamic imaging of ictal oscillations using non-invasive high-resolution EEG”. In: *Neuroimage* 56.4 (June 2011). [DOI:here], pp. 1908–1917.

[104] P. Boon et al. “Ictal source localization in presurgical patients with refractory epilepsy”. In: *J Clin Neurophysiol* 19.5 (Oct. 2002). [DOI:here], pp. 461–468.

[105] L. Ding et al. “Ictal source analysis: localization and imaging of causal interactions in humans”. In: *Neuroimage* 34.2 (Jan. 2007). [PubMed Central:PMC1945182] [DOI:here], pp. 575–586.

[106] J. S. Ebersole. “Noninvasive localization of epileptogenic foci by EEG source modeling”. In: *Epilepsia* 41 Suppl 3 (2000). [DOI:10.1111/j.1528-1157.2000.tb01531.x] [PubMed:11001333], pp. 24–33.

[107] M. A. Habib et al. “Ictal EEG Source Imaging for Presurgical Evaluation of Refractory Focal Epilepsy”. In: *World Neurosurg* 88 (Apr. 2016). [DOI:10.1016/j.wneu.2015.10.096] [PubMed:26548833], pp. 576–585.

[108] L. Koessler et al. “Source localization of ictal epileptic activity investigated by high resolution EEG and validated by SEEG”. In: *Neuroimage* 51.2 (June 2010). [DOI:here], pp. 642–653.

[109] S. Kovac et al. “Ictal EEG source imaging in frontal lobe epilepsy leads to improved lateralization compared with visual analysis”. In: *J Clin Neurophysiol* 31.1 (Feb. 2014). [DOI:10.1097/WNP.0000000000000022] [PubMed:24492441], pp. 10–20.

[110] B. E. Mouthaan et al. “Current use of imaging and electromagnetic source localization procedures in epilepsy surgery centers across Europe”. In: *Epilepsia* 57.5 (May 2016). [DOI:pmid27012361], pp. 770–776.

[111] P. Nemtsas et al. “Source localization of ictal epileptic activity based on high-density scalp EEG data”. In: *Epilepsia* 58.6 (June 2017). [DOI:here], pp. 1027–1036.

[112] P. M. Bossuyt et al. “STARD 2015: updated reporting guidelines for all diagnostic accuracy studies”. In: *Ann Transl Med* 4.4 (Feb. 2016). [PubMed Central:PMC4779779] [DOI:here], p. 85.

[113] V. Montes-Restrepo et al. “The Role of Skull Modeling in EEG Source Imaging for Patients with Refractory Temporal Lobe Epilepsy”. In: *Brain Topogr* 29.4 (July 2016). [DOI:here], pp. 572–589.

[114] G. Strobbe et al. “Bayesian model selection of template forward models for EEG source reconstruction”. In: *Neuroimage* 93 Pt 1 (June 2014). [DOI:10.1016/j.neuroimage.2014.02.022] [PubMed:24582919], pp. 11–22.

[115] B. Vanrumste et al. “The validation of the finite difference method and reciprocity for solving the inverse problem in EEG dipole source analysis”. In: *Brain Topogr* 14.2 (2001). [DOI:10.1023/a:1012909511833] [PubMed:11797813], pp. 83–92.

[116] S. Beniczky et al. “Standardized computer-based organized reporting of EEG: SCORE - Second version”. In: *Clin Neurophysiol* 128.11 (Nov. 2017). [DOI:10.1016/j.clinph.2017.07.418] [PubMed:28838815], pp. 2334–2346.

[117] P. F. Griner et al. “Selection and interpretation of diagnostic tests and procedures”. English (US). In: *Annals of Internal Medicine* 94.4 II (Jan. 1981). ISSN: 0003-4819.

[118] N. D. Mercaldo, K. F. Lau, and X. H. Zhou. "Confidence intervals for predictive values with an emphasis to case-control studies". In: *Stat Med* 26.10 (May 2007). [DOI:10.1002/sim.2677] [PubMed:16927452], pp. 2170–2183.

[119] Martin Bland. *An introduction to medical statistics*. Oxford university press, 2015.

[120] M. Scherg et al. "Fast evaluation of interictal spikes in long-term EEG by hyper-clustering". In: *Epilepsia* 53.7 (July 2012). [DOI:10.1111/j.1528-1167.2012.03503.x] [PubMed:22578143], pp. 1196–1204.

[121] G. Lantz et al. "Propagation of interictal epileptiform activity can lead to erroneous source localizations: a 128-channel EEG mapping study". In: *J Clin Neurophysiol* 20.5 (2003). [DOI:10.1097/00004691-200309000-00003], pp. 311–319.

[122] Mihai Dragos Măliia et al. "Epileptiform discharge propagation: analyzing spikes from the onset to the peak". In: *Clinical Neurophysiology* 127.4 (2016), pp. 2127–2133.

[123] P. Sharma et al. "Ictal and interictal electric source imaging in presurgical evaluation: a prospective study". In: *Eur J Neurol* 25.9 (Sept. 2018). [DOI:10.1111/ene.13676] [PubMed:29751364], pp. 1154–1160.

[124] W. O. Tatum et al. "Clinical utility of EEG in diagnosing and monitoring epilepsy in adults". In: *Clin Neurophysiol* 129.5 (May 2018). [DOI:10.1016/j.clinph.2018.01.019] [PubMed:29483017], pp. 1056–1082.

[125] Bernd J. Vorderwülbecke et al. "Automated interictal source localisation based on high-density EEG". In: *Seizure* 92 (2021), pp. 244–251. ISSN: 1059-1311. DOI: https://doi.org/10.1016/j.seizure.2021.09.020.

[126] Evelina Iachim et al. "Automated electrical source imaging with scalp EEG to define the insular irritative zone: Comparison with simultaneous intracranial EEG". In: *Clinical Neurophysiology* 132.12 (2021), pp. 2965–2978. ISSN: 1388-2457. DOI: https://doi.org/10.1016/j.clinph.2021.09.004.

[127] Roberto Santalucia et al. "Clinical added value of interictal automated electrical source imaging in the presurgical evaluation of MRI-negative epilepsy: A real-life experience in 29 consecutive patients". In: *Epilepsy & Behavior* 143 (2023), p. 109229. ISSN: 1525-5050. DOI: https://doi.org/10.1016/j.yebeh.2023.109229.

[128] L. Spinelli et al. "Semiautomatic interictal electric source localization based on long-term electroencephalographic monitoring: A prospective study". In: *Epilepsia* 64.4 (Apr. 2023). [DOI:10.1111/epi.17460] [PubMed:36346269], pp. 951–961.

[129] URL: https://classic.clinicaltrials.gov/ct2/show/NCT04218812.

[130] G. Miron et al. “Integration of interictal EEG source localization in presurgical epilepsy evaluation - A single-center prospective study”. In: *Epilepsia Open* 8.3 (Sept. 2023). [DOI:10.1002/epi4.12754], pp. 877–887.

[131] Amir G. Baroumand et al. “Automated EEG source imaging: A retrospective, blinded clinical validation study”. In: *Clinical Neurophysiology* 129.11 (2018), pp. 2403–2410. ISSN: 1388-2457. DOI: https://doi.org/10.1016/j.clinph.2018.09.015.

[132] Simone Vespa et al. “Ictal EEG source imaging and connectivity to localize the seizure onset zone in extratemporal lobe epilepsy”. In: *Seizure* 78 (2020), pp. 18–30. ISSN: 1059-1311. DOI: https://doi.org/10.1016/j.seizure.2020.03.001.

[133] C. Czarnetzki et al. “Yield of non-invasive imaging in MRI-negative focal epilepsy”. In: *J Neurol* (Nov. 2023). [PubMed Central:5082694] [DOI:10.1111/epi.13116] [PubMed:26250432].

[134] Pieter van Mierlo et al. “T12. Automated EEG analysis of long-term EEG to localize the epileptogenic zone in extra-temporal lobe epilepsy”. In: *Clinical Neurophysiology* 129 (2018). Abstracts of the 31st International Congress of Clinical Neurophysiology (ICCN) of the IFCN, May 1–6, 2018, Washington, DC, USA, e5–e6. ISSN: 1388-2457. DOI: https://doi.org/10.1016/j.clinph.2018.04.013.

[135] P van Mierlo et al. “Added Value Of Eeg Source Localization In Extra-Temporal Lobe Epilepsy”. In: *EPILEPSIA*. Vol. 59. WILEY 111 RIVER ST, HOBOKEN 07030-5774, NJ USA. 2018, S267–S267.

[136] P van Mierlo et al. “Automated EEG Source Imaging: A Retrospective, Blinded Clinical Validation Study”. In: *EPILEPSIA*. Vol. 60. WILEY 111 RIVER ST, HOBOKEN 07030-5774, NJ USA. 2019, pp. 143–143.

[137] Bernd Vorderwuelbecke et al. “Accuracy of automated interictal source localisation based on high-density EEG”. In: *EPILEPSIA*. Vol. 62. WILEY 111 RIVER ST, HOBOKEN 07030-5774, NJ USA. 2021, pp. 125–126.

[138] Laurent Spinelli et al. “Semiautomatic interictal electric source localization based on long-term electroencephalographic monitoring: A prospective study”. In: *Epilepsia* 64.4 (2023), pp. 951–961. ISSN: 0013-9580. DOI: 10.1111/epi.17460.

[139] R Santalucia et al. “Clinical added value of interictal automated electrical source imaging in the presurgical evaluation of MRI-negative epileptic patients: a monocentric prospective study”. In: *EPILEPSIA*. Vol. 64. WILEY 111 RIVER ST, HOBOKEN 07030-5774, NJ USA. 2023, pp. 85–86.

[140] S. W. Cramer et al. “Resective epilepsy surgery: assessment of randomized controlled trials”. In: *Neurosurg Rev* 44.4 (Aug. 2021). [DOI:here], pp. 2059–2067.

[141] P. Sharma, M. Seeck, and S. Beniczky. "Accuracy of Interictal and Ictal Electric and Magnetic Source Imaging: A Systematic Review and Meta-Analysis". In: *Front Neurol* 10 (2019). [PubMed Central:PMC6382058] [DOI:10.1212/WNL.0000000000006877] [PubMed:30610090], p. 1250.

[142] Brian E. Mouthaan et al. "Diagnostic accuracy of interictal source imaging in presurgical epilepsy evaluation: A systematic review from the E-PILEPSY consortium". In: *Clinical Neurophysiology* 130.5 (2019), pp. 845–855. ISSN: 1388-2457. DOI: https://doi.org/10.1016/j.clinph.2018.12.016.

[143] Mette Thrane Foged et al. "Diagnostic added value of electrical source imaging in presurgical evaluation of patients with epilepsy: A prospective study". In: *Clinical Neurophysiology* 131.1 (2020), pp. 324–329. ISSN: 1388-2457. DOI: https://doi.org/10.1016/j.clinph.2019.07.031.

[144] Pieter van Mierlo et al. "Ictal EEG source localization in focal epilepsy: Review and future perspectives". In: *Clinical Neurophysiology* 131.11 (2020), pp. 2600–2616. ISSN: 1388-2457. DOI: https://doi.org/10.1016/j.clinph.2020.08.001.

[145] Sándor Beniczky et al. "Source localization of rhythmic ictal EEG activity: a study of diagnostic accuracy following STARD criteria". In: *Epilepsia* 54.10 (2013), pp. 1743–1752.

[146] Moritz Dannhauer et al. "Modeling of the human skull in EEG source analysis". In: *Human Brain Mapping* 32.9 (2011), pp. 1383–1399. DOI: https://doi.org/10.1002/hbm.21114.

[147] Massoud Akhtari et al. "Conductivities of three-layer live human skull". In: *Brain topography* 14 (2002), pp. 151–167.

[148] Jens Haueisen et al. "On the influence of volume currents and extended sources on neuromagnetic fields: a simulation study". In: *Annals of biomedical engineering* 23 (1995), pp. 728–739.

[149] Stephen B Baumann et al. "The electrical conductivity of human cerebrospinal fluid at body temperature". In: *IEEE transactions on biomedical engineering* 44.3 (1997), pp. 220–223.

[150] S.I. Goncalves et al. "In vivo measurement of the brain and skull resistivities using an EIT-based method and realistic models for the head". In: *IEEE Transactions on Biomedical Engineering* 50.6 (June 2003), pp. 754–767. ISSN: 1558-2531. DOI: 10.1109/TBME.2003.812164.

[151] S. Goncalves, J.C. de Munck, and J.P.A. Verbunt. "In vivo measurement of skull and brain resistivities with EIT based method and analysis of SEF/SEP data". In: *2001 Conference Proceedings of the 23rd Annual International Conference of the IEEE Engineering in Medicine and Biology Society*. Vol. 1. 2001, 1006–1008 vol.1. DOI: 10.1109/IEMBS.2001.1019124.

[152] Lene Duez et al. “Electromagnetic source imaging in presurgical workup of patients with epilepsy”. In: *Neurology* 92.6 (2019), e576–e586. ISSN: 0028-3878. DOI: 10.1212/WNL.0000000000006877.

[153] In: (). URL: https://neupsykey.com/nasopharyngeal-anterotemporal-and-sphenoidal-electrodes/.

[154] Amir G. Baroumand et al. “Automated ictal EEG source imaging: A retrospective, blinded clinical validation study”. In: *Clinical Neurophysiology* 141 (2022), pp. 119–125. ISSN: 1388-2457. DOI: https://doi.org/10.1016/j.clinph.2021.03.040.

[155] Simone Vespa et al. “Ictal EEG source imaging and connectivity to localize the seizure onset zone in extratemporal lobe epilepsy”. In: *33rd International Epilepsy Congress*. 2019.

[156] Amir G Baroumand et al. “TH-289. Evaluation of ictal EEG source imaging with sliding window approach to localize the epileptogenic focus”. In: *Clinical Neurophysiology* 141 (2022), S180.

[157] AG Baroumand et al. “Bicentric retrospective study to evaluate the performance of ictal EEG source imaging to localize the epileptogenic focus”. In: *EPILEPSIA*. Vol. 63. WILEY 111 RIVER ST, HOBOKEN 07030-5774, NJ USA. 2022, pp. 108–108.

[158] AG Baroumand et al. “Interictal and ictal EEG source imaging in children below 6 years of age with curative epilepsy surgery: a retrospective, blinded clinical study”. In: *EPILEPSIA*. Vol. 64. WILEY 111 RIVER ST, HOBOKEN 07030-5774, NJ USA. 2023, pp. 257–257.

[159] F. Sperli et al. “EEG source imaging in pediatric epilepsy surgery: a new perspective in presurgical workup”. In: *Epilepsia* 47.6 (June 2006). [DOI:10.1111/j.1528-1167.2006.00550.x] [PubMed:16822244], pp. 981–990.

[160] Odysseas Kargiotis et al. “Localization of the epileptogenic tuber with electric source imaging in patients with tuberous sclerosis”. In: *Epilepsy Research* 108.2 (2014), pp. 267–279. ISSN: 0920-1211. DOI: https://doi.org/10.1016/j.eplepsyres.2013.11.003.

[161] V. Brodbeck et al. “Electrical source imaging for presurgical focus localization in epilepsy patients with normal MRI”. In: *Epilepsia* 51.4 (May 2010). [DOI:10.1111/j.1528-1167.2010.02521.x], pp. 583–591.

[162] G Lantz et al. “Epileptic source localization with high density EEG: how many electrodes are needed?” In: *Clinical Neurophysiology* 114.1 (2003), pp. 63–69. ISSN: 1388-2457. DOI: https://doi.org/10.1016/S1388-2457(02)00337-1.

[163] Gwénael Birot et al. “Head model and electrical source imaging: A study of 38 epileptic patients”. In: *NeuroImage: Clinical* 5 (2014), pp. 77–83. ISSN: 2213-1582. DOI: https://doi.org/10.1016/j.nicl.2014.06.005.

[164] C. M. Michel et al. “128-channel EEG source imaging in epilepsy: clinical yield and localization precision”. In: *J Clin Neurophysiol* 21.2 (2004). [DOI:10.1097/00004691-200403000-00001] [PubMed:15284597], pp. 71–83.

[165] V. Brodbeck et al. “Accuracy of EEG source imaging of epileptic spikes in patients with large brain lesions”. In: *Clin Neurophysiol* 120.4 (May 2009). [DOI:10.1016/j.clinph.2009.01.011] [PubMed:19264547], pp. 679–685.

[166] M. Centeno et al. “Combined electroencephalography-functional magnetic resonance imaging and electrical source imaging improves localization of pediatric focal epilepsy”. In: *Ann Neurol* 82.2 (Aug. 2017). [DOI:10.1002/ana.25003] [PubMed:28749544], pp. 278–287.

[167] Rui Feng et al. “Application of 256-channel dense array electroencephalographic source imaging in presurgical workup of temporal lobe epilepsy”. In: *Clinical Neurophysiology* 127.1 (2016), pp. 108–116. ISSN: 1388-2457. DOI: https://doi.org/10.1016/j.clinph.2015.03.009.

[168] R. Feng et al. “Accurate source imaging based on high resolution scalp electroencephalography and individualized finite difference head models in epilepsy pre-surgical workup”. In: *Seizure* 59 (July 2018). [DOI:10.1016/j.seizure.2018.05.009] [PubMed:29843085], pp. 126–131.

[169] D. Maziero et al. “A Comparison of Independent Component Analysis (ICA) of fMRI and Electrical Source Imaging (ESI) in Focal Epilepsy Reveals Misclassification Using a Classifier”. In: *Brain Topogr* 28.6 (Nov. 2015). [DOI:10.1007/s10548-015-0436-4] [PubMed:25998855], pp. 813–831.

[170] C. J. Park et al. “EEG Source Imaging in Partial Epilepsy in Comparison with Presurgical Evaluation and Magnetoencephalography”. In: *J Clin Neurol* 11.4 (Oct. 2015). [PubMed Central:PMC3504419] [DOI:10.3988/jcn.2015.11.4.319] [PubMed:17574913], pp. 319–330.

[171] E. Rikir et al. “Electrical source imaging in cortical malformation-related epilepsy: a prospective EEG-SEEG concordance study”. In: *Epilepsia* 55.6 (June 2014). [DOI:10.1111/epi.12591] [PubMed:24702598], pp. 918–932.

[172] L. Jehi. “Commentary on Interictal epileptogenic zone localization in patients with focal epilepsy using electric source imaging and directed functional connectivity from low-density EEG”. In: *Epilepsia Open* 5.3 (Sept. 2020). [PubMed Central:PMC6218499] [DOI:10.1002/epi4.12426] [PubMed:30397245], pp. 342–343.

[173] Aurélie Wanders et al. “High density electric source imaging in childhood-onset epilepsy due to focal cortical dysplasia”. In: *Clinical Neurophysiology Practice* 7 (2022), pp. 245–251. ISSN: 2467-981X. DOI: https://doi.org/10.1016/j.cnp.2022.07.002.

[174] Michael Scherg et al. “Relative Source Power: A novel method for localizing epileptiform EEG discharges”. In: *Clinical Neurophysiology* 133 (2022), pp. 9–19. ISSN: 1388-2457. DOI: https://doi.org/10.1016/j.clinph.2021.10.005.

[175] M. Heers et al. “Spatial correlation of hemodynamic changes related to interictal epileptic discharges with electric and magnetic source imaging”. In: *Hum Brain Mapp* 35.9 (Sept. 2014). [PubMed Central:PMC2977852] [DOI:10.1002/hbm.22482] [PubMed:17586868], pp. 4396–4414.

[176] L. Elshoff et al. “The value of EEG-fMRI and EEG source analysis in the presurgical setup of children with refractory focal epilepsy”. In: *Epilepsia* 53.9 (Sept. 2012). [DOI:10.1111/j.1528-1167.2012.03587.x] [PubMed:22779700], pp. 1597–1606.

[177] S. Beniczky et al. “Source localization of rhythmic ictal EEG activity: a study of diagnostic accuracy following STARD criteria”. In: *Epilepsia* 54.10 (Oct. 2013). [DOI:10.1111/epi.12339] [PubMed:23944234], pp. 1743–1752.

[178] Johannes Koren et al. “Automatic ictal onset source localization in presurgical epilepsy evaluation”. In: *Clinical Neurophysiology* 129.6 (2018), pp. 1291–1299. ISSN: 1388-2457. DOI: https://doi.org/10.1016/j.clinph.2018.03.020.

[179] B. A. Assaf and J. S. Ebersole. “Visual and quantitative ictal EEG predictors of outcome after temporal lobectomy”. In: *Epilepsia* 40.1 (Jan. 1999). [DOI:10.1111/j.1528-1157.1999.tb01988.x] [PubMed:9924902], pp. 52–61.

[180] Chunsheng Li et al. “Epileptogenic Source Imaging Using Cross- Frequency Coupled Signals From Scalp EEG”. In: *IEEE Transactions on Biomedical Engineering* 63.12 (2016), pp. 2607–2618. DOI: 10.1109/TBME.2016.2613936.

[181] M. A. Habib et al. “Recursive independent component analysis (ICA)-decomposition of ictal EEG to select the best ictal component for EEG source imaging”. In: *Clin Neurophysiol* 131.3 (Mar. 2020). [DOI:here], pp. 642–654.

[182] C. Plummer et al. “Interictal and ictal source localization for epilepsy surgery using high-density EEG with MEG: a prospective long-term study”. In: *Brain* 142.4 (Apr. 2019). [DOI:10.1093/brain/awz015], pp. 932–951.

[183] Yunfeng Lu et al. “Seizure source imaging by means of FINE spatio-temporal dipole localization and directed transfer function in partial epilepsy patients”. In: *Clinical Neurophysiology* 123.7 (2012), pp. 1275–1283. ISSN: 1388-2457. DOI: https://doi.org/10.1016/j.clinph.2011.11.007.

[184] D. J. Englot et al. “Epileptogenic zone localization using magnetoencephalography predicts seizure freedom in epilepsy surgery”. In: *Epilepsia* 56.6 (June 2015). [DOI:10.1111/epi.13002], pp. 949–958.

[185] Salah Almubarak et al. “The correlation of magnetoencephalography to intracranial EEG in localizing the epileptogenic zone: A study of the surgical resection outcome”. In: *Epilepsy Research* 108.9 (2014), pp. 1581–1590. ISSN: 0920-1211. DOI: https://doi.org/10.1016/j.eplepsyres.2014.08.016.

[186] Bassam A Assaf et al. “Magnetoencephalography source localization and surgical outcome in temporal lobe epilepsy”. In: *Clinical Neurophysiology* 115.9 (2004), pp. 2066–2076. ISSN: 1388-2457. DOI: https://doi.org/10.1016/j.clinph.2004.04.020.

[187] E. F. Chang et al. “Magnetic source imaging for the surgical evaluation of electroencephalography-confirmed secondary bilateral synchrony in intractable epilepsy”. In: *J Neurosurg* 111.6 (Dec. 2009). [DOI:10.3171/2009.6.JNS081376], pp. 1248–1256.

[188] W. Jeong, C. K. Chung, and J. S. Kim. “Localization value of magnetoencephalography interictal spikes in adult nonlesional neocortical epilepsy”. In: *J Korean Med Sci* 27.11 (Nov. 2012). [DOI:here], pp. 1391–1397.

[189] Kitti Kaiboriboon et al. “Interictal MEG/MSI in intractable mesial temporal lobe epilepsy: Spike yield and characterization”. In: *Clinical Neurophysiology* 121.3 (2010), pp. 325–331. ISSN: 1388-2457. DOI: https://doi.org/10.1016/j.clinph.2009.12.001.

[190] Burkhard S. Kasper et al. “Coregistrating magnetic source and magnetic resonance imaging for epilepsy surgery in focal cortical dysplasia”. In: *NeuroImage: Clinical* 19 (2018), pp. 487–496. ISSN: 2213-1582. DOI: https://doi.org/10.1016/j.nicl.2018.04.034.

[191] H. Kim et al. “Magnetoencephalography in pediatric lesional epilepsy surgery”. In: *J Korean Med Sci* 27.6 (June 2012). [DOI:here], pp. 668–673.

[192] R. C. Knowlton et al. “Magnetoencephalography in partial epilepsy: clinical yield and localization accuracy”. In: *Ann Neurol* 42.4 (Oct. 1997). [DOI:10.1002/ana.410420413] [PubMed:9382474], pp. 622–631.

[193] A. N. Mamelak et al. “Magnetoencephalography-directed surgery in patients with neocortical epilepsy”. In: *J Neurosurg* 97.4 (Oct. 2002). [DOI:10.3171/jns.2002.97.4.0865] [PubMed:12405375], pp. 865–873.

[194] F. Schneider et al. “Magnetic source imaging in non-lesional neocortical epilepsy: additional value and comparison with ICEEG”. In: *Epilepsy Behav* 24.2 (June 2012). [DOI:10.1016/j.yebeh.2012.03.029] [PubMed:22542998], pp. 234–240.

[195] J. R. Smith et al. “A 10-year experience with magnetic source imaging in the guidance of epilepsy surgery”. In: *Stereotact Funct Neurosurg* 80.1-4 (2003). [DOI:10.1159/000075153] [PubMed:14745202], pp. 14–17.

[196] W. W. Sutherling et al. “Influence of magnetic source imaging for planning intracranial EEG in epilepsy”. In: *Neurology* 71.13 (2008), pp. 990–996. ISSN: 0028-3878. DOI: 10.1212/01.wnl.0000326591.29858.1a.

[197] Z. I. Wang et al. “Linking MRI postprocessing with magnetic source imaging in MRI-negative epilepsy”. In: *Ann Neurol* 75.5 (May 2014). [DOI:10.1002/ana.24169], pp. 759–770.

[198] Yuchun Wang et al. “Use of interictal 18F-fluorodeoxyglucose (FDG)-PET and magnetoencephalography (MEG) to localize epileptogenic foci in non-lesional epilepsy in a cohort of 16 patients”. In: *Journal of the Neurological Sciences* 355.1 (2015), pp. 120–124. ISSN: 0022-510X. DOI: https://doi.org/10.1016/j.jns.2015.05.039.

[199] X. T. Wu et al. “Interictal magnetoencephalography used in magnetic resonance imaging-negative patients with epilepsy”. In: *Acta Neurol Scand* 127.4 (Apr. 2013). [DOI:10.1111/j.1600-0404.2012.01712.x] [PubMed:22882005], pp. 274–280.

[200] X. T. Wu et al. “Complementary use of video-electroencephalography and magnetoencephalography in frontal lobe epilepsy”. In: *Seizure* 21.6 (June 2012). [DOI:10.1016/j.seizure.2012.04.007] [PubMed:22578278], pp. 426–430.

[201] I. S. Mohamed et al. “Utility of magnetic source imaging in nonlesional focal epilepsy: a prospective study”. In: *Neurosurg Focus* 48.4 (Apr. 2020). [DOI:10.3171/2020.1.FOCUS19877] [PubMed:32234989], E16.

[202] D. M. Sindhu et al. “Role of magnetoencephalography in predicting the epileptogenic zone and post-operative seizure outcome - A retrospective study”. In: *Seizure* 113 (Nov. 2023). [DOI:here], pp. 41–47.

[203] Bhargava Gautham et al. “Magnetic source imaging in presurgical evaluation of paediatric focal drug-resistant epilepsy and its predictive value of surgical outcome in lesional cases: A single-centre experience from South India”. In: *Seizure* 91 (2021), pp. 22–28. ISSN: 1059-1311. DOI: https://doi.org/10.1016/j.seizure.2021.05.015.

[204] B. A. Assaf et al. “Ictal magnetoencephalography in temporal and extratemporal lobe epilepsy”. In: *Epilepsia* 44.10 (Oct. 2003). [DOI:here], pp. 1320–1327.

[205] D.S. Eliashiv et al. “Ictal magnetic source imaging as a localizing tool in partial epilepsy”. In: *Neurology* 59.10 (2002), pp. 1600–1610. ISSN: 0028-3878. DOI: 10.1212/01.WNL.0000032493.83875.0B.

[206] M. Medvedovsky et al. “Sensitivity and specificity of seizure-onset zone estimation by ictal magnetoencephalography”. In: *Epilepsia* 53.9 (Sept. 2012). [DOI:10.1111/j.1528-1167.2012.03574.x], pp. 1649–1657.

[207] J. M. Badier et al. “Ictal Magnetic Source Imaging in Presurgical Assessment”. In: *Brain Topogr* 29.1 (Jan. 2016). [DOI:10.1007/s10548-015-0445-3] [PubMed:26264375], pp. 182–192.

[208] Hisako Fujiwara et al. “Ictal MEG onset source localization compared to intracranial EEG and outcome: Improved epilepsy presurgical evaluation in pediatrics”. In: *Epilepsy Research* 99.3 (2012), pp. 214–224. ISSN: 0920-1211. DOI: https://doi.org/10.1016/j.eplepsyres.2011.11.007.

[209] Woorim Jeong, June Sic Kim, and Chun Kee Chung. “Usefulness of multiple frequency band source localizations in ictal MEG”. In: *Clinical Neurophysiology* 127.2 (2016), pp. 1049–1056. ISSN: 1388-2457. DOI: https://doi.org/10.1016/j.clinph.2015.07.015.

[210] B. Ramanujam et al. “Can ictal-MEG obviate the need for phase II monitoring in people with drug-refractory epilepsy? A prospective observational study”. In: *Seizure* 45 (Feb. 2017). [DOI:here], pp. 17–23.

[211] A. Sohrabpour et al. “Noninvasive electromagnetic source imaging of spatiotemporally distributed epileptogenic brain sources”. In: *Nat Commun* 11.1 (Apr. 2020). [DOI:here], p. 1946.

[212] X. Jiang et al. “Imaging the extent and location of spatiotemporally distributed epileptiform sources from MEG measurements”. In: *Neuroimage Clin* 33 (2022). [DOI:10.1016/j.neuroimage.2013.09.070], p. 102903.

[213] Stefan Rampp et al. “Magnetoencephalography for epileptic focus localization in a series of 1000 cases”. In: *Brain* 142.10 (Aug. 2019), pp. 3059–3071. ISSN: 0006-8950. DOI: 10.1093/brain/awz231.

[214] Z. Cai et al. “Noninvasive high-frequency oscillations riding spikes delineates epileptogenic sources”. In: *Proc Natl Acad Sci U S A* 118.17 (Apr. 2021). [DOI:10.1073/pnas.2011130118].

[215] H. Becker et al. “SISSY: An efficient and automatic algorithm for the analysis of EEG sources based on structured sparsity”. In: *NeuroImage* 157 (2017), pp. 157–172. ISSN: 1053-8119. DOI: https://doi.org/10.1016/j.neuroimage.2017.05.046.